CRANFIELD UNIVERSITY

Boštjan Naglič

MODELLING AND ANALYSIS OF SOIL WETTING PATTERNS UNDER SURFACE DRIP IRRIGATION

School of Applied Sciences

MSc by Research
Academic year: 2010 - 2011

Supervisor: Dr. Cédric Kéchavarzi

October, 2011

CRANFIELD UNIVERSITY

School of applied sciences

MSc by Research

Academic year: 2010 - 2011

Boštjan Naglič

MODELLING AND ANALYSIS OF SOIL WETTING PATTERNS UNDER SURFACE DRIP IRRIGATION

Supervisor: Dr. Cédric Kéchavarzi

October, 2011

This thesis is submitted in partial fulfilment of the requirements for the degree of Master by Research

Abstract

Knowledge of the horizontal and vertical distances by which water spreads in soils under a point source is essential to the design of cost effective and efficient surface drip irrigation systems. The size of this wetting pattern is influenced by soil properties as well as emitter discharge rate and is a limiting factor determining the minimum number of emitters along drip lines. Numerical simulations were carried out with Hydrus-2D/3D to investigate the effects of volume of water applied, emitter discharge rate and initial soil moisture conditions on the dimension of wetting patterns under point source surface drip irrigation for a series of soils with different textures. In addition, the dimensions of the wetting patterns estimated with Hydrus-2D/3D for three soils and various flow rates were compared those observed with two-dimensional soil tank experiments. Finally, the wetting pattern dimensions obtained numerically were also compared to values estimated using a simple analytical model. Simulation results showed that at a given volume of applied water the wetted radius tended to be larger for fine-textured soils and smaller for coarse-textured soils. Conversely, the wetted depth was larger for coarse-textured soils and smaller for fine-textured soils. The wetted depth increased more than the wetted radius for increasing volumes of applied water. In the coarse-textured soils the wetting pattern was elongated in the vertical direction, but in fine-textured soils the wetting pattern lengths were about the same in both directions. In general, a decrease in discharge rate resulted in a slight increase in the wetting pattern radius for all soils. Conversely, emitter discharge rate had no effect on the wetted depth in the sand and clay soils, but a small effect in the silt loam soil where lower discharge rates resulted in lower wetted depth. Importantly, higher emitter discharge rates resulted in larger saturated wetting pattern radius and depth for all three soils. Higher initial soil moisture conditions caused larger wetting pattern sizes in both horizontal and vertical directions but the increase was larger in the vertical direction. Hydrus-2D/3D predicted accurately the vertical distribution of water for all three tank experiments, with RMSE values < 2.6 cm. Good predictions of horizontal distribution were also obtained for the sand for all flow rates (RMSE < 2.2 cm) and the silty clay loam (RMSE = 5.0 cm) but the model simulations did not match the horizontal spreading as well in the sandy loam (RMSE < 9.9 cm). A multiple linear regression analysis revealed that the volume of applied water, V, the available pore space, θ_f, the saturated hydraulic conductivity, *Ks*, and the van

Genuchthen retention parameter, α, explained 92 % of variability in the wetted radius. On the other hand, 92 % of variability in wetted depth was explained by V, θ_f, *Ks* and the emitter discharge rate, *Q*, but this latter had a small effect. The Schwartzman and Zur (1986) model was tested against the wetting depth and radius obtained with the Hydrus-2D/3D simulations for the 11 soil textural classes, three different emitter discharge rates and different initial soil moisture conditions. The values of the model constants were fitted to the data. The predictive capability of the model was remarkable considering that the only parameters used were V, *Ks* and *Q*, It therefore provides a simple analytical tool for estimating wetting patterns dimensions and emitter spacing from readily available parameters without the added experimental complexity associated with the characterisation of other hydraulic parameters.

Acknowledgement

I would like to express my gratitude to my supervisor Dr. Cédric Kéchavarzi for all the help, support and encouragement during the year of this project.

Many thanks to Dr. Marina Pintar, from University of Ljubljana, for offering me the opportunity to study at Cranfield University.

I would like to thank to Martina Zupančič, from the Slovenian Institute of Hop Research and Brewing, who recommended studying abroad to enhance my experience.

A special thanks to Nataša Hrastnik and Plima d.o.o. for enabling me to study at Cranfield and for financial support.

The project was partly founded by the European Union (European Social Found) and Cranfield University.

Table of contents

List of figures

List of tables

Nomenclature

Roman alphabet

Symbol	Description	Dimension
A	Surface area	L^2
A_1	Constant for the cylindrical flow model	[-]
A_2	Constant for the cylindrical flow model	[-]
EF	Modelling efficiency	[-]
h	Soil water pressure head	L
$h_a^{\ i}$	Average water tension	L
$\boldsymbol{K_{ij}^A}$	Components of the dimensionless anisotropy tensor KA	[-]
$K(h)$	Unsaturated hydraulic conductivity function	(L/T)
K^A	Dimensionless anisotropy tensor for the unsaturated hydraulic conductivity K	[-]
Ks	Saturated hydraulic conductivity of the soil	L/T
l	Shape parameter (pore connectivity parameter)	[-]
m	Parameter in the soil water retention function	[-]
$\boldsymbol{\bar{M}}$	Mean of observed data	[-]
Mi	Observed (measured) values	[-]
n	Shape parameter (exponent of soil water retention function)	[-]
n	Number of observations	[-]
n_1	Constant for the cylindrical flow model	[-]
n_2	Constant for the cylindrical flow model	[-]
Q	Discharge rate	L^3/T
q	Water flux per unit area	L/T/L
Q	Emitter discharge rate	L^3/T
Qa	Actual flow rate	L^3/T
q_i	Volumetric flux density	L/T
r	Radius	L
S	Sink term	L^3/L^3T
S_e	Effective soil water saturation	[-]
Si	Simulated values	[-]
t	Time	T
V	Applied volume of water	L^3
V	Total amount of water in the soil	L^3
V^*	Dimensionless parameter amount of water applied	[-]
x^*	Dimensionless parameter wetted radius	[-]
x_i	Spatial coordinate	L
y^*	Dimensionless wetted depth	[-]
$\boldsymbol{\bar{M}}$	Mean of observed data	[-]

Greek symbols

Symbol	Description	Dimension
α	Shape parameters (coefficient in the soil water retention function)	1/L
$\Delta\theta$	Average change in volumetric water content	L^3/L^3
θ	Volumetric water content	L^3/L^3
θ_a^i	Average water content	L^3/L^3
θ_f	Free pore space	L^3/L^3
θ^i	Initial water content	L^3/L^3
θ_r	Residual water content	L^3/L^3
θ_s	Saturated water content	L^3/L^3

Abbreviations

2D	Two-dimensional
3D	Three-dimensional
AEi	Improved Amin and Ehhmaj (2006) model
AEi	Existing Amin and Ekhmaj model
ASAE	American Society Of Agricultural Engineers
AW	Available water
Aw	Area wetted by one emitter
BC	Boundary condition
BD	Bulk density
DLL	Dynamically Linked Library
DOS	Disk operating system
E	Existing Schwartzman and Zur model
E	Evaporation
ET	Evapotranspiration
ETc	Crop water requirements (crop evapotranspiration)
ETo	Reference crop evapotranspiration
FAO	Food and agricultural organisation
FC	Field capacity
GUI	Hydrus graphical user interface
IC	Soil moisture initial conditions
IR	Irrigation requirement
Kc	Crop coefficient
Le	Existing Li *et al*. model
Li	Improved Li et al. (2003)
M	Modified Schwartzman and Zur model
NSRI	National Soil Resource Institute
PTF	Pedotransfer functions
Pw	Percentage of the wetted area
PWP	Permanent wilting point
Qw	Application rate

RMSE	Root mean square error
SDI	Subsurface drip irrigation
Se	Emitter spacing
SEISMIC	Spatial Environmental Information System for Modelling the Impact of Chemicals
T	Transpiration
UK	United Kingdom
USA	United States of America
VG	van Genuchten
Vw	Volume of water applied
X	Wetted radius (horizontal direction)
Y	Wetted depth (vertical direction)

1 Introduction

1.1 Background and rationale

With the population increase in the last century and the increasing pressure on land, land use has become more vulnerable to the effects of climatic events. Irrigated crops, according to Fischer *et al.* (2007), present around 18 % of total cultivated land today and produce about 40 % of total agricultural output. Since 1960 the area of irrigated land worldwide has increased, at a rate of around 2 % per year, from 140 million hectares (ha) in 1961/63 to 270 million ha in 1997/99.

Changes in availability and demand of water under climate change will affect security of food and agricultural activities in the 21st century. Modified precipitation patterns and water storage cycles will change annual, interannual and seasonal availability of water for terrestrial and aquatic agro-eco systems. In the majority of world regions the climate change will increase irrigation demand because of a combination of decreased rainfall and increased evapotranspiration caused by higher temperatures. Climate change could have a big effect on irrigation water requirements.

Worldwide about 70% of total water withdrawals is due to irrigation causes. That represents more than 90% of consumptive water use. *"For countries in development a 14% increase in irrigation water withdrawal is expected by 2030"* in a study by Bruinsma (2003) where the impacts of climate change were not taken into account. As mentioned by Bruinsma (2003), the *"practices that increase the productivity of irrigation water use (crop output per unit water use) may provide significant adaptation potential under future climate change"*. Therefore, irrigation improvements in the future (modified irrigation techniques or technology, including timing and amount) will play a very important role. In other words, the water availability both for production of food and for competing environmental and human needs will need to be assured (Bates *et al.*, 2008).

"Drip irrigation offers a great potential to improve water management by improving crop yield and quality using less water, and by localising fertiliser and chemical

applications to enhance their efficient use and to reduce pollution risk" (Fischer *et al*., 2007). Drip irrigation systems consist of point or line source emitters which are usually operated intermittently. The emitters sometimes interact, for instance, for irrigation of row crops, emitters have to be closely spaced along the laterals to maintain the necessary strip of wetted soil along the row. During irrigation (water infiltration) the water content in the soil changes spatially and temporally. Water distribution in the soil is strongly dependent on the design parameters of the irrigation system (drip lateral spacing, system pressure, flow rate, trickle emitter type), climatic conditions, root distribution, soil type, rates of water application and vegetation. For effective design of drip irrigation systems, the water dynamics in the soil needs to be predited using all above mentioned variables. Information about temporal evolution of the wetted volume in specific soil can help in establishing the optimal spacing between the emitters and the irrigation duration as a function of the soil volume where the crop roots are located (Provenzano, 2007).

There are some guidelines published to help end-users operate, maintain and install surface drip irrigation systems (for instance FAO, 2002a). Unfortunately there are few, if any, clear guidelines helping to design surface drip irrigation systems taking into account differences in soil hydraulic properties. Systems are, in engineering terms, often designed to an economic optimum, which may result in excessive or insufficient irrigation, which then fails to produce the desired output. Some irrigation manuals, such as Vermairen and Jobling (1984), propose excavation of the soil beneath the emitter to visually observe the geometry of the wetting pattern. This poses several problems since it is not practically possible to test all the design parameters mentioned above.

On the other hand, models that simulate soil water dynamics beneath surface drip emitters can help predict soil water movement, taking into account most of the above mentioned variables. One such model is the numerical model Hydrus-2D/3D (Šimůnek *et al*., 2006), which solves the governing flow equation for soil water movement and root water uptake. It has recently been used extensively to simulate water distribution under surface and subsurface drip irrigation systems (e.g. Aussaline, 2001; Cote *et al*., 2003; Skaggs *et al*., 2004, 2010; Lazarovitch *et al*., 2005; Provenzano, 2007; Bufon *et al*., 2011; Kandelous et al., 2011; Phogat et al., 2011). Use of such models can save

time, financial resources and laborious work in comparison to field experiments, which would have to be undertaken to examine wetting patterns under different irrigation strategies and field conditions. Once all the necessary soil parameters are measured, Hydrus-2D/3D can simulate water distribution under drip irrigation systems for a wide range of conditions, including different drip irrigation scheduling, flow rates, volumes of water applied, pulsing irrigation and different initial soil moisture conditions.

1.2. Aims and Objectives

1.1.1 Aim

The aim of this study is to investigate numerically and experimentally the influence of soil texture and hydraulic properties on the size of the wetted area and therefore emitter spacing under surface drip irrigation.

1.1.2 Objectives

- To simulate water infiltration and measure depth and width of the wetted area using the numerical model Hydrus-2D/3D for a series of soils with contrasting textures;
- To compare numerical results with simple two-dimensional tank experiments for three soils with different textures;
- To study the influence of emitter flow rates and initial soil moisture content on wetted geometry;
- To investigate the relationship between design parameters, soil properties and the geometry of the wetting patterns;

2 Literature review

2.1 Drip irrigation

2.1.1 Principles

Microirrigation is a general, broadly defined term and means slow application of water on or below the soil surface. It can be also called localised irrigation, to emphasize that only part of the soil volume is wetted (Lamm *et al*., 2007). Microirrigation systems can be classified as a surface drip, subsurface drip, bubbler and microsprinklers systems. Drip irrigation is, according to ASAE, 2007, defined as a *"method of microirrigation wherein water is applied to the soil surface as drops or small streams through emitters. Discharge rates are generally less than 8 L/h for single-outlet emitters and 12 L/h per meter for line-source emitters"*. In the literature, trickle irrigation is used interchangeably with drip irrigation. In this work the term drip irrigation will be used.

After the World War II the technological development on an industrial scale came about with the ″plastic revolution″, initially it started in glasshouses in England, between 1945-1948 and later in Israel and in the USA (Dasberg and Or, 1999). Equipment for installing subsurface drip had been developed by the 1970s. About the same time surface drip irrigation systems, including fertilizer injection were being developed in Israel. When tubing and drip emitters became more reliable, surface drip irrigation systems grew at a greater rate than subsurface systems. This was because of problems with root intrusions and emitter clogging of the latter (Camp, 1998). After Reinders, 2007, the area irrigated by microirrigation in the world increased from 436,590 ha in 1981 to more than 6.089,534 ha in 2006 (Table 2.1).

Table 2.1 The area of microirrigation in the world (after Reinders, 2007)

Year	**1981**	**1986**	**1991**	**2000**	**2006**
Area (ha)	436590	1030578	1826287	3201300	6089534
Increase (%)		136.1	77.2	75.3	90.2

2.1.2 Design

Drip irrigation systems are designed to transport water from source, to a crop, through a delivery network of a pipes and emission water devices. The general goal of drip

irrigation system design is to provide irrigation water efficiently and uniformly to a crop, to help meet the evapotranspiration (*ET*) needs. At the same time, maintaining desired water content at a depth of the root zone, which is increasing the crop yield and quality, is of great importance (Lamm *et al*., 2007; FAO, 2002a).

When the field is cropped, water can be lost from the soil surface and wet vegetation through evaporation (*E*). The process is affected by climatological factors such as solar radiation, air temperature, air humidity and wind speed. The second process of water loss is called transpiration (*T*), where liquid water from the plant tissues vaporizes into the atmosphere through stomata, located on the plant leaves. Transpiration, like evaporation, depends on the energy supply, vapour pressure gradient and wind. Air temperature, air humidity, solar radiation, and wind speed should be considered when assessing transpiration. Transpiration rate is also determined by many other factors, such as crop characteristics, cultivation practices, environmental aspects, soil salinity, waterlogging and the soil water content, and its ability to transport water to the plant roots. When those two above mentioned separate processes, where water is on one hand lost from evaporation from the soil surface and, on the other hand, when water is lost from transpiration from a plant, combined they are called evapotranspiration (*ET*).

Evaporation and transpiration occur together, and distinguishing between them is not easy. At the beginning of the crop growth, while the crop is small, the main process is evaporation. Later in crop development, or when the crop is fully grown, it completely covers the ground and then transpiration becomes the prevailing process. It has been estimated that at crop sowing, 100% of the total *ET* comes from evaporation. But when the crop develops its full cover, evaporation accounts for only about 10% of *ET* and transpiration for the remaining 90%. Crop water requirements encompass the total amount of water used in evapotranspiration (FAO, 2002b).

Irrigation requirements (*IR*) refer to the water that must be supplied through the irrigation system to ensure that the crop receives its full crop water requirements. In this case the ET_c (crop water requirements) have to be calculated by multiplying ET_o (reference crop evapotranspiration), which is defined as the evapotranspiration from a

reference surface, not short of water, with crop coefficient (K_c), which varies with the crop, its growth stage, growing season and weather conditions. If irrigation is the sole source of water supply for the plant, the irrigation requirement will always be greater than the crop water requirement to allow for inefficiencies in the irrigation system. If the crop receives some of its water from other sources (rainfall, water stored in the ground, upward seepage, etc.), then the irrigation requirement can be considerably less than the crop water requirement. (Dorenbos *et al*., 1984; FAO, 2002b).

Once the crop water irrigation requirements are considered, irrigation scheduling can be prepared. Scheduling has to integrate all elements of the system's hydraulic design and maintenance with various aspects of the soil and the crop characteristics with the atmospheric evaporative demand. In short, drip irrigation scheduling is controlled by measuring or estimating of crop water needs, soil water status and plant water status property (Lamm *et al*., 2007). As noted in FAO (2002a), many factors influence the soil water movement, its water holding capacity and plant ability to use water the drip irrigation system used has to match most of them.

The primary objective of a drip system design is to choose appropriate components and layout to achieve suitable water distribution over the field and, at the same time, meet crop need with consideration of economical, operational, water quality and quantity. Well designed drip irrigation systems should provide equal soil water availability to all plants in the irrigated field at high irrigation efficiency (in ASAE, 2007 is defined *"as the ratio of the average depth of irrigation water that is beneficially used to the average depth of irrigation water applied, expressed as a percentage"*). Water distribution, by drip irrigation systems, can be applied as a line source or point source applications for both tapes and tubings. Line sources apply water in a continuous or near-continuous pattern along the length of the lateral. In this category are soaker hoses or porous pipes (line-source emitters) in which the entire pipe wall is a seepage (and filtration) surface, as well as drip tapes with closely spaced (e.g., 15-30 cm) emission points whose water application patterns overlap. Polyethylene drip tubing, with on line, or built in, or fused drip emitters, is most commonly used. Thin walled collapsible emitting hoses, also called drip tapes, are used to irrigate annual crops, but seldom used for irrigation of

permanent crops because these drip lines don't have the longevity required. Point source emitters can be grouped based on their flow characteristics. Thin walled driplines with periodically spaced emitters infiltrate upon pressurization. Emitter spacings are ranging from about 50 mm to 1m. The combination of emitter discharge rate and emitter spacing determines the dripline discharge rate (L/h-100 m). Water discharge from the emission points which are spaced more than 1 m apart (usually 1 m or more) is called point source application. Water discharged from closely spaced outlets is called line-source application. These devices apply water at discrete points, and overlap between wetting patterns may or may not occur, depending on emitter spacing, irrigation duration, and emitter flow rate (Evans *et al*., 2007; Lamm *et al*., 2007)

Preliminary design steps therefore include: determination of crop water requirements, irrigation requirements, leeching requirements, percentage wetted area, number of emitter per plant and emitter spacing, irrigation frequency and duration, emitter selection, design emission uniformity and allowable pressure variation (FAO, 2002a)

Surface drip irrigation (SD)

Surface drip irrigation systems have been primarily used for irrigation of widely spaced perennial crops, but today they can be used for annual row crops too. Typical components of surface drip irrigation systems are filters, control and system valves, injection systems, underground pipelines and other components, as shown on Figure 2.1 (Lamm *et al*., 2007).

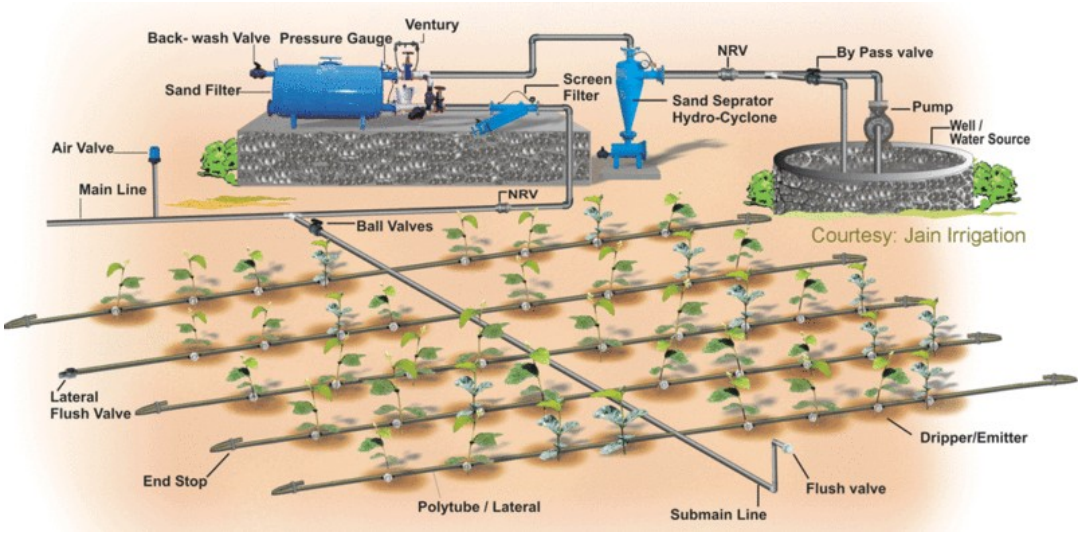

Figure 2.1: Drip irrigation Layout and its parts (source: http://en.wikipedia.org/wiki/File:Dripirrigation.gif)

Advantages and disadvantages of surface drip irrigation systems

As described by Lamm *et al*. (2007) and Keller and Bliesner (1990) surface drip irrigation, when compared to other systems of irrigation, has many advantages, such as: Increased water use efficiency, improved water management (surface drip irrigation has lower evaporative losses than surface, sprinkler or microsprinkler irrigation, because a smaller surface area is wetted), improved crop establishment (a surface drip irrigation is ideal for establishing orchards and vineyards because the emitters can target water to the limited root zone of the young trees), crop yield and quality (because surface drip systems wet only a proportion of soil, the irrigation right up to time of harvest is possible), improved weed control (weed control is much easier with surface drip irrigation systems than with full coverage irrigation systems or sprinklers), improved crop yields and quality (soil water content in the root zone is constant because water is applied slowly and frequently), reduced nonbeneficial use (water requirements are smaller than with traditional irrigation methods, because of irrigation of smaller soil volume, decreased surface evaporation, reduced or eliminated runoff, and reduced deep percolation), reduced deep percolation (drip irrigation offers great opportunities to reduce the losses to a minimum), improved fertilizer and other chemical application (fertilizers, herbicides, insecticides, fungicides, rodenticides, nematocides, growth regulators and carbon dioxide can be efficiently applied to improve crop production),

lower costs (surface drip irrigation systems are often less expensive when compared to microsprinkler or sprinkler irrigation systems, reduced insects problems (surface drip systems are less likely to be plugged by insects than microsprinklers, because of smaller discharge openings) and decreased energy requirements (because the operating pressures are low, the energy costs of pumping water can be reduced).

Surface drip irrigation systems also have disadvantages (Lamm *et al*., 2007; Keller and Bliesner, 1990). High system costs (extensive lateral networks and supportive equipment, like valves, controllers and filters, make trickle irrigation systems initially expensive. Actual costs may depend on the crop, specific system design attributes, filtration equipment or automation. Operational costs are comparable to other pressurized irrigation systems), limited wetting of crop root zone (difficulties may occur with achieving sufficient wetted soil volume), cover crop limitations (if the rainfall is low, surface drip irrigation may exclude the use of cover crops), persistent maintenance requirements (drip emitters of surface drip irrigation systems have smaller flow passageways than mikrosprinkler irrigation systems and are thus more easily clogged), extensive maintenance requirements (complete or partial clogging still represents a serious problem. Also the damages of pipelines and other components (rodent) or leeks can occur), potential for excess deep percolation (because crop water demand is applied to a small volume of soil, deep percolation losses can occur), difficulties in visual inspection (clogging problems are difficult to detect through visual inspection), cleaning difficulties (if the emitter gets clogged it is almost impossible to clean it), minimum frost protection capabilities, salt accumulation near plants (if the high salinity waters are used, salts tend to accumulate at the soil surface and along the borders of the wetting patterns) and restricted root development (root development may be limited to the wetted soil volume near each emitter or along each lateral line, because water is applied to a specific part of a soil volume occupied by a plant).

Surface drip irrigation for row crops

Design and management of surface irrigation systems for perennial crops and for annual row crops is different. For certain vegetable crops, flower beds or other density-planted crops with limited lateral root zones, wetting of the entire area is needed by overlapping

the soil volumes by each emitter. With row crops the aim is to wet the plat row uniformly, while between rows the soil can be left dry. For perennial crops, like trees or vines, a dry zone may separate each tree from its neighbour. Because of that, the distance between, and along, the laterals must be adapted to crop water requirements. Usually for irrigation of row crops the drip tape emitting hose is used, but also point source emitters, which are usually used to irrigate trees in orchards, are used. Emitters have to be closely spaced along the laterals to maintain the necessary strip of wetted soil along the row.

Surface drip irrigation of row crops has some advantages, as discussed by Lamm *et al*. (2007), when compared to the row crops subsurface drip irrigation:
Cultivation alternatives (Extensive cultivation is possible between crops because the dripline is removed prior to harvest), reduced system damage (because the dripline is removed prior to harvest, the damage to driplines during harvest is removed), salinity (seedbed soil salinity can be better controlled by surface drip irrigation than by subsurface drip irrigation), reuse of drippers (the driplines can be recovered and used elsewhere), better leeching capabilities (leeching can occur from soil surface downwards , but no leeching occurs above driplines of subsurface drip irrigation systems), repairs (very easy to repair or replace damaged dripline), underground pests (less damage because of burrowing rodents and insects), visual inspection (potential clogging problems can be seen and quickly repaired), also the problems, such as dripline crimping, root and soil intrusion like with subsurface drip irrigation systems, are eliminated.

Surface drip irrigation of row crops also has some disadvantages (Lamm *et al*., 2007). This includes dripline installation and removal issues (installation and removal costs are needed for each crop. Laterals have to be removed prior to harvest to prevent damage), damage to driplines (surface installed driplines are more susceptible to damage during cultural operations and also from animal pests compared with subsurface drip irrigation systems), length limitations (lateral lengths may be limited because of the need to extract driplines), clogging potential (clogging problems can be caused because of temperature variations and accumulation of salts at the emitters).

2.2 Characterization and modelling of wetting patterns

2.2.1 Introduction

Importance of wetted volume

As already mentioned, one of the important preliminary design steps, or planning factors of surface drip irrigation systems, is to get more information about the dimensions of the wetted soil zone or moisture distribution patterns.

In order to answer the question: ″How many emitters per plant are required? ″ It is important to know how big an area of the soil is wetted by one emitter and what is the desired percentage of the wetted area (Pw), we want to achieve. As discussed by Keller and Bliesner (1990) and FAO (2002a), the percentage wetted area (Pw) compared with the entire cropped area depends on the volume and rate of discharge at each emission point, spacing of emission points (drippers) and type of soil which is irrigated. Wetted area at each emitter is at the soil surface usually quite small. It expands with depth and forms an inverted bulb shaped cross section. Pw is determined from an estimate of the average area wetted at a depth of 150 to 300 mm beneath the emitters, divided by the total cropped area served. So far, no proper minimum value for Pw has been established. A reasonable objective of design for widely spaced crops (vines, bushes, trees) is to wet at least one-third, and as much as two-thirds, of the potential horizontal cross-sectional area of the root systems (33%<Pw>67%). For widely spaced crops Pw should be held below 67% to keep the strips between the rows relatively dry, for agricultural practices. Low Pw values also reduce loss of water due to evaporation even where cover crops are used. Also it is less costly to have a low Pw, because more emitters per plant (and laterals) are needed to obtain a larger coverage. In closely spaced crops, where rows or emitter laterals are spaced less than 1.8 m apart, Pw often approaches 100%. In order to determine the number of emitters per plant, the desirable Pw and area wetted by one emitter (Aw) must be known. The Aw along a horizontal plane about 30 cm below the soil surface depends on the rate and volume of emitter discharge, soil texture, structure, slope and horizontal layering of the soil.

The information, gathered from other drip irrigation systems cannot help in the designing and operation of a drip irrigation system, because water distribution is

dependent on soil type and specific design parameters. Conversely, design parameters, such as Pw, location and emitter spacing, application rates, amount of water applied, frequency of irrigation under surface drip irrigation are governed by the moisture distribution patterns, or dimensions of the wetted area in the soil. Those have to be carefully investigated because they indicate the boundaries of the irrigated soil volume and therefore determine emitter spacing.

When installing the surface drip irrigation system, the placement of the emitter directly above the soil surface enables infiltration within a very small area compared to the total area, of the soil surface. The shape of the wetted volume of soil under single drip emitter is, according to Cote *et al*. (2003), Vermeiren and Jobling, (1984), Skaggs *et al*. (2010), Gardenas *et al*. (2005), influenced by soil texture, soil structure, soil hydraulic properties, anisotropy such as horizontal and vertical permeability and impermeable layers. Under field conditions when the wetting and drying are continuous processes, patterns of soil water content depend also on water management (volume of water applied per irrigation, the rate of application (irrigation frequency), emitter distance (number of drippers), dripper placement (above or below soil surface), lateral positioning with respect to the plant row and initial soil moisture content. Lamm *et al.* (2007) mentioned that management, monitoring and modelling of soil water distribution under cropped conditions, also requires information on water uptake patterns by plants. Uptake patterns influence water distribution and are essential for obtaining reliable predictions of water and matric potential distributions within the wetted soil volume. Information on root water uptake is important for design purposes to match application uniformity, emitter spacing and discharge with the extent of plant root systems, and to ensure uniform root accessibility to wetted soil volume. Lubana and Narda (2001) presented a review of modelling of soil water dynamics under drip emitter, and pointed that still not much is known about the water movement in soil in response to surface point sources. This is mainly because of the complex nature of the surface boundary condition. There is also a lack of understanding of how the soil water distribution is affected by the unsaturated hydraulic properties, which has sometimes resulted in non-optimal management and low water-use efficiency in drip irrigation systems. A better

understanding of the interactions of irrigation method, soil type, crop root distribution, uptake patterns and rates of water applied, is needed to improve drip irrigation practices.

It not possible to test all possible drip irrigation scheduling strategies under different field conditions because of the lack of time and necessary financial resources. A practical approach is to use soil-water flow, root growth, and water uptake models to simulate different irrigation strategies or to evaluate possible scheduling strategies. Then, the most promising strategies could be selected and tested under field conditions. This is a concept that is widely accepted to study and evaluate complex agricultural systems and to select a technology that has best economic effect at the farm level. In this context the adoption of drip irrigation technologies in combination with models that describe water infiltration from a point source can play a major role.

2.2.2 Field and laboratory studies

Li *et al*. (2003) studied the effect of discharge rates and applied volume of water on the shape of the wetted area, from a surface point source for a loam soil. The application rates varied from 0.6 to 7.8 L/h. Results for surface and vertical wetting for all experiments showed that the wetting front moved fast at the beginning and slowed down with increasing time. The wetting front moved outward in a circular arc shape and the surface saturated wetted radius increased with increase of application rate. The surface wetted radius and wetted depth were proportional to the volume of water applied. Saturated water entry zone radius become larger as time increased, and approached a constant value after around 3.5 h. The bigger the application rate, the faster the constant surface saturated wetted radius was reached. Higher application rate resulted in faster wetting front movement in both, radial and vertical directions. Increase in application rate after adding the same volume of water, resulted in an increase in the horizontal direction and decrease in the wetted depth, which has been reported from other studies (e.g. Khan *et al.,* 1996). In addition, the bigger volumes of water applied produced higher water content within the wetted volume. Increase in the applied volume of water increased the wetted depth and had little effect on horizontal wetted area. Li *et al.* (2004) followed his work from Li *et al.* (2003) but this time he monitored the wetting front movement in sand soil too and concluded that for the same volume

applied, the increase in application rate allowed more water to be distributed in the horizontal direction. A decrease in application rate allowed more water to distribute in the vertical direction. They mentioned that further research is necessary to verify whether those results are true in other soil types.

Similarly, Ah Koon *et al.* (1990) studied three emitter discharge rates (1, 2 and 3 L/h) on the distribution and drainage of water beneath a sugarcane crop and fallow plot on clay/silty clay soil. Results showed that higher emitter discharge rate (4 L/h) increased lateral spread of water and are in agreement with Li *et al.* (2003, 2004) results.

Bar-Yosef and Sheikholslami (1976) studied the distribution of water in sand soil, irrigated from a surface drip source. They found that, when adding identical amounts of water, but increasing the emitter discharge rate, the wetting depth increased and horizontal water movement decreased.

Bresler *et al.* (1971) studied the effect of surface emitter discharge rate on the water content distribution in loam and sand soil. Laboratory and field experiments showed that increase in emitter discharge rate resulted in increased wetted area in horizontal direction and decreased soil wetted depth. Research done by Levin *et al.* (1979) for sand soil, confirmed the findings of Bresler *et al.* (1971).

Study about effect of drip irrigation frequency on wetting pattern and potato growth was done by Feng-Xin Wang *et al.* (2006). They used six different irrigation frequencies (once every day (N1, once every two days (N2), once every three days (N3), once every four days (N4), once every six days (N6) and once every eight days (N8)). They applied equal amount of water for all studied frequencies. The results showed that irrigation frequency affected water distribution, wetted soil depth and distance from the emitter. Water distribution varied with the potato growing stage. The wetting pattern developed under treatment N1, showed larger change than those for N4 and N8. In the middle of the planting season, at the depth below 30 cm, water content variations increased as irrigation frequency decreased. During the late growth stages the treatment N8 showed larger variation at depth of 50 – 90 cm than other treatments. This was due to longer

application duration, which led to larger wetted soil in the horizontal direction. Denser root distribution at that depth depleted water more quickly. The higher the frequency, the higher the root length density in 0 – 60 cm of soil depth and the lower root length density at 0 – 10 cm of soil depth. Also the reduction in irrigation frequency from N1 to N8 resulted in significant yield reduction.

2.2.3 Empirical models

For prediction of wetting patterns from a point source a number of models exist. We can group them in empirical, analytical or numerical models.

Empirical models have been developed, based on field observations or regression analysis. Keller and Karmeli (1974) presented a table which serves as a guide for estimating an average percentage of wetted area (Pw). As already mentioned earlier, the optimum value for Pw is unclear; but, considering the current state of knowledge, the Pw for widely spaced crops should be held below 67%. But for closely spaced crops (crops spaced less than 1.8 m apart) Pw can approach to 100%. Table 2.2 estimates Pw for coarse (C), medium (M) and fine (F) textured soils at various emitter discharge rates and spacings. The emitter spacings, suggested in the table, should provide a continuous wetted strip of soil with uniform width approximately 30 cm beneath the soil surface. The values presented in the table are valid for predictions of Pw for a single straight lateral, with uniformly spaced emitters, when applying approximately 40 mm of water per irrigation cycle.

Table 2.2: Percentage of soil wetted by various emitter discharge rates and spacing for emission points in a straight line applying 40 mm of water per cycle (after Keller and Karmeli (1974).

Effective spacing between laterals, m* (1.0 m = 3.3 ft)	Effective emission point discharge rate†														
	under 1.5 lph (0.4 gph)			2 lph (0.5 gph)			4 lph (1 gph)			8 lph (2 gph)			over 12 lph (3 gph)		
	Soil texture and recommended emission point spacing on the lateral - m‡														
	C 0.2	M 0.5	F 0.9	C 0.3	M 0.7	F 1.0	C 0.6	M 1.0	F 1.3	C 1.0	M 1.3	F 1.7	C 1.3	M 1.6	F 2.0
	Percentage of soil wetted§														
0.8	35	88	100	50	100	100	100	100	100	100	100	100	100	100	100
1.0	33	70	100	40	80	100	80	100	100	100	100	100	100	100	100
1.2	25	58	92	33	67	100	67	100	100	100	100	100	100	100	100
1.5	20	47	73	26	53	80	53	80	100	80	100	100	100	100	100
2.0	15	35	55	20	40	60	40	60	80	60	80	100	80	100	100
2.5	12	28	44	16	32	48	32	48	64	48	64	80	64	80	100
3.0	10	23	37	13	26	40	26	40	53	40	53	67	53	67	80
3.5	9	20	31	11	23	34	23	34	46	34	46	57	46	57	68
4.0	8	18	28	10	20	30	20	30	40	30	40	50	40	50	60
4.5	7	16	24	9	18	26	18	26	36	26	36	44	36	44	53
5.0	6	14	22	8	16	24	16	24	32	24	32	40	32	40	48
6.0	5	12	18	7	14	20	14	20	27	20	27	34	27	34	40

* Where double laterals (or laterals with multiple outlet emitters) are used in orchards, enter the table with both the spacing between outlets to either side of the tree row and across the space between the rows and proportion the percentages

† Where relatively short pulses of irrigation area applied, the effective emission point discharge rate should be reduced to approximately half of the instantaneous rate for safety

‡ The texture of the soil is designated by C, course; M, medium; and F, fine. The emission point spacing is equal to approximately 80 percent of the largest diameter of the wetted area of the soil underlying the point. (Closer spacings on the lateral will not affect the percentage area wetted)

§ The percentage of soil wetted is based on the area of the horizontal section approximately 0.30 m (1.0 ft) beneath the soil surface. Caution should be exercised where less than 1/3 of the soil volume will be wetted.

Keller and Bliesner (1990) presented a table for estimation of wetted area (Aw). Estimation is based on a standard 4 L/h emitter for different soil types and depths. They state that the Aw, wetted by one emitter at the soil surface, is usually less than a half as large as Aw measured at a depth of 15 to 30 cm. The values in Table 2.3 are given for different soil texture classes, soil depths and degrees of soil stratification. The values shown are based on daily or every-other-day irrigations, which apply sufficient volumes of water to slightly exceed the water crops need. Wetted area is given as a rectangle; the long dimension, w, is the expected maximum horizontal diameter of the wetted soil volume caused by one emitter. Se is the short dimension and is representing 80 % of maximum expected diameter. Se represents the emitter spacing, which should give a continuous wetted strip of soil. If those two values are multiplied, the result is approximately the same as the circular wetted area. It is clearly mentioned that this table should serve for estimation purposes only.

Table 2.3: Estimated wetted area by 4 L/h drip emitter operating under various field conditions (after Keller and Bliesner, 1990).

Soil or root depth and soil structure	Degree of soil stratification and equivalent wetted soil area (m×m)		
	Homogeneous	**Stratified**	**Layered**
Depth 0,75 m			
Coarse[1]	0.4 × 0.5	0.6 × 0.8	0.9 × 1.1
Medium	0.7 × 0.9	1.0 × 1.2	1.2 × 1.5
Fine	0.9 × 1.1	1.2 × 1.5	1.5 × 1.8
Depth 1,5 m			
Coarse	0.6 × 0.8	1.1 × 1.4	1.4 × 1.8
Medium	1.0 × 1.2	1.7 × 2.1	2.2 × 2.7
Fine	1.2 × 1.5	1.6 × 2.0	2.0 × 2.4

[1]Coarse includes coarse to medium sands; medium includes loamy sands to loams; fine includes sandy clay to loam to clays.

Schwartzman and Zur (1986) developed a semi-empirical model for determining width and depth of the wetted soil volume under the point source. Wetted soil volume was assumed to depend on the hydraulic conductivity of the soil (*Ks*), on emitter discharge rate (*Q*) and on the total amount of water in the soil (V). Using dimensional analysis, analytical expressions for wetted depth and width were obtained as functions of the above parameters. The equations coefficients were then obtained empirically based on experiments carried out on two types of soils (Gilat loam and Sinai sand). This model is one of the most practical for determination of soil wetted geometry for point sources. However, using the model for a wide range of conditions is questionable because it was calibrated only on two sets of experimental data, with only two soil types and two emitter discharge rates. The Schvartzman and Zur (1986) model is presented in more detail in the results and discussion part of this thesis (section 4.1.6.).

Amin and Ekhmaj (2006) presented an empirical model for estimating surface wetted radius (X) and vertical (Y) distances of the wetting pattern front from the surface drip emitter. Their model is based on average change of volumetric water content within the wetted zone, total volume of water applied, application rate and saturated hydraulic conductivity. In their work they verified and modified the Schwartzman and Zur (1986) model, by adding volumetric water content as one of the parameters in their equation. They used already published experimental data from Taghavi *et al*. (1984), Anglelakis *et al*. (1993), Hammami *et al.* (2002), and Li *et al.* (2003), which include sand soil,

loamy sand, loam, silty clay and sandy loam type of soil, to determine the coefficients in their equation, using nonlinear regression:

$$X = \Delta\theta^{-0.5626} V_W{}^{0.2686} Q_w{}^{-0.0028} k_s{}^{-0.344} \quad 1$$

$$Y = \Delta\theta^{-0.383} V_W{}^{0.365} Q_w{}^{-0.101} k_s{}^{0.195} \quad 2$$

where $\Delta\theta$ is the average change in volumetric water content of the wetted zone (L^3/L^3), Vw is the total volume of water applied (ml), Q_w is the application rate (ml/h), Ks is the saturated hydraulic conductivity (cm/h). They concluded, based on the experiments, that the soil type, volume of applied water and emitter discharge rate are the most important factors that affect the wetted zone width and depth.

Kandelous and Šimůnek (2010a) compared the above two empirical models of Schwartzman and Zur (1986) and Amin and Ekhmaj (2006) against field data, to evaluate their accuracy in predicting wetted zone dimensions. Results showed better prediction capability of the Amin and Ekhmaj (2006) model in comparison with the Schwartzman and Zur (1986) model. In some cases the Amin and Ekhmaj (2006) model predicted wetting pattern geometry even better than the numerical models results. The better predictive capability of the Amin and Ekhmaj (2006) model can be explained by its use of $\Delta\theta$. Kandelous and Šimůnek (2010a) concluded that soil water content plays an important role when predicting wetted geometry for surface drip irrigation systems.

2.2.4 Analytical models

Analytical models for prediction of geometry of wetting patterns, under surface point source, usually solve the governing water flow equation under specific conditions. Analytical models rely on assumptions, such as soil homogeneity, and they do not take into account root water uptake.

Cook *et al*. (2003) developed a user friendly Microsoft Windows-based software programme, WetUp, that provides visualisation of the wetting patterns (Figure 2.2). The programme estimates dimensions of the wetting patterns, in different soil textures, with

different soil hydraulic characteristics, for surface or subsurface point sources (emitters). WetUp contains a database of predefined soil types, emitter flow rates (from 0.503 to 2.7 L/h), application times (1 – 24 h), initial soil moisture conditions (3, 6 and 10 m of suction) and emitter position (surface or subsurface).

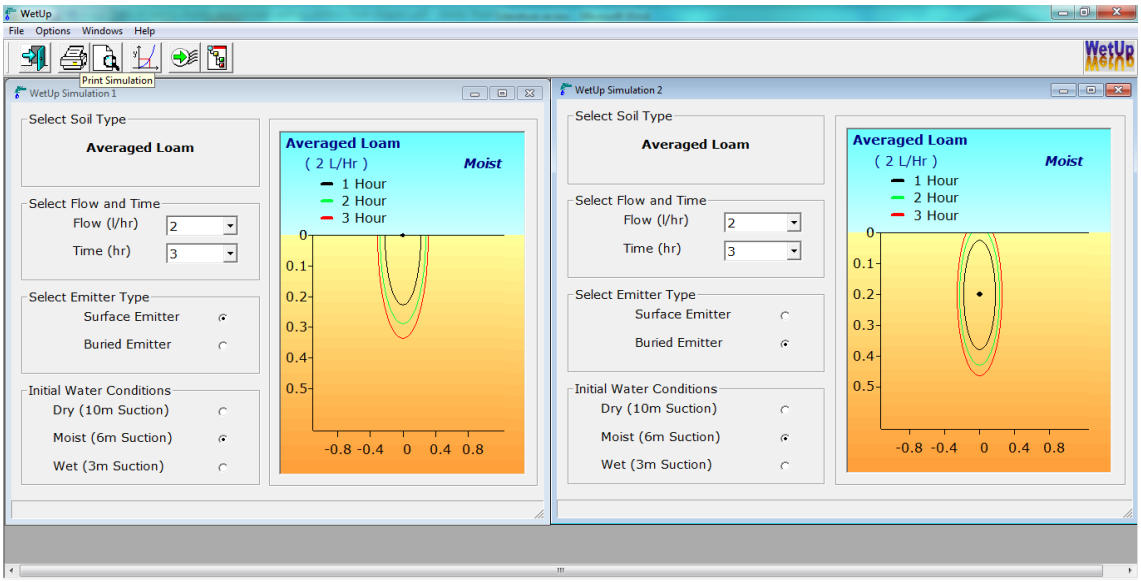

Figure 2.2: WetUp window showing wetted patterns for loamy soil, at 2 l/h emitter flow rate, 2 h of application and initial soil moisture content of 6 m, for surface and subsurface irrigation

WetUp uses a Philip's (1984) solution for flow from a surface and subsurface point source. The solution determines the travel time of water and is based on a quasi-linear analysis of steady three dimensional unsaturated water flow.

Kandelous and Šimůnek (2010a) compared WetUp to other empirical and numerical solutions, for estimating the size of the wetting pattern. WetUp predictions of the geometry of the wetting pattern were less precise compared to Amin and Ekhmaj (2006) or numerical model Hydrus-2D (Šimůnek *et al.,* 1999). Cook *et al.* (2003) also reported that WetUp tends to underestimate horizontal wetting at large volumes of water applied for coarse textured soils.

Other analytical solutions have been derived for steady infiltration from a buried point source and from cavities (Philip, 1968, 1984), from a surface point (Warrick, 1974), and, from shallow circular ponds (Wooding, 1968). Mmolawa and Or (2000) presented

a semi-analytical model for calculating water flow and non-reactive solute transport with and without plant uptake for a buried or surface point source.

Application of analytical models in trickle irrigation management is limited because the solutions are based on limiting assumptions with regards to source configurations, the linearization of the flow equation and homogeneous soil hydraulic properties. Most of them also do not take into account root water uptake.

2.2.5 Numerical studies

There are a number of numerical models developed with the purpose of simulating the surface and subsurface point source water infiltration. Brandt *et al*. (1971) developed a model to analyse multidimensional transient infiltration from a trickle source. Bresler *et al*. (1971) compared the theory, discussed by Brandt *et al*. (1971), with experimental results. Calculated and measured locations of wetting fronts and soil water content distribution were examined. They concluded that, despite the dissimilarity between the theoretical and experimental results, the agreement is sufficient for the practical implementation of the theory.

In 1975 Bresler reported a study about numerical model simulations for analysis of multidimensional simultaneous transfer of a non-interacting water and solute transport, applicable to the infiltration from a trickle source. Mostaghimi *et al*. (1982) studied water movement in silty clay loam soil under single emitter source. They used the numerical method of Bresler (1975) and compared it to laboratory experimental results. The study showed that increasing discharge rate of an emitter results in an increase in the vertical direction and decrease in horizontal direction of the wetted zone. Those results are in contraindication with the results of Li *et al*. (2003), Bar-Yosef and Sheikholslami (1976) and Khan *et al*. (1996). Bresler (1975) also found quite good agreement between predicted and measured soil water content. Lafolie *et al*. (1989) presented the numerical solution which allows predictions of water content distribution under drip irrigation.

Šimůnek *et al.* (1996) developed a software package, Hydrus-2D, which was updated to provide a third dimension, now called Hydrus-2D/3D (Šimůnek *et al.,* 2006). The software enables implementation of three-dimensional water flow, solute transport, and root–water and nutrient uptake based on finite-element numerical solutions of the flow and transport equations. For the water flow module, the program numerically solves Richards equation (Richards, 1931) for variably saturated flow. The flow equation also incorporates a sink term to simulate water uptake by plant roots. In 2011 a 2.0. version of Hydrus-2D/3D has been released. It includes many new features as compared to version 1.0. The most important ones, which can be used for simulating drip irrigation design and management, are various new boundary conditions (i.e. surface and subsurface drip irrigation) and triggered irrigation (irrigation can be triggered by the program when the pressure head drops below specified value) (Šejna *et al*. 2011). The main unit of the programme is the Hydrus graphical user interface (GUI) which defines the overall computational environment of the system (Figure 2.3).

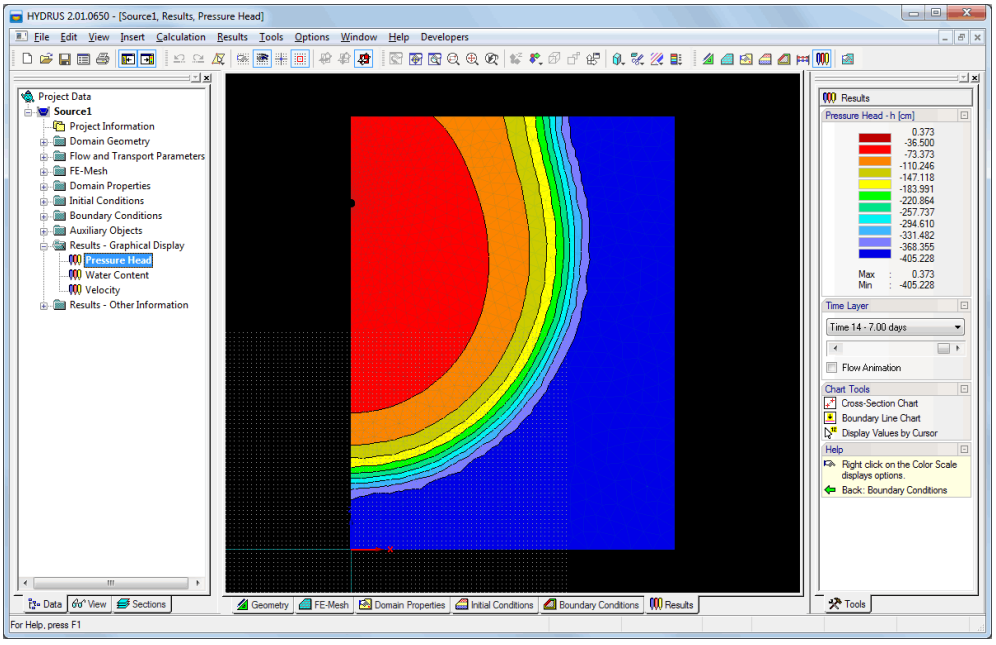

Figure 2.3: The main window of the Hydrus GUI, including his main components.

Soil-water flow and solute transport modelling are useful for water resources and ecological management and, due to the increasing computer speed and availability of more comprehensive numerical models, Hydrus-2D/3D is now increasingly being used

for evaluating water flow in trickle irrigation systems. The number of such studies is extensive and has been growing steadily in recent years (Assouline, 2001; Schmitz *et al*., 2002; Cote *et al*., 2003; Skaggs *et al*., 2004; Lazarovitch *et al*., 2005, 2007; Fernandez-Galvez and Simmonds, 2006; Dahiya *et al*., 2007; Provenzano, 2007; Patel and Rajput, 2008; Elmaloglou and Diamantopolus, 2009; Kandelous and Šimunek, 2010a, b; Rodriguez-Sinobas *et al*., 2010; Skaggs *et al*., 2010). Some of these studies simulated subsurface drip irrigation (SDI) process as a line source (a lateral) (Ben-Gal *et al*., 2004; Skaggs *et al*., 2004;Patel, 2008), while others simulated SDI by means of a point source, as individual emitter (Lazarovitch *et al.*, 2005; Provenzano, 2007; Kandelous and Šimůnek, 2010a, b). While some other authors assessed the ability of Hydrus to simulate water movement from surface drip irrigation systems (Assouline, 2001; Gardenas *et al*. 2005), the number of studies on surface drip irrigation has been limited by the lack of appropriate boundary conditions (a problem which is now resolved by the introduction of version 2.0 in 2011). All of these studies were done using either planar or axisymmetrical two-dimensional models, which is valid as long as the flow domain studied is not influenced by neighbouring emitters.

Kandelous *et al.* (2011) used Hydrus-2D/3D to analyse field data, assuming the modelling approaches in which emitters were represented, either as a point source in an axisymmetrical two-dimensional domain, a line source in a planar two-dimensional domain or a point source in a fully three - dimensional domain. Results showed, that SDI systems can be accurately described, using an axisymmetrical two-dimensional domain, only before wetting patterns start to overlap, and a planar two-dimensional domain, only after full merging of the wetting fronts from neighbouring emitters. Fully three-dimensional model appears to be required to entirely describe the subsurface trickle irrigation process.

Kandelous and Šimůnek (2010a) compared numerical, analytical and empirical models to estimate wetting patterns for surface and subsurface irrigation. They evaluated the accuracy of several approaches used to estimate wetting zone dimensions by comparing their predictions with field and laboratory data, including the numerical Hydrus-2D model, the analytical WetUp software and selected empirical models (Schwarzman and

Zur, 1986; Amin and Ekhmaj, 2006; Kandelous *et al*., 2008). They used the mean absolute error to compare the model predictions and observations of wetting zone dimension. Mean absolute error for different experiments and directions varied from 0.9 to 10.4 cm for Hydrus, from 1 to 58.1 cm for WetUp and from 1.3 to 12.2 cm for other empirical models.

Skaggs *et al*. (2010) used numerical simulations with Hydrus-2D to investigate the effect of application rate, antecedent water content and pulsed water application on horizontal water spreading from drip irrigation emitters. Results showed that higher antecedent water content increases water spreading from trickle irrigation systems, but the increase is bigger in a vertical than a horizontal direction. Also, lower application rates and pulsing, produced minor increases in horizontal spreading of water. Some irrigation treatments were tested in field trials and they confirmed the simulation results. Overall they found out that soil texture (hydraulic properties), and antecedent water content largely determine the spreading and distribution of a given water application, with pulsing and flow rate having very little effect.

Cote *et al*. (2003) also used numerical model Hydrus -2D to investigate the effect of pulsed water applications on the size of the wetting pattern for subsurface drip irrigation for sand, silty and silty clay loam soils. They found that soil hydraulic properties greatly influence the geometry of wetting pattern. Irrigation frequency (pulsing) has slightly increased the dimensions of the wetting pattern in highly permeable coarse textured soil. Also, similarly to Skaggs *et al*. (2010), high discharge rates from a SDI tend to increase vertical spreading more than horizontal. The simulations also highlighted that, in order to achieve desired wetted volume, the drip irrigation system discharge rate has to be regulated according to particular soil type and consequently its hydraulic properties are of great importance.

Provenzano (2007) studied wetted soil volume for subsurface drip irrigation numerically, with Hydrus-2D, and experimentally. He presented the dimensions of the wetted soil volume as a function of duration of irrigation, Q and initial soil moisture conditions as shown in Figure 2.4.

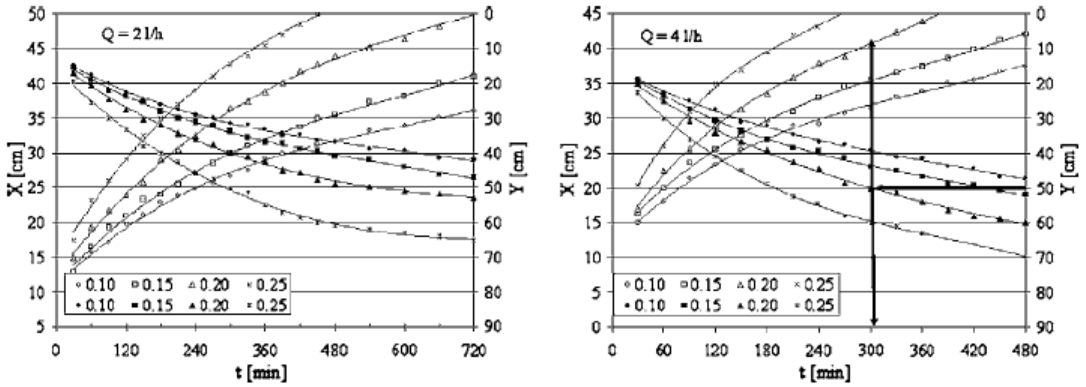

Figure 2.4: Dimensions of the wetted soil volume for horizontal (X) and vertical (Y) direction, as a function of flow rate (*Q*), initial soil moisture conditions (varying from 0.10 cm^3/ cm^3 to 0.25 cm^3/ cm^3 and irrigation duration (min). After Provenzano (2007)

Results clearly showed that, for fixed initial soil moisture content, wetting pattern increased with irrigation duration. If a duration of application is fixed, the wetting pattern increases with increase in initial soil moisture content.

Assouline (2001) presented a study about the effect of different emitter discharge rates, including microdrip emitters (emitter discharge rate <0.5 L/h), on different water regimes in drip irrigated corn. In his study, three emitter discharge rates (0.25, 2.0 and 8 L/h) were compared in field experiments and for numerical simulations using Hydrus-2D. Field experiments showed that, under microdrip irrigation, the highest relative water content occurred in the upper 30 cm of the soil profile and the lowest in the 60 to 90 cm layer. Numerical results showed that, under microdrip irrigation treatment, wetted volume of soil was smallest in both, horizontal and vertical directions. The water content gradients for microirrigation treatment were also less extreme in both directions, compared to 2.0 and 8.0 L/h discharge rates. The saturated zone of soil was maintained only beneath the 8.0 L/h dripline (Figure 2.5). The depth of the wetting front below the dripline was shallowest under microdrip irrigation treatment.

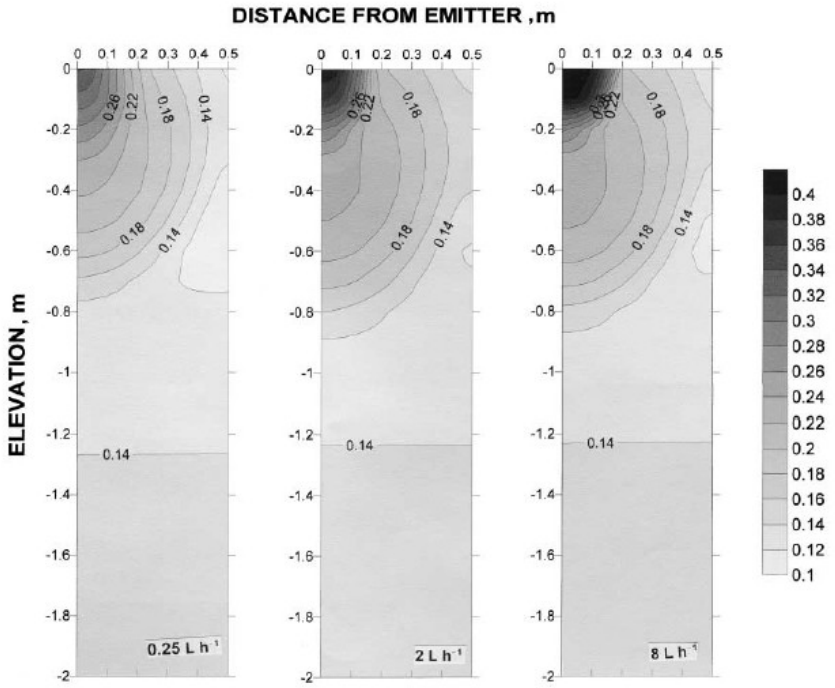

Figure 2.5: Simulated water content distribution beneath the dripline for three emitter discharge rates at the end of application cycle. After Assouline, 2001

Those results are in agreement with findings of Mostaghimi *et al*. (1982) but in contradiction with Khan *et al*. (1996) and Li *et al*. (2003) which concluded that higher emitter discharge rates extend soil water movement in a horizontal direction. This was likely to be caused by the differences in hydraulic properties of different soils or water uptake patterns of plant.

3 Materials and methods

3.1 Hydrus-2D/3D model

The modelling of water flow under single drip surface emitter, in this research, was performed using the numerical model Hydrus-2D/3D Version 2.0 (v.2) and v.1.0. This Microsoft Windows based software, which was developed by Šimůnek *et al*. (2006), can simulate water, solute and heat flow in two and three dimensional variably saturated media. The software package is a replacement and extension of Hydrus-2D (v. 2.0) (Šimůnek *et al*., 1999) and SWMS_3D. SWMS_3D is the Disk operating system (DOS) computer programme for water and solute movement simulations in three dimensional (3D) variably saturated media, developed by Šimůnek *et al*. (1995). Recently, in 2011, Hydrus-2D/3D v.1.0 was upgraded and replaced by Hydrus-2D/3D v.2.0. (Šejna *et al.,* 2011; Šimůnek *et al*., 2011). A notable new feature is new boundary condition, which allows the dynamic evaluation of the wetted area for surface drip irrigation. Although most of the simulations in this study had already been carried out with version 1.0. prior to the release of version 2.0, the simulations of soil water movement in the tank experiments were carried out with this new boundary condition (BC).

3.1.1 Soil hydraulic model and water flow parameters

The theory behind Hydrus-2D/3D is given by Šimůnek *et al*. (2006), and more recently by Radcliffe and Šimůnek (2010). This section only focuses on details which are relevant to this research.

The description of variably saturated water flow in soils, as is the case when water enters the soil surface in the form of precipitation or irrigation, is based on the equation of Richards (1931), which combines the Darcy-Buckingham equation (Equation 3) for unsaturated water flow with a mass balance or continuity equation (Equation 4):

$$q_i = K(h)\left(K_{ij}^{A}\frac{\partial h}{\partial x_j} + K_{iz}^{A}\right) \qquad 3$$

$$\frac{\partial \theta}{\partial t} = \frac{\partial q_i}{\partial x_i} - S \qquad 4$$

where, *K(h)* is the unsaturated hydraulic conductivity function (L/T), h is the soil water pressure head (L), x_i (*i=1,2* for two-dimensional model and *i=1,2,3* for three-dimensional model) are spatial coordinates (L), K_{ij}^A and K_{iz}^A are components of a dimensionless anisotropy tensor K^A (which reduces to the unit matrix when the medium is isotropic), θ is the volumetric water content (L^3/L^3), t is time (T), q_i is the volumetric flux density (L/T) and S is a sink term (L^3/L^3T), usually representing the root water uptake.

Combining these two equations leads to the Richards equation (Equation 5):

$$\frac{\partial \theta}{\partial t} = \frac{\partial}{\partial x_i}\left[K(h)\left(K_{ij}^A \frac{\partial h}{\partial x_j} + K_{iz}^A\right)\right] - S \qquad 5$$

The unsaturated soil hydraulic properties *θ(h)* and *K(h)* in Equation 5 are usually highly nonlinear functions of the pressure head. The water retention curves are usually expressed in terms of simplified analytical solutions to enable their use in numerical models. The soil hydraulic properties in Hydrus can be determined using five different analytical models. The Mualem-Van Genucten hydraulic functions (van Genuchten, 1980; Mualem, 1976), the most widely implemented functions, were used in this study (Equation 6 and 7):

$$\theta(h) = \begin{cases} \theta_r + \dfrac{\theta_s - \theta_r}{[1 + |\alpha h|^n]^m} & h < 0 \\ \theta_s & h \geq 0 \end{cases} \qquad 6$$

$$K(h) = K_s S_e^l \left[1 - (1 - S_e^{1/m})^m\right]^2 \qquad 7$$

where

$$m = 1 - \frac{1}{n} \qquad n > 1$$

where θ_s and θ_r are saturated and residual water content (L^3/L^3), α (1/L), n and l are shape parameters, and S_e is the effective soil water saturation, given as:

$$S_e = \frac{\theta - \theta_r}{\theta_s - \theta_r}$$

The pore connectivity parameter l in Equation 7 is equal to 0.5 for most soils (Mualem, 1976; Šimůnek *et al*., 2011).

Richards equation (Equation 5) is a nonlinear, partial differential equation governing variably saturated water flow. Most practical applications of this equation require a numerical solution. In order to solve it initial (*IC*) and BC have to be specified. In Hydrus-2D/3D the initial conditions can be specified in terms of water content or pressure head to characterise the initial state of the system. Two types of BC along the boundaries of flow region can be specified. The first one is the system-independent BC, for which the specified values does not depend on the soil system status. They are usually used for simulations of ponded infiltration, to explain the hydrostatic pressure between the soil, and standing or running water boundary and to define the position of the water table, or when the flux along BC is known and does not depend on the soil system (this is not the case in modelling precipitation and irrigation event, where the flux may exceed the infiltration capacity of the soil).

Dirichlet or type-1 BC can be used when the pressure head at the boundary is known. When the water flux across the BC is known, the Neumann or type-2 BC is used. The second type of BC is a system-dependent BC for which the actual BC (as water content, pressure head, water flux or gradient) depends on the system status and is calculated by the model itself. System-dependent BC are: Atmospheric BC, Seepage face, Tile drains, Special time-variable flux/head BC, Snow BC, Gradient-type BC, Subsurface drip

characteristic function, Irrigation scheduling (triggered irrigation) and Surface drip irrigation – dynamic evaluation of the wetted area.

Finite elements and finite differences are the two most common numerical methods used to solve Richards equation (Radcliffe and Šimůnek, 2010). Hydrus-2D/3D uses a numerical finite element approach in space, and finite difference approach in time. The Galerkin linear finite element method is used to obtain a solution of Richards equation and can be used to solve two and three dimensional problems (Šimůnek *et al.,* 2011, 2006). The two-dimensional form of Richards equation can be also solved for three-dimensional problems. In this case the z coordinate (vertical axis) must coincide with the vertical axis of symmetry. These problems are then called axisymmetrical or quasi-three-dimensional problems and are good to simulate water flow from a point source.

3.1.2 Dynamic boundary conditions for drip irrigation simulations

The new special BC for surface drip irrigation with dynamic evaluation of the wetted area, which is now implemented in the recent version 2.0. of Hydrus-2D/3D, was first used by Gärdenas *et al.* (2004) who had access to the source code. With this BC, a Neumann boundary condition (the discharge rate, Q) is applied to the node representing the dripper. As the pressure head needed to maintain this constant flux at the node exceeds 0, the BC is switched from a Neumann (flux) to a 0 pressure head Dirichlet (head) BC and the actual flow rate (Qa) corresponding to this head is computed (Šimůnek *et al*., 2011). The excess flux (irrigation flux) ($Q - Q_a$), again with a specified Neumann BC, is then applied to the neighbouring node., This procedure is repeated iteratively until the entire specified Q is applied over a radius corresponding to the wetted area.

To implement this BC the Time-Variable flux at the surface boundary has to be selected. The boundary length has to be sufficient to accommodate for the entire wetting zone. As shown of Figure 3.1, the node where irrigation starts (position of the dripper) has to be selected.

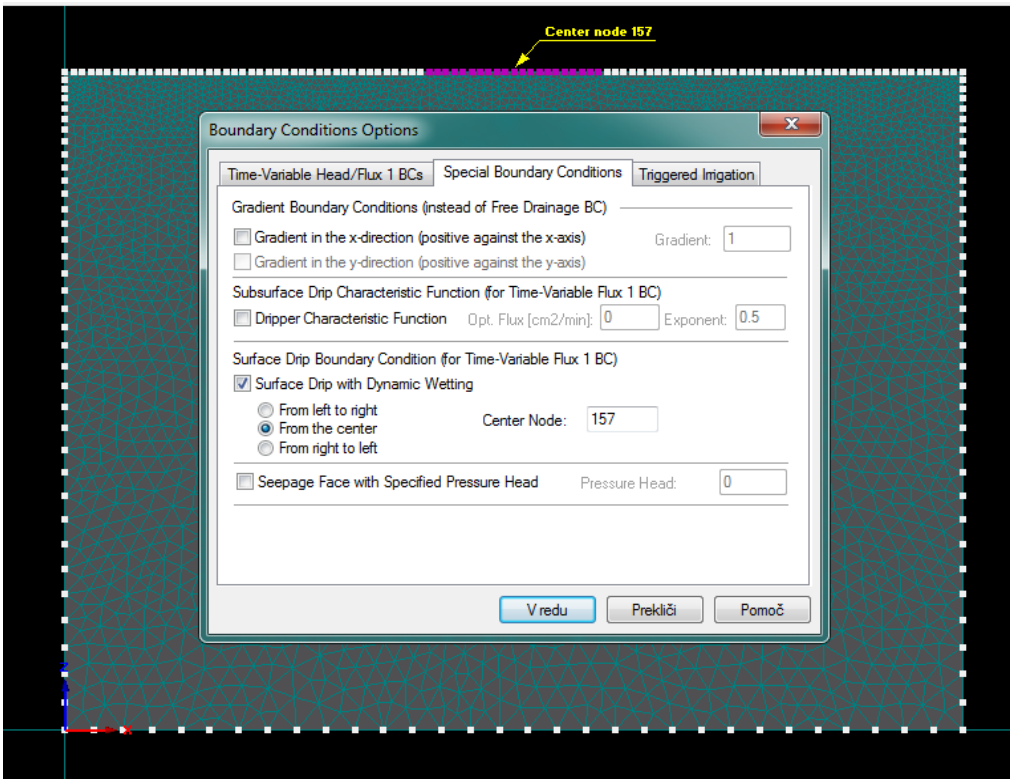

Figure 3.1: The new surface drip boundary condition window

Three options are available; irrigation can start in the right, left or centre node. If the centre node is selected, the wetting pattern will spread on both sides of the node (Figure 3.1).

3.2 Numerical and experimental study of wetting patterns

3.2.1 Numerical simulations for numerical soils

Soil textural classes and hydraulic parameters

Study of water infiltration under drip irrigation was conducted for eleven hypothetical textural classes from United Kingdom (UK) textural triangle. The percentages of sand, silt and clay were determined from the middle of each texture class (Figure 3.2) and are presented in Table 3.1.

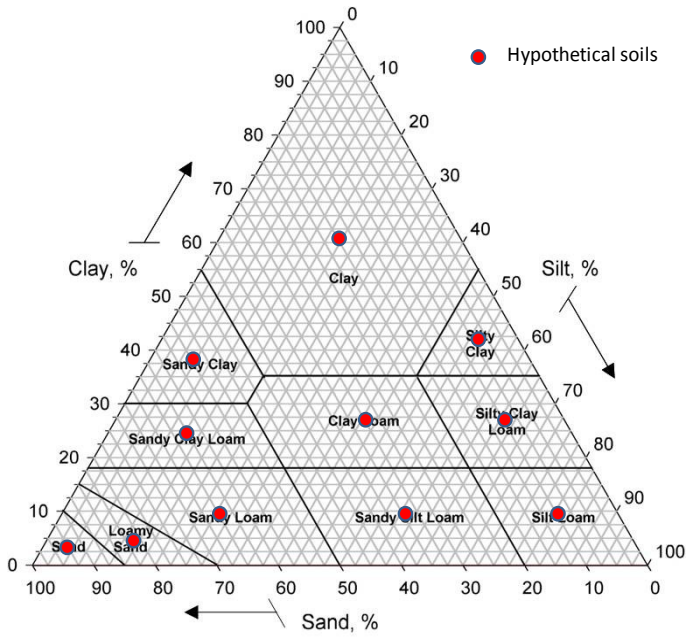

Figure 3.2: Middle values for each texture class (UK textural triangle)

Table 3.1: Percentages of sand, silt and clay determined from UK textural triangle

Determined from UK textural triangle			
Sand (%)	**Clay (%)**	**Silt (%)**	**UK Texture**
32.5	27.5	40.0	Clay Loam
93.0	3.5	3.5	Sand
82.5	5.0	12.5	Loamy Sand
65.0	10.0	25.0	Sandy Loam
35.0	10.0	55.0	Sandy Silt Loam
10.0	10.0	80.0	Silt Loam
10.0	27.5	62.5	Silty Clay Loam
62.5	25.0	12.5	Sandy Clay Loam
55.0	37.5	7.5	Sandy Clay
20.0	60.0	20.0	Clay
6.25	42.5	51.25	Silty Clay

The Hydrus-2D/3D code is coupled with the Rosetta Lite DLL (Dynamically Linked Library) v. 1.1. (Schaap *et al*., 2001). Rosetta implements five hierarchical pedotransfer functions (PTFs) for prediction of van Genuchten (1980) water retention parameters and saturated hydraulic conductivity (*Ks*) from soil textural class only, to soil textural distribution, bulk density (BD) and water content at 33 or 1500 kPa as inputs (Figure 3.3). The program is based on neural network analyses, which is combined with the bootstrap method.

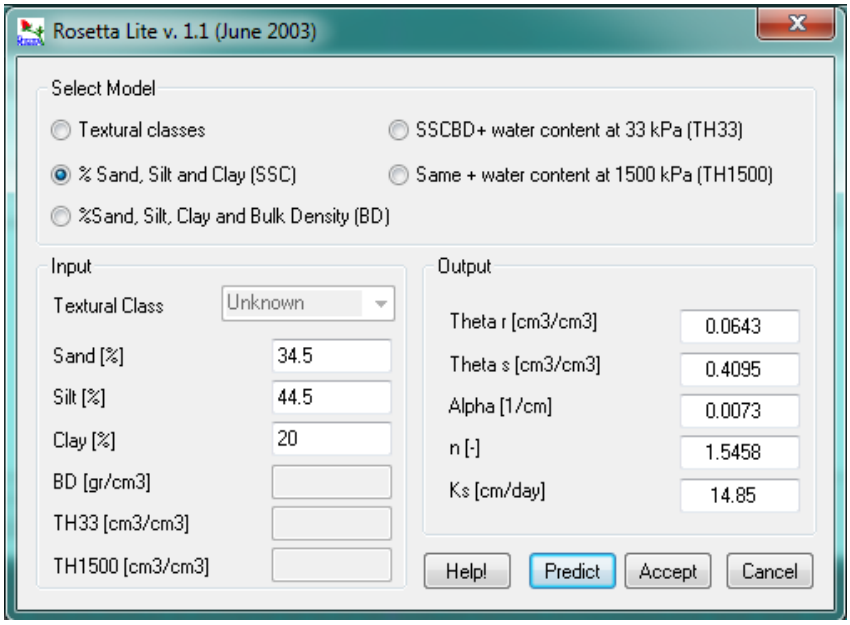

Figure 3.3: The dialog window of Rosetta Lite (Neural Network Predictions).

The use of more input data (predictors) often leads to better predictions, but if only texture is available, Rosetta can still be very useful (Schaap *et al*., 2001). In this case only soil texture data, as presented in Table 3.1, was used as input. The hydraulic parameters obtained for each soil texture class are listed in Table 3.2.

Table 3.2: Parameters for the van Genuchten–Mualem model

UK Texture	α (cm-1)	θs	θr	n	m	Ks (cm/d)	l
Clay Loam	0.01	0.43	0.08	1.48	0.32	10.97	0.50
Sand	0.03	0.38	0.05	3.08	0.68	589.39	0.50
Loamy Sand	0.04	0.38	0.04	1.82	0.45	122.34	0.50
Sandy Loam	0.03	0.39	0.04	1.40	0.29	40.01	0.50
Sandy Silt Loam	0.01	0.41	0.05	1.65	0.39	40.44	0.50
Silt Loam	0.01	0.47	0.06	1.67	0.40	30.78	0.50
Silty Clay Loam	0.01	0.46	0.08	1.57	0.36	11.88	0.50
Sandy Clay Loam	0.03	0.38	0.07	1.31	0.24	14.28	0.50
Sandy Clay	0.03	0.39	0.08	1.23	0.19	14.93	0.50
Clay	0.02	0.49	0.10	1.21	0.17	17.73	0.50
Silty Clay	0.01	0.50	0.10	1.41	0.29	13.48	0.50

Hydrus-2D/3D setup

The time of irrigation was 31 days with 16 irrigation cycles. Each irrigation cycle lasted for 15 hours and was followed by 33 hours of redistribution (Figure 3.4). Assouline (2002) noted that effects of initial soil moisture conditions in the soil vanishes after 10 irrigation cycles. With these considerations in mind the size of the wetting pattern was measured on the last (16^{th}) irrigation cycle to minimize the effect of initial soil moisture content and study the wetting patterns under conditions close to field capacity (more realistic soil moisture conditions were studied in the next set of numerical simulations as presented in the next section).

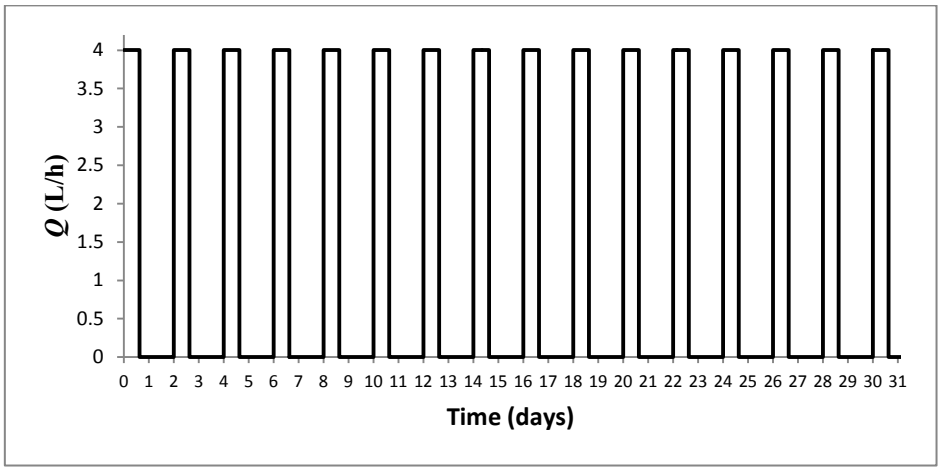

Figure 3.4: Irrigation cycles for period of 31 days for surface emitter discharge rate (Q) of 4 L/h.

In Hydrus-2D/3D only the right side of axisymmetrical domain was simulated, as was shown previously for subsurface drip irrigation (e.g. Guseppe, 2007) and surface drip irrigation (e.g. Gardenas *et al*., 2005; Kandelous and Šimůnek, 2010b). The measured horizontal dimension (X) of the wetting patterns represents only half of the wetted diameter and have to be therefore multiplied by 2 (Figure 3.5). Simulations were done considering a 200 cm deep and 400 cm wide rectangular flow domain, where a single drip emitter resulted in a specific infiltration area on top left side of the domain.

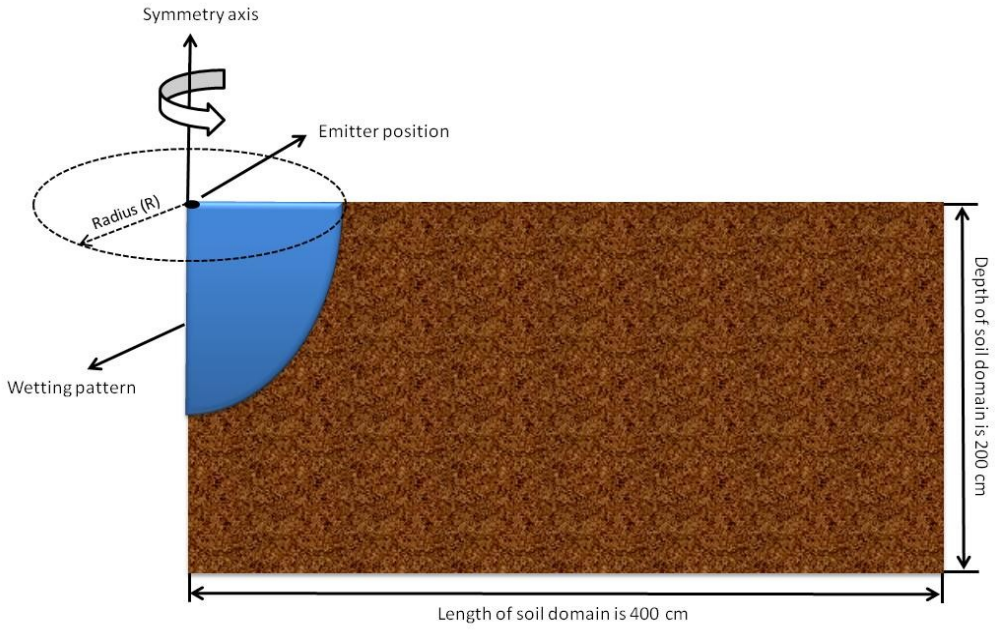

Figure 3.5: Scheme of the flow domain used in numerical simulations

An unstructured mesh was automatically generated to discretise the flow domain into between 1737 and 1892 nodes, depending on the infiltration area. Finite elements were smaller around the emitter, where the hydraulic gradient is higher, and larger with increasing distance from the emitter (Figure 3.6). The transport domain was assumed to have uniform soil hydraulic properties and to be isotropic. It was also assumed to have uniform initial conditions, which were expressed in terms of pressure heads. These were selected to correspond to water contents close to field capacity, varying between -100 and -450 cm, depending on the soil type.

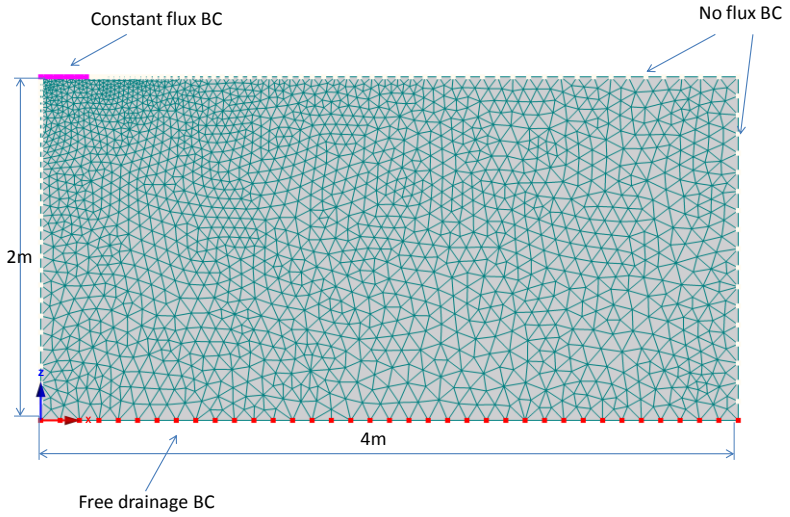

Figure 3.6: Spatial discretization of the 2D axisymmetrical flow domain and its BC.

Absence of flux was considered along the upper boundary except on the left side along the emitter boundary surface where a constant flux boundary condition (BC) representing the dripper discharge rate (4 L/h or 96000 cm^3/day) was used. A free drainage BC was used along the bottom boundary and a zero-flux boundary for all remaining boundaries (Figure 3.6).

As mentioned in section 3.1, the new boundary condition for surface drip irrigation developed in the latest version of Hydrus-2D/3D (v 2.0) was not used for these simulations. Since Hydrus-2D/3D v.1.0. cannot simulate surface flow, which occurs at the onset of drip irrigation, as the discharge rate exceeds the infiltration capacity of the soil, a constant flux boundary was applied to a fixed surface area representing the infiltration area that is achieved at steady state, after water has spread across the soil surface. In other words, this area represents the area that would be obtained with the new BC in v 2.0 after all the fluxes have been redistributed, assuming a maximum pressure head of zero (i.e. no ponding) at the soil surface (see section 3.1.2). The radius of this surface area (Equation 13) is calculated by considering that, at zero pressure head, the flow rate per unit area is equal to the soil saturated hydraulic conductivity (Equation 8, 9, 10, 11):

$$q = \frac{Q}{A} \quad (8)$$

$$A = \pi r^2 \quad (9)$$

$$q = Ks \quad (10)$$

$$r = \sqrt{\frac{Q}{\pi \times Ks}} \quad (11)$$

where Q is the flow rate (cm^3/h), A is surface area (cm^2), K_s is saturated hydraulic conductivity (cm/day), q is the water flux per unit area (cm/day) and r is the radius (cm) of the infiltrating surface.

To investigate the possible discrepancy between the wetting pattern dimensions obtained with the new boundary condition, and those obtained by assuming steady state across the infiltration surface, subsequent simulations were carried out using v 2.0. This is investigated in subsection 3.2.4.

The location of wetted radius (X) and depth (Y) were defined as the point in the wetted front where water content just exceeds the initial water content, as suggetsd by Bresler *et al.* (1971). For this purpose the boundary line chart function in Hydrus-2D/3D was used, resulting in a cross section graph, where water content was presented as a function of length (Figure 3.7). As an example, Figure 3.7 shows that the wetted depth is observed at 29 cm.

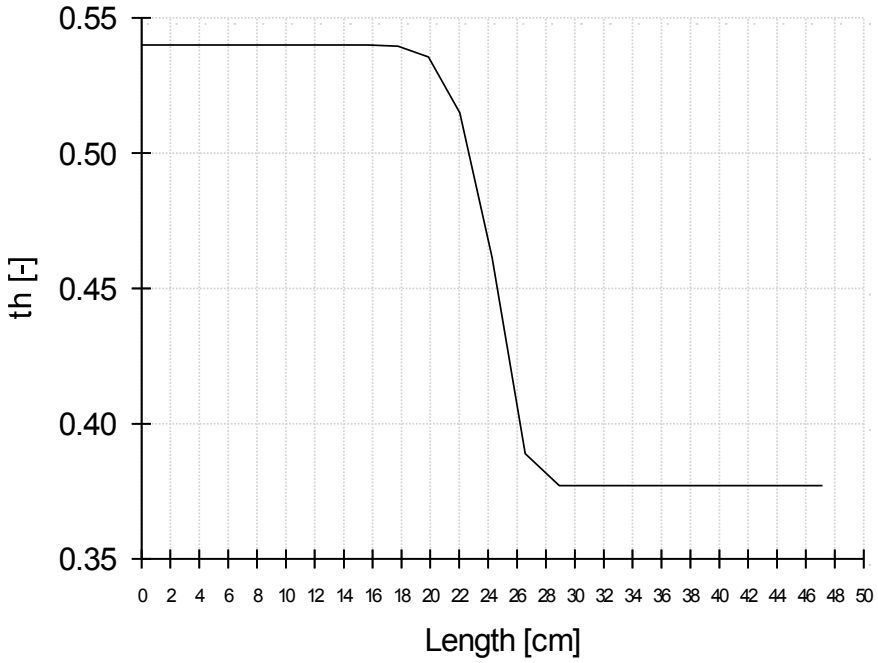

Figure 3.7: Water content (θ) as a function of wetted depth (Y)

This procedure was repeated for every hour during water application (after every 4 L of water applied) and in both directions (X and Y).

3.2.2 Numerical simulations for real soils from SEISMIC database

Soil textural classes and hydraulic parameters

Real soils, from arable land use, covering all texture classes according to the UK soil textural triangle, were selected from the Spatial Environmental Information System for Modelling the Impact of Chemicals (SEISMIC) database. The SEISMIC database was developed by the National Soil Resource Institute (NSRI) at Cranfield University. It provides soil data for 412 soil series of England and Wales. The data is available for each soil layer to a depth of 1.5 m and for different land uses. The database provides data of % total silt, % Total Clay %, Organic Carbon %, pH (1:25 H2O), Bulk density (BD), % volume water at 5 kPa, % volume water at 10 kPa, % volume water at 40 kPa. The texture, particle sizes, BD (g/cm^{-3}), van Genuchten α (cm^{-1}) and n and sub-vertical Ks (cm/day) from the SEISMIC database for each of the textural classes chosen are summarized in Table 3.3. According to Mualem (1976) the l value was taken as 0.5 for all soils.

Table 3.3: Soil classification, texture, bulk density (BD) and van Genuchten (VG) parameters

Soil series	Texture	Layer	Particle size fraction (%)			BD (g/cm^3)	VG		*Ks* (cm/day)
			Clay	Silt	Sand		α (cm^{-1})	*n*	
Blackwood	Sandy Loam	A	11	19	70	1.3	0.08	1.32	242.6
Bridgnorth	Loamy Sand	A	8	8	84	1.48	0.11	1.41	117
Isleham	Sandy Clay Loam	A	20	13	67	1.03	0.08	1.29	333
Bridgnorth	Sand	BW1	7	6	87	1.42	0.12	1.48	289.8
Wittering	Silty Clay	A	38	49	13	0.88	0.03	1.21	141
Carswell	Sandy Clay	Bc	31	16	53	1.37	0.06	1.24	161.2
Fladbury	Clay	A	50	30	20	1.05	0.04	1.2	78.9
Chatteris	Silty Clay Loam	A	30	54	16	0.83	0.03	1.22	185.6
Coprolite washing	Clay Loam	A	25	52	23	1.38	0.04	1.23	47.9
Rowton	Silt Loam	A	16	79	5	1.25	0.03	1.25	80.8
Poundgate	Sandy Silt Loam	A	4	68	28	1.1	0.06	1.35	226.9

For the numerical simulations performed for these soils, the different initial soil moisture conditions are presented as % of depletion of the available water (AW) which corresponds to the amount of water between field capacity (FC) and permanent wilting point (PWP). % depletion represents the % of AW that is no longer available. A field capacity corresponding to moisture content at 10 kPa (-100 cm) matric potential was chosen for all soils. Soil water initial conditions for three most contrasting soil textural classes, with which the simulations were done, are presented in Table 3.4.

Table 3.4: Water content at different depletion rates for 11 soil types

	Depletion (initial conditions)		
Texture	**30%**	**50%**	**70%**
Sandy Loam	0.24	0.21	0.18
Loamy Sand	0.20	0.17	0.15
Sandy Clay Loam	0.30	0.26	0.22
Sand	0.15	0.13	0.11
Silty Clay	0.42	0.37	0.33
Sandy Clay	0.27	0.25	0.23
Clay	0.41	0.38	0.34
Silty Clay Loam	0.41	0.36	0.31
Clay Loam	0.32	0.28	0.25
Silt Loam	0.33	0.29	0.24
Sandy Silt Loam	0.30	0.25	0.21

Hydrus-2D/3D setup

Three distinct sets of numerical simulations were carried out. 20 L of water was applied in all cases (sets). The first set of simulations, aimed at studying the influence of texture alone, was performed for the eleven soils at a given discharge rate (Q) of 2 L/h and a fixed initial soil moisture depletion rate of 50 % (Table 3.5).

Table 3.5: Emitter discharge rate, soil initial condition and soil textures used for first set of simulations.

***Q* (L/h)**	**Initial conditions (% depletion)**	**Soil texture**
2	50	Sandy Loam Loamy Sand Sandy Clay Loam Sand Silty Clay Sandy Clay Clay Silty Clay Loam Clay Loam Silt Loam Sandy Silt Loam

The second set of simulations aimed at illustrating the influence of initial moisture content on wetting patterns and was carried out on three soils with contrasting textures (sand, silt loam and clay) at one given emitter discharge rate of 2 L/h, on the three initial moisture depletion rates of 30, 50 and 70% (Table 3.6).

Table 3.6: Emitter discharge rates, soil initial conditions and soil textures used for second set of simulations.

Q (l/h)	Initial conditions (% depletion)	Soil texture
2	30	Sand Silt loam Clay
2	50	Sand Silt loam Clay
2	70	Sand Silt loam Clay

The third set of simulations aimed at studying the influence of three different emitter discharge rates (1.5, 2 and 4 L/h). The initial soil moisture conditions were kept the same and set to 50 % depletion for all cases. Measurements of wetting pattern dimensions for these three emitter discharge rates were carried out for three contrasting soil texture classes (sand, silt loam and clay) (Table 3.7).

Table 3.7: Emitter discharge rates, soil initial conditions and soil textures used for second set of simulations.

Q (L/h)	Initial conditions (% depletion)	Soil texture
1.5	50	Sand Silt loam Clay
2	50	Sand Silt loam Clay
4	50	Sand Silt loam Clay

Sizes of the wetting patterns in both directions were measured for every litre of applied water. Hence, for simulations with 1.5 L/h, measurements were carried out every 0.03 days (40 min), for 2 L/h every 0.02 days (30 min) and for 4 L/h after every 0.01days (15 min). The total irrigation time was 0.56 days (13.3 h) for the 1.5 L/h emitter discharge rate, 0.42 days (10 h) for the 2 L/h emitter discharge and 0.21 days (5 h) for the 4 L/h emitter discharge.

Figure 3.8 shows the three different emitter discharge rates, used in Hydrus-2D/3D numerical simulations, and the corresponding time of continuous water application necessary for each emitter to apply up to 20 L of water.

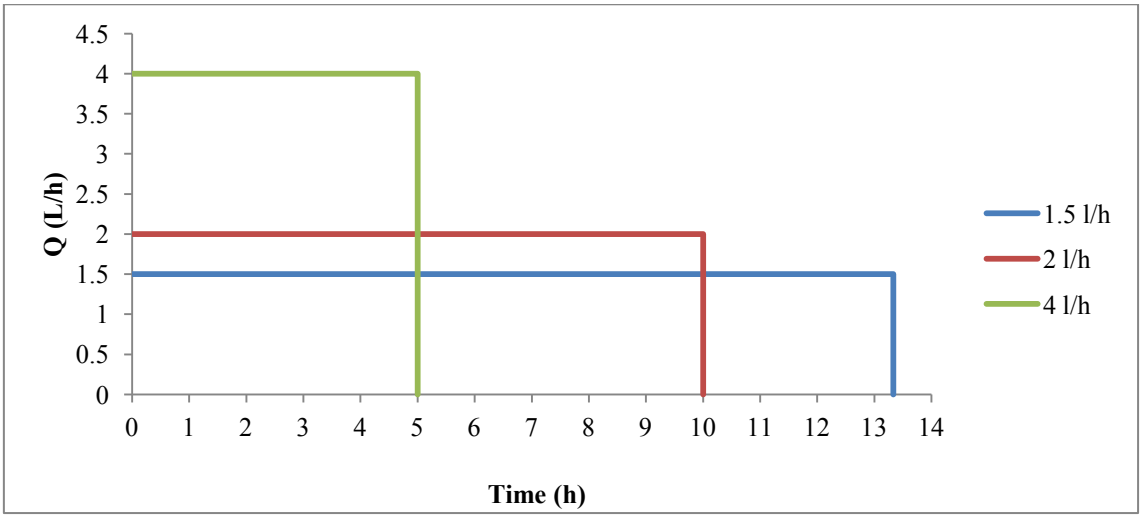

Figure 3.8: Three emitter discharge rates (*Q*) and corresponding time of application needed to apply 20 L of water.

As for the numerical soils, only the right side of the axisymmetrical domain was simulated and the measured horizontal dimension (X) of the wetting patterns represent only half of the wetted diameter and have to be therefore multiplied by 2 (Figure 3.9). Simulations were done using a 150 cm deep and 100 cm wide rectangular flow domain, where a single drip emitter resulted in a specific infiltration area on the top left side of the domain (Figure 3.9). The radius (X) and depth (Y) were measured exactly the same way as presented in previous section (Numerical soils).

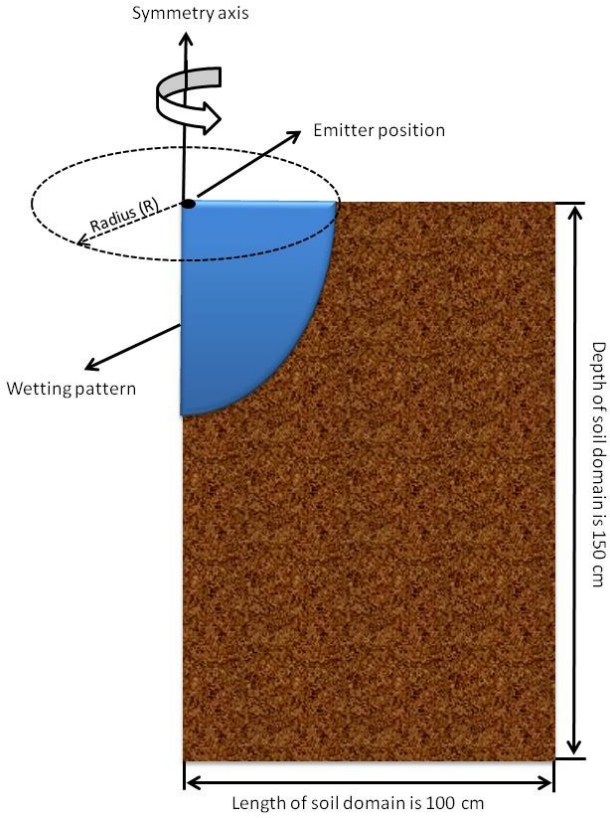

Figure 3.9: Scheme of the flow domain used in real soils simulations

An unstructured mesh was automatically generated to discretise the flow domain into between 1789 and 1917 nodes, depending on the infiltration area of the soil. Finite elements were smaller around the emitter, where the hydraulic gradient is higher, and larger with increasing distance from the emitter (Figure 3.10).

Absence of flux was considered along the upper boundary except on the left side, where a constant flux boundary condition (BC), representing the dripper was used. A free drainage BC was used along the bottom boundary, and a zero-flux boundary for all remaining boundaries (Figure 3.10).

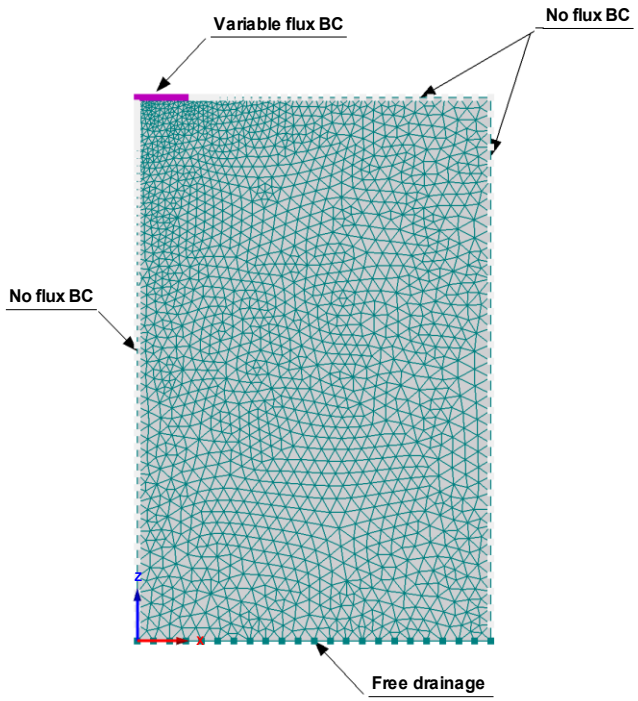

Figure 3.10: Spatial discretization of the 2D axisymmetrical flow domain and its BC.

The radius of the constant flux BC corresponding to discharge rates between 1.5 and 4 L/h was calculated following the same procedure as presented in section 3.2.1 (Equation 11). The flow domain was assumed to have uniform hydraulic properties and to be isotropic. Initial conditions were selected corresponding to Table 3.4. The size of the wetting pattern was measured for every litre of water applied, for all emitter discharge rates. For measurements the same boundary line chart function was used, as described in the previous section.

3.2.3 Soil tank experiments

Experimental setup

The soil tank experiments were conducted in the Soil Laboratory at Cranfield University. Experiments were carried out on a 40.3 cm long, 30 cm high and 2.45 cm deep two-dimensional soil tank. The front wall of the soil tank was transparent and made of tempered glass, back panels were made from stainless steel alloy (Figure 3.11).

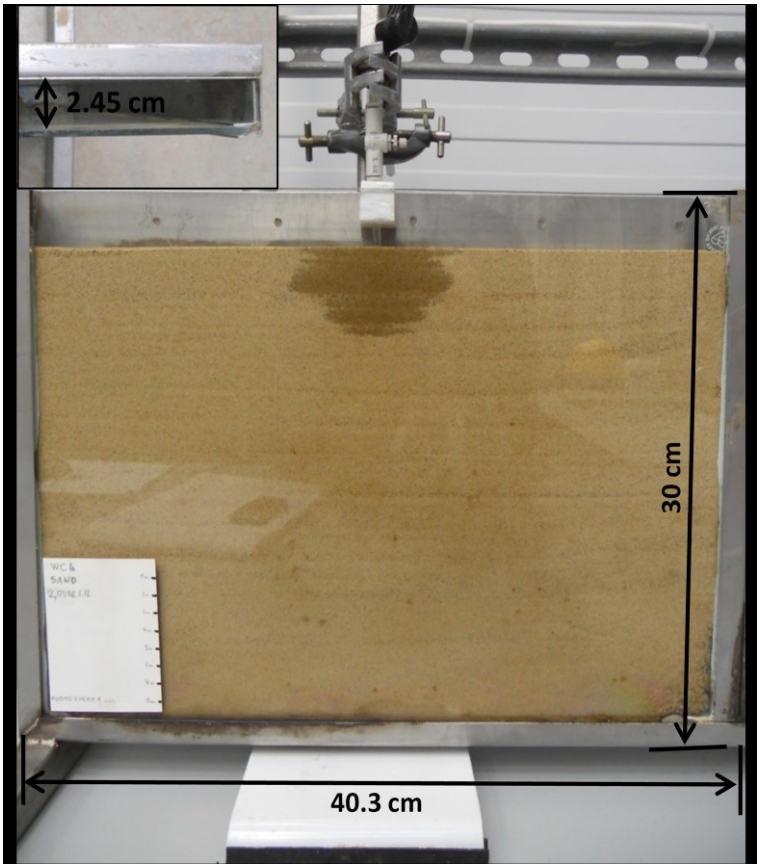

Figure 3.11: Soil tank experiment layout

Experiments were conducted for three different types of soils: sand, sandy loam and silty clay loam. Soil physical properties are presented in Table 3.8. A thin 4 mm diameter polyethylene pipe fitted with a water flow regulator, representing a surface emitter, was installed at the upper boundary of the soil tank, 5 mm above the soil surface. The pipe was connected to a Mariotte bottle filled with water, located above the soil tank, providing a constant water pressure head of h = 92 cm. The soil was first sieved through a 2 mm sieve and packed in the soil tank in 2 cm layers. The soil BD was determined after packing, using a steel tube with known volume.

Table 3.8: Soil texture and bulk density for selected soils

Soil texture	Sand (%)	Silt (%)	Clay (%)	Soil BD (g/cm^3)
Sand	99.52	0.32	0.16	1.58
Sandy loam	67.96	16.26	15.78	1.49
Silty clay loam	18.27	46.77	34.96	1.29

Desired and averaged emitter discharge rates for different soil types are shown in Table 3.9. The total amount of water applied for 0.5, 1, 1.5 and 2 L/h emitter discharge was around 0.4 L. For 0.1 L/h treatments, around 0.2 L was applied. However, all the emitter flow rates could not be used with every soil type because of different infiltration characteristics (determined by *Ks*) of the soils. In the sand soil, with high *Ks* value, all the different emitter flow rates were tested. However, because of surface ponding and water spreading to the sides of the soil tank, the experiments in sandy loam and silty clay loam soils could only be conducted using emitter discharge rates up to 0.5 and 0.1 L/h, respectively.

Table 3.9: Desired and averaged emitter discharge rates

Soil	Q (l/h)	
	Desired	Average
Sand	0,1	0,11
	0,5	0,49
	1	0,99
	1,5	1,51
	2	2,05
Sandy loam	0,1	0,09
	0,5	0,49
Silty clay loam	0,1	0,12

When the experiment started, the shapes of the wetting patterns in both directions were recorded, taking pictures at different predetermined times. The interval between two pictures depended on the emitter discharge rate and soil type. A scale was drawn on the soil tank which enabled determination of the wetting pattern dimensions from the pictures using the computer software programme ImageJ 1.43u (National Institutes of Health, USA).

Soil hydraulic properties

Water retention data for the sand soil were determined using a pressure-plate apparatus. The RETC (Code for Quantifying the Hydraulic Functions of Unsaturated Soils) software (van Genuchten *et al*. 1991) was used to fit the unknown van Genuchten - Mualem equation parameters (α and n) from observed water retention data. Results are

presented in Table 3.10 and Figure 3.12. For sandy loam and silty clay loam the laboratory evaporation method HYPROP® was used to determine water retention data and to fit to van Genuchten-Mualem model.

Table 3.10: Parameters of van Genuchten-Mualem model for selected soils.

Soil texture	θ_s (V/V)	θ_r (V/V)	α (1/cm)	n	K_s(cm/min)	l
Sand	0.459	0.018	0.029	3.437	0.481	0.5
Sandy loam	0.432	0.084	0.0228	2.077	0.057	0.5
Silty clay loam	0.52	0.13	0.0215	1.281	0.007	0.5

Hyprop is a registered trademark of the UMS Company (Germany). Evaporation method is a fast and simple technique to determine the soil water retention curves. The method was proposed by Wind, 1968 (cited in Peters and Durner, 2008). Hyprop uses the simplified evaporation method, developed by Schindler, 1980 (cited in Peters and Durner, 2008), where two pressure heads measurements, are carried out at two different depths (two small tensiometers). The soil in between the two tensiometers represent the volume of soil being characterised. The soil sample in a 250 ml soil sampling ring is saturated, placed on the scale and closed on the bottom. The upper side of the sample is open, so the water from the sample can evaporate to the atmosphere. The mean water content is derived from the mean pressure head and column weight, and is assessed at every time step, to get the water flow rate and volumetric water content. From the total loss of water the initial water content (θ^i) can be determined. Average water content $\theta_a{}^i$ can be derived from the θ^i and weight loss and the average water tension $h_a{}^i$ gives a retention function value $\theta_a{}^i(h_a{}^i)$ at every time step. The measurements lasts until the tensiometers run dry or the change in mass becomes negligible. The procedure is based on the assumption that water content and water tension distribute through the column linearly. Another assumption is that the changes between the water tension and weight of the sample are linear between two tensiometer heights. The data obtained with the method was fitted with the van Genuchten-Mualem model (Table 3.10, Figure 3.12).

For all three soils K_s was determined in the laboratory using a falling head method. All soils used in soil tank experiment were air-dried and initial soil moisture content was close to θ_r.

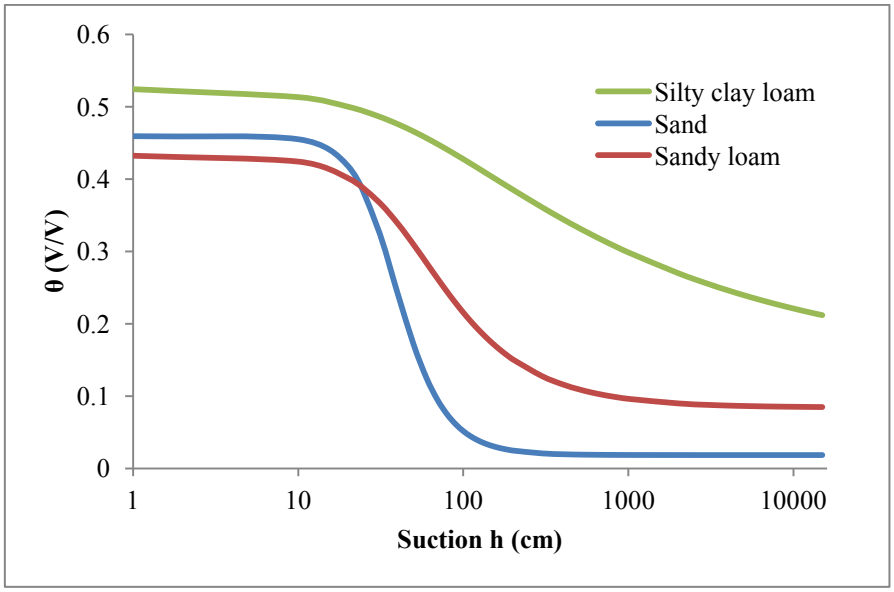

Figure 3.12: Sand hydraulic properties for sand, sandy loam and silty clay loam

The hydraulic parameters obtained were used as inputs for the numerical model Hydrus-2D/3D which was used simulate the experiments as described below.

Hydrus-2D/3D setup

The emitter discharge rates and total volumes of applied water for numerical simulations are presented in Table 3.11 and are equal to those used in soil tank experiments.

Table 3.11: Irrigation duration and volume of applied water for all trials

Soil	Q (L/h)	Irrigation time (min)	Applied volume (L)
Sand	0,11	84	0.15
	0,49	50	0.41
	0,99	28	0.47
	1,51	19	0.48
	2,05	13	0.44
Sandy loam	0,09	130	0.20
	0,49	49	0.40
Silty clay loam	0,12	120	0.23

In Hydrus-2D/3D the planar two-dimensional geometry was selected because of the nature of the soil tank shape. The dripper lateral on the soil surface was assumed to

represent a 2.45 cm section of an infinite line source. Simulations were done considering a 30 cm deep and 40.3 cm wide rectangular transport domain (Figure 3.13), where a single emitter was placed at the centre of domain.

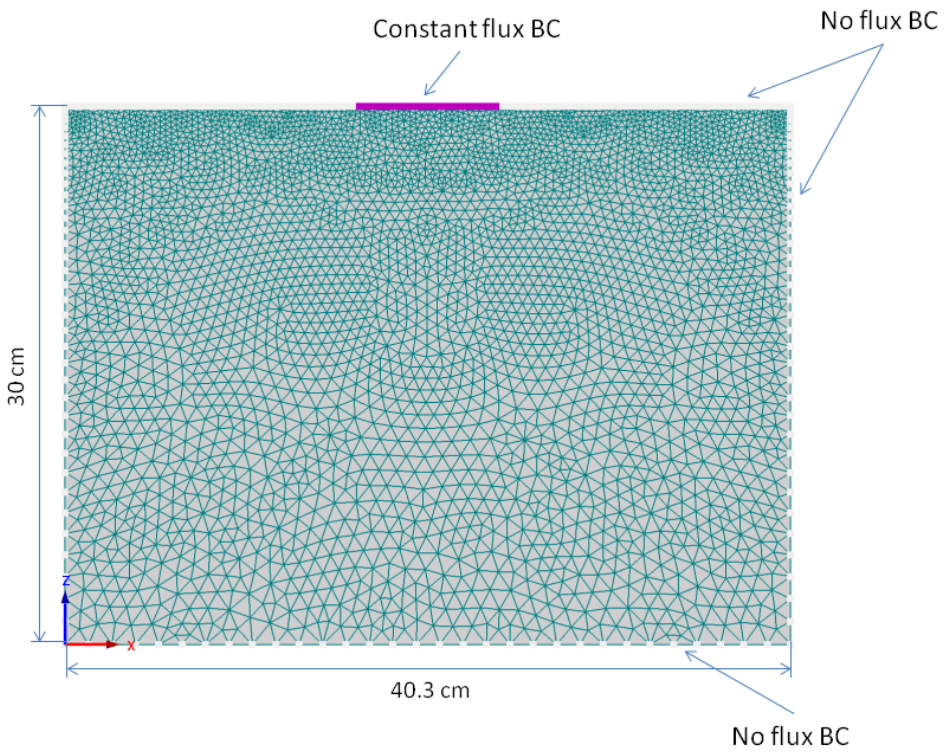

Figure 3.13: Spatial discretization of the 2D flow domain and its BC.

An unstructured mesh was automatically generated to discretise the flow domain into 3733 nodes in all cases. Finite elements were smaller at the upper boundary of the transport domain, where the hydraulic gradient is higher, and larger with increasing depth. Absence of flux was considered for all boundaries, except at the centre of the domain where a time-constant flux boundary condition (BC), representing the dripper, was used (Figure 3.13). A new special BC for surface drip with dynamic wetting, incorporated into recent second version of Hydrus-2D/3D, was used. This BC was previously used by Gardenas *et al.* (2004).

The constant water flux per unit area (q) is equal to the emitter discharge rate (Q) at the modelled drip surface length (2.45 cm wide) (Equation 12), which varied from 0.1 to 2 L/h, and was calculated as below:

$$q = \frac{QL/h * 1000}{60 * 2.45\ cm}\ in\ cm^3/min \qquad 12$$

The flow domain was assumed to be uniform and isotropic. Initial conditions were selected close to the θ_r and were 0.02, 0.09 and 0.14 for sand, sandy loam and silty clay loam, respectively.

3.2.4 Old and new Boundary condition

All simulations, except soil tank tests, have been done with version 1.0. of the Hydrus-2D/3D, assuming that the flow rate per unit area was equal to the saturated hydraulic conductivity of the soil (Ks) (constant flux boundary was applied to a fixed surface area). The simulations comparing the soil tank experiments were carried out with new surface drip irrigation BC which was included in Hydrus-2D/3D Version 2.0. To test, if new BC causes different dimensions of wetting patterns, some randomly selected simulations, where old BC was used, were rerun using new BC. The results are presented in Figures 3.14 to 3.20.

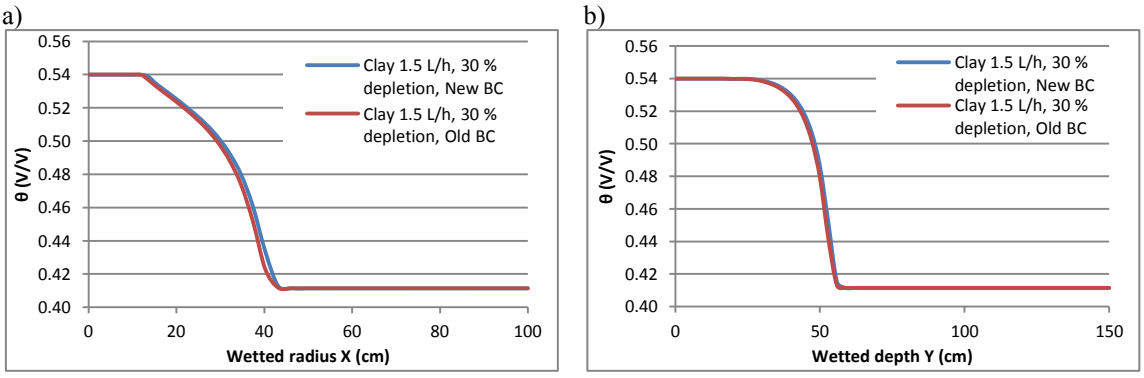

Figure 3.14: Comparison of simulated wetted radius (a) and wetted depth (b) using old and new BC for 1.5 L/h emitter discharge rate and 30 % depletion for clay soil at the end of irrigation (20 L of water applied).

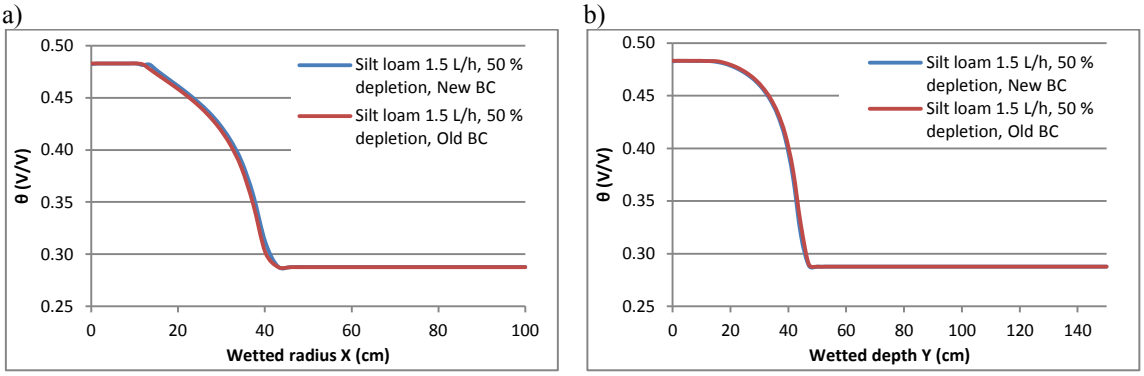

Figure 3.15: Comparison of simulated wetted radius (a) and wetted depth (b) using old and new BC for 1.5 L/h emitter discharge rate and 50 % depletion for silt loam soil at the end of irrigation (20 L of water applied).

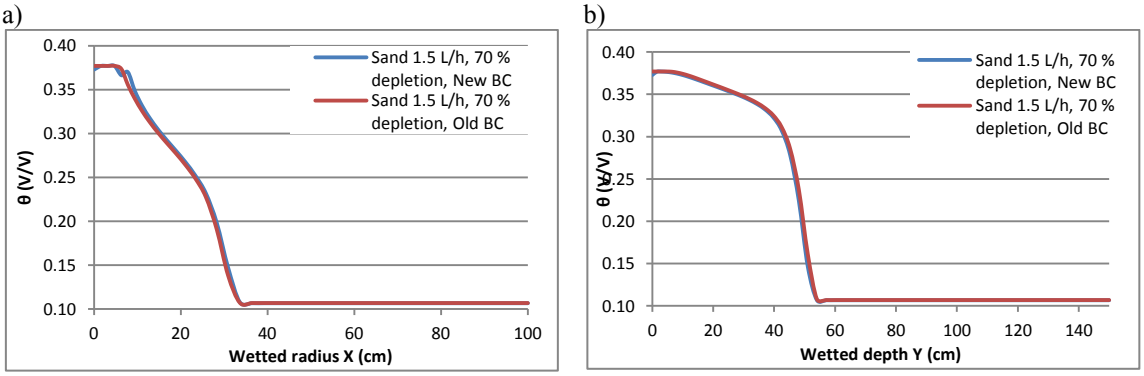

Figure 3.16: Comparison of simulated wetted radius (a) and wetted depth (b) using old and new BC for 1.5 L/h emitter discharge rate and 70 % depletion for sand soil at the end of irrigation (20 L of water applied).

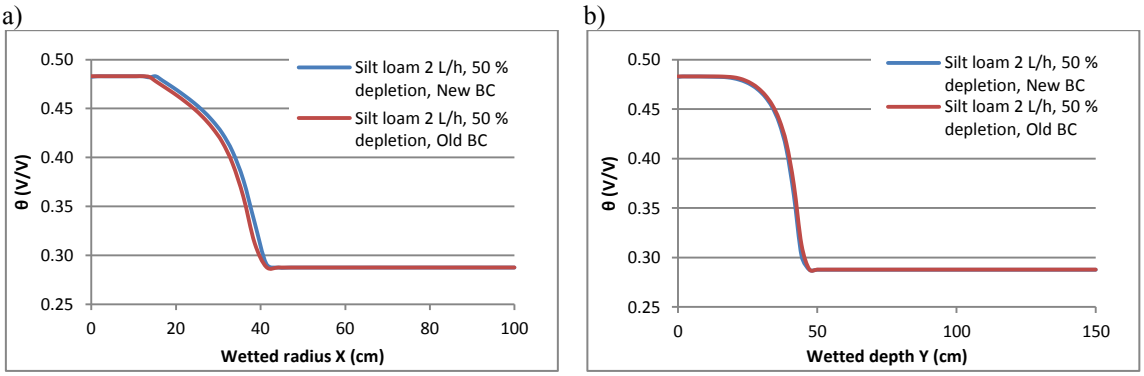

Figure 3.17: Comparison of simulated wetted radius (a) and wetted depth (b) using old and new BC for 2 L/h emitter discharge rate and 50 % depletion for silt loam soil at the end of irrigation (20 L of water applied).

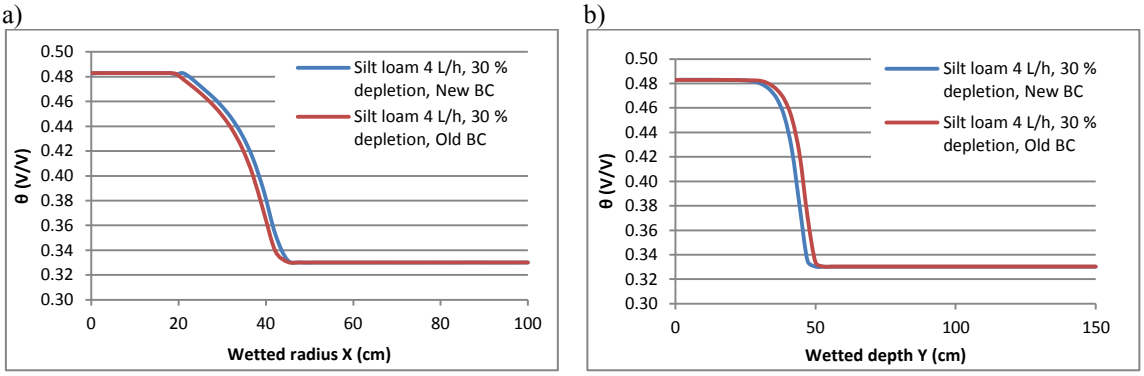

Figure 3.18: Comparison of simulated wetted radius (a) and wetted depth (b) using old and new BC for 4 L/h emitter discharge rate and 30 % depletion for silt loam soil at the end of irrigation (20 L of water applied).

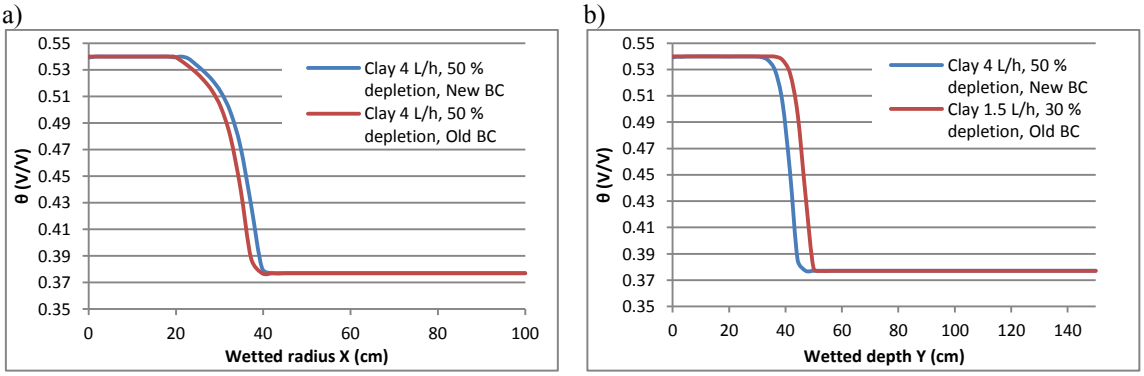

Figure 3.19: Comparison of simulated wetted radius (a) and wetted depth (b) using old and new BC for 4 L/h emitter discharge rate and 50 % depletion for clay soil at the end of irrigation (20 L of water applied).

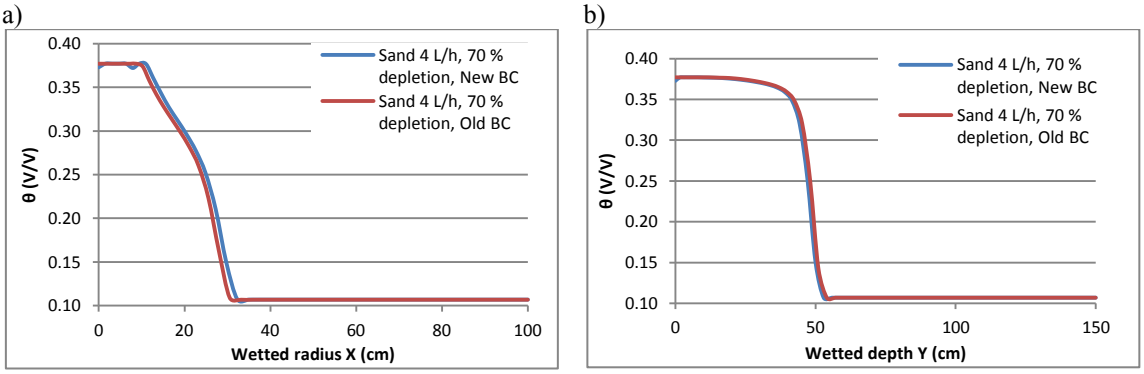

Figure 3.20: Comparison of simulated wetted radius (a) and wetted depth (b) using old and new BC for 4 L/h emitter discharge rate and 70 % depletion for sand soil at the end of irrigation (20 L of water applied).

For 1.5 and 2 L/h emitter discharge rates and different initial soil moisture conditions (depletions) for sand, silt loam and clay soils, no difference between old (constant flux

applied to fixed surface) and new BC (dynamic evaluation of wetted area) in observed wetted geometry at the end of irrigation was observed. For 4 L/h treatment some differences occurred in all soils but were in general small. For silt loam soil at 30 % depletion the radius of wetting pattern was 45 cm for old and 46 cm for new BC. Observed wetted depth for old and new BC was 52 and 50 cm, respectively. In clay soil at 50 % depletion the radius of wetting pattern was 39.5 cm for old and 40 cm for new BC, the wetted depth was 51.5 cm for old and 44.5 cm for new BC. In sand soil at 70 % depletion the radius of wetting pattern was 32.5 cm for old and 31 cm for new BC, no difference between old and new BC in wetted depth was observed and resulted in 54 cm in both cases. In general the differences between the position of the wetted front between old and new BC was remarkably small. This is likely to be due to the fact that spreading of water over the surface until the discharge rate can be accommodated for, as modelled by the new BC, is fast and that infiltration after this proceeds as we have assumed, at a steady rate equivalent to *Ks*.

3.2.5 Statistical analysis

A multiple linear regression analysis was done to identify whether soil texture, emitter discharge rates (*Q*), volume of applied water (V) and soil hydraulic properties *(α, n, Ks*) and free pore space *(θ_f)* can explain the variation in soil wetting pattern radius and depth. The software package STATISTICA Version 10 (StatSoft, Inc., USA) was used for this purpose.

4 Results and discussion

4.1 Simulations of wetting patterns for all soil textural classes

4.1.1 Effect of soil texture and volume of applied water on horizontal and vertical wetting pattern dimensions

Numerical soils with hydraulic properties predicted using Rosetta Lite v. 1.1

As mentioned in Chapter 3, the texture of the numerical soils was determined from the middle of each texture class from UK textural triangle and their hydraulic properties determine using Rosetta Lite v. 1.1. The time of irrigation was 31 days with 16 irrigation cycles. Each irrigation cycle lasted for 15 hours and was followed by 33 hours of redistribution.

Hydrus-2D/3D simulations were carried out and the measurements of wetting patterns in horizontal (X) and vertical (Y) direction were observed after every hour of irrigation (after every 4 L of applied water) for the 16th irrigation cycle.

Figures 4.1 to 4.3 show the 2D moisture content distribution obtained with the Hydrus-2D/3D simulations for three of the eleven soils for the last (16th) irrigation cycle after 10 h of irrigation (40 L of water applied).

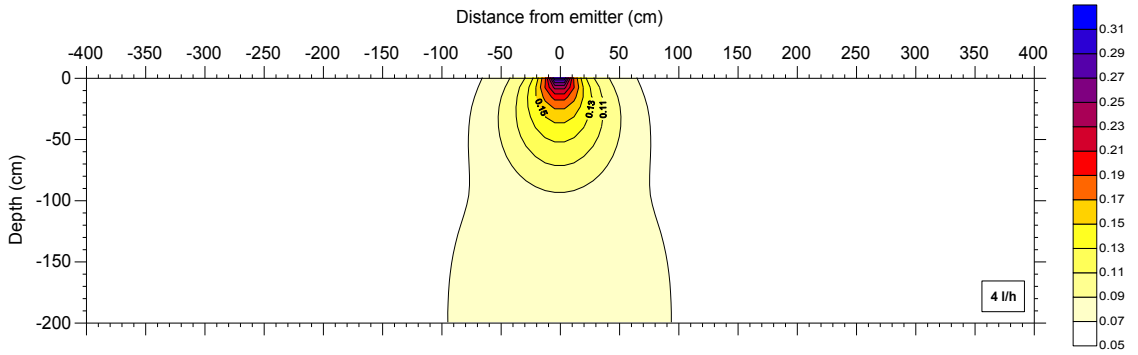

Figure 4.1: Simulated geometry of wetting pattern for sand soil after 15 irrigation cycles and 10 h of irrigation (40 L of water applied).

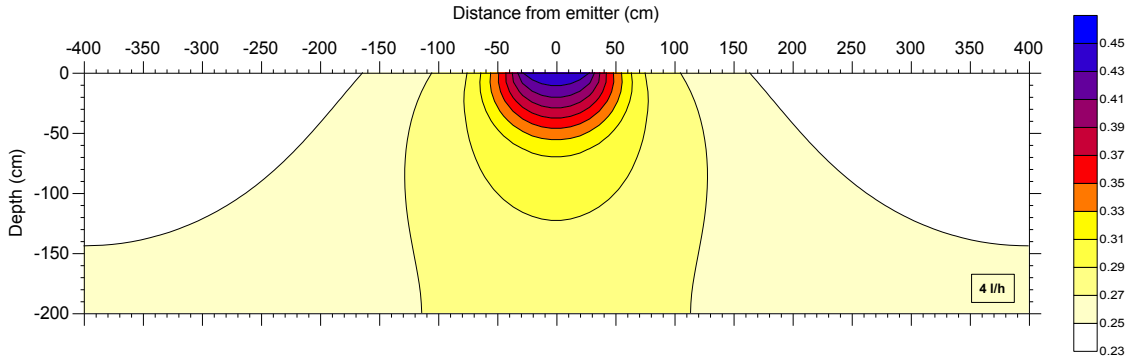

Figure 4.2: Simulated geometry of wetting pattern for silt loam soil after 15 irrigation cycles and 10 h of irrigation (40 L of water applied).

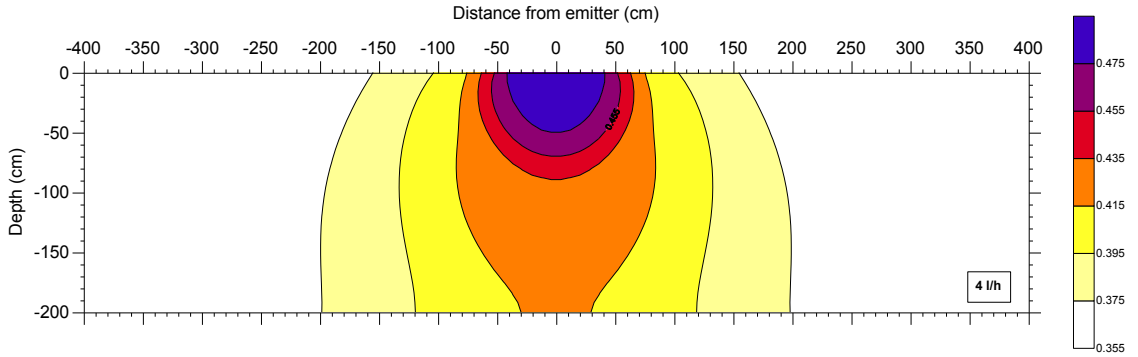

Figure 4.3: Simulated geometry of wetting pattern for clay soil after 15 irrigation cycles and 10 h of irrigation (40 L of water applied).

The results in Figures 4.1 to 4.3 show that, at the high value of cumulative infiltration (irrigation), the soil type importantly affects the size of the wetting pattern. The wetting pattern in the coarser textured soils (sand) is elongated in a vertical direction (the wetting pattern is elliptical), and the wetted depth is larger than the wetted diameter. The contours show that there is not much water stored in the soil profile. In both fine-textured soils, as silt loam and clay soil, the wetting pattern is elongated in a horizontal direction and the wetted diameter is larger than the wetted depth, and has a more circular shape. The contours show higher water storage capability of fine textured soils, which is even more profound in clay soil. Further analysis and causes for this behaviour are explained in the following section.

The influence of soil type on the wetting patterns is shown in figures 4.4 and 4.5 which are a plot of the dimension of the wetted soil in the horizontal (X) and vertical (Y) directions, as a function of volume of water applied, for all soil texture classes. As it was expected, both X and Y dimensions increase with increasing volume of water applied. Wetted radius (X) at a given volume of applied water tends to be larger for fine-textured soils (clay loam, clay, silty clay) and smaller for course-textured soils (sand, sandy loam, loamy sand). The wetted depth (Y) tends to be larger for coarse-textured soils (sandy clay, sandy clay loam and sand). The smallest wetted depth occurred in fine-textured soils (silty clay loam, clay loam and silty clay).

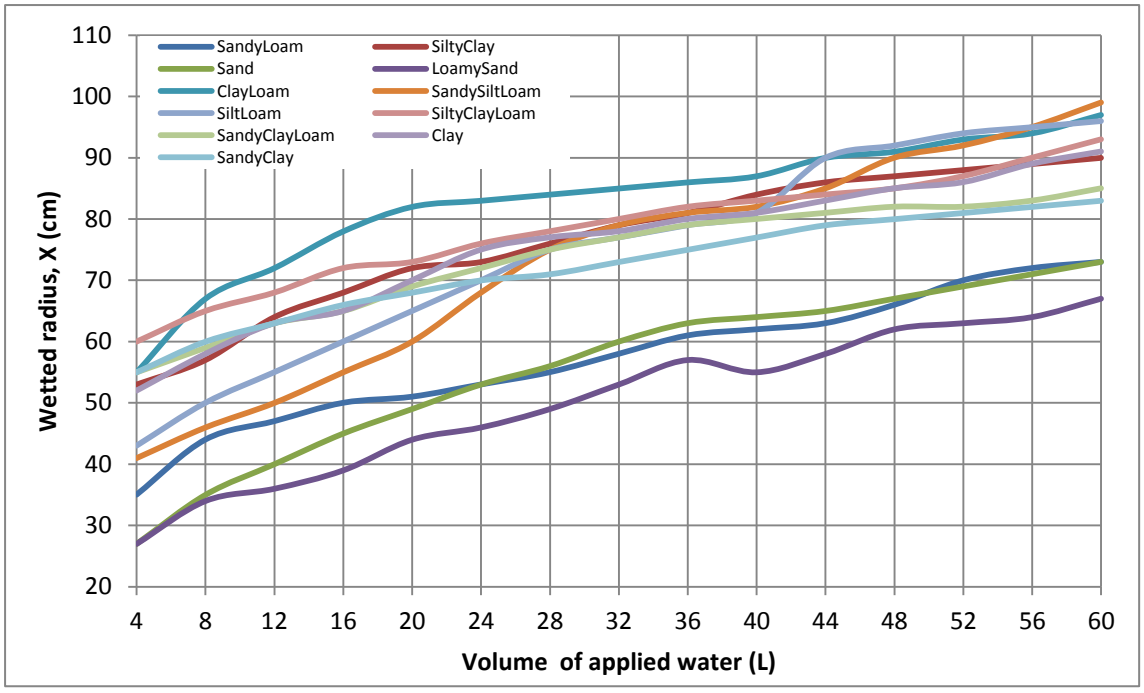

Figure 4.4: Dimensions of the wetted soil radius (X) as a function of volume of applied water.

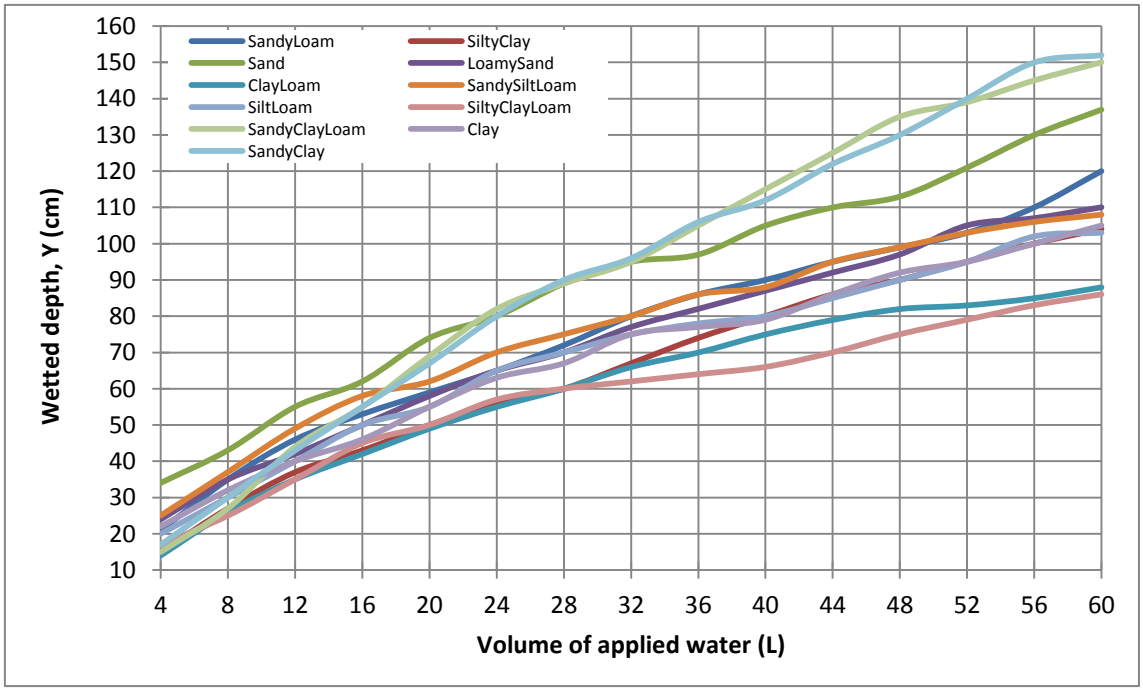

Figure 4.5: Main dimensions of the wetted soil volume in vertical direction (Y) as a function of volume of applied water.

For example, in order to irrigate the root depth (Y) equal to 40 cm, in sand soil and with emitter discharge rate of 4 L/h, it is necessary to apply 7 L of water and to irrigate for 105 min. The wetted radius is equal to 34 cm, so the emitter spacing should be at least 68 cm to maintain a continuous wet strip of soil for irrigation of row crops. To irrigate to the root depth of 40 cm in the clay soil it is necessary to apply 12 L of water and to irrigate for 180 min. The wetted radius at that volume of water applied will be 63 cm, so the emitter spacing should be at least 126 cm to maintain a continuous wet strip of soil.

The maximum X and Y obtained for each soil at the end of last cycle of irrigation are compared in Figure 4.6. It can be seen that the maximum water spread in horizontal (X) direction occurred for the sandy silt loam (99 cm), silt loam and sand but in horizontal (Y) direction for sandy clay (152 cm) soil. Minimum water spread in horizontal (X) direction can be observed for loamy sand (56 cm) soil and in vertical (Y) for silty clay loam (86 cm) soil. The results show that the wetting patterns for coarse-textured soils tend to extend in vertical (Y) direction more than in horizontal (X) direction. This is due to high infiltration capacity of coarse-textured soils, where water drains easily through the soil profile because gravity dominates. The opposite is observed for fine-textured

soils, where, because of high capillarity forces, the wetting patterns tends to move more in the horizontal (X) direction. The bigger storage capacity in fine-textured soils and consecutive shape of the wetted radius can be explained by porosity, which is an index of the relative pore space in the soils. Coarse-textured soils tend to be less porous than fine-textured soils, which explains their lower storage capacity.

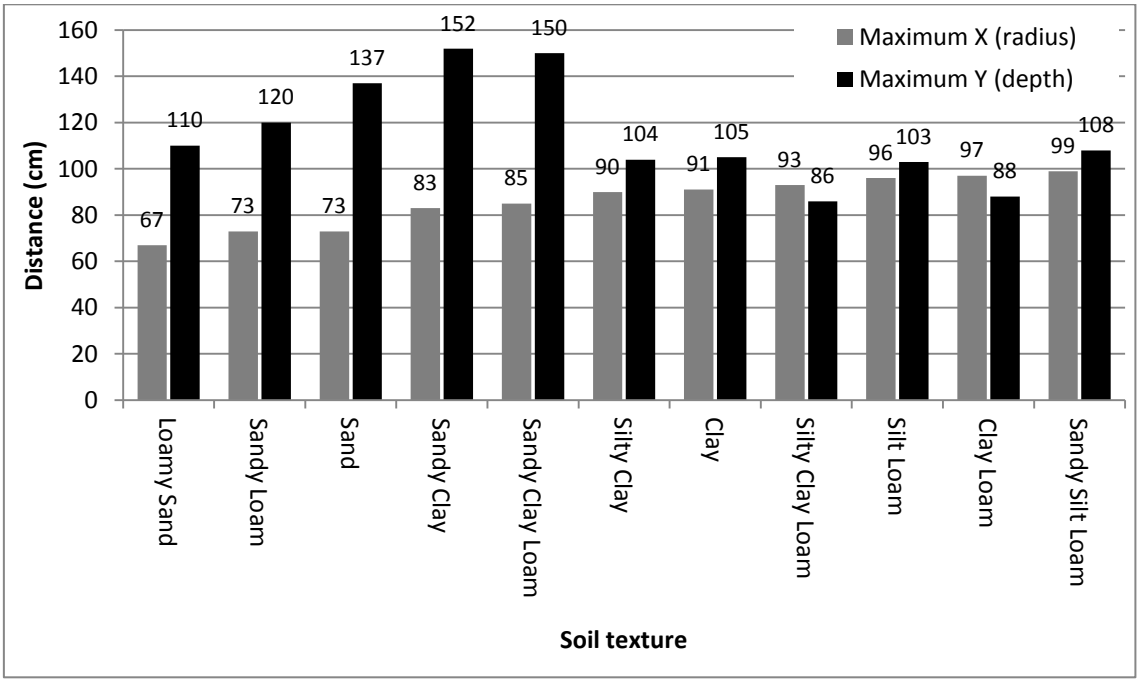

Figure 4.6: Maximum horizontal and vertical wetting pattern dimension at the end of the irrigation cycle (15 h).

To illustrate how soil texture affects the geometry of wetting pattern the Figure 4.7 shows the ratio of wetted depth (Y) to wetted radius (X) at the end of irrigation cycle (60 L of water applied). The Y/X ratio of 1 means that wetted depth (Y) and wetted radius (X) have about the same distance – the wetting pattern shape is round. Ratio higher than 1 shows that the wetted depth is larger than the wetted diameter and values lower than 1 show that the wetted diameter is larger than the wetted depth. Coarse-textured soils (sand, sandy clay, sandy clay loam, loamy sand) have Y/X ratio above 1.64, showing that the wetting pattern depth is larger than the wetted diameter. The ratio for fine-textured soils, as clay loam, silty clay loam, silt loam, sandy silt loam, clay and silty clay, is just above or under 1, showing that the wetting pattern depth and diameter have about the same length. The Y/X ratio gives information about the relative

contribution of gravity and capillarity forces. Gravity dominates in soils with large Y/X ratio whereas it is negligible compared to the capillarity forces in soils with a ratio close to 1.

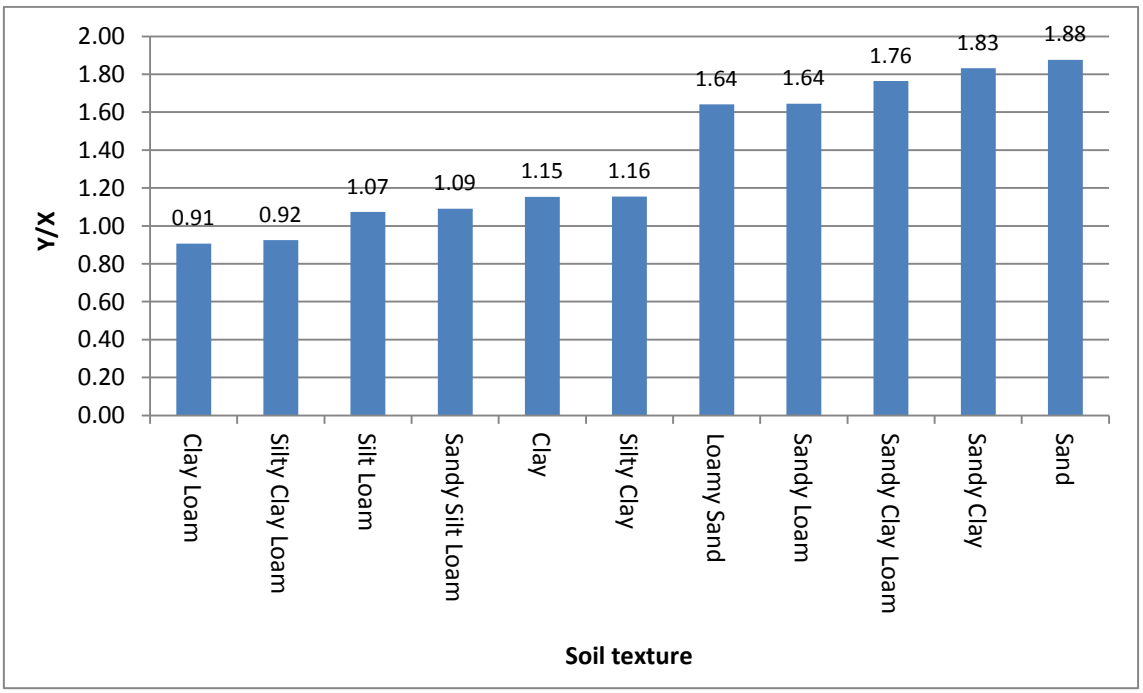

Figure 4.7: The ratio of wetted depth (Y) to wetted radius (X) at the end of the irrigation cycle (60 L of water applied).

PTF models, like Rosetta Lite v. 1.1 estimate water retention and *Ks* reasonably well when more predictors, such as soil texture, bulk density and water retention points, are used (Schaap *et al*., 2001). In the case of these numerical soils, only soil texture was used as a predictor. It is therefore possible that the estimations of the hydraulic parameters of these soils are not always accurate. Since the dimensions of the wetting patterns simulated with Hydrus-2D-3D are likely to be highly dependent on these hydraulic parameters, the above simulation results were not used for further statistical analysis of the influence of soil texture and volume of applied water, on wetting pattern dimensions. A second set of numerical simulations was run, where real soils, corresponding to all soil textural classes from UK textural triangle, were used. These were selected from the SEISMIC database, developed by NSRI at Cranfield University. The database provided all the soil parameters needed for this study (soil texture, bulk density, saturated hydraulic conductivity, and water retention parameters).

Real soils from SEISMIC database

In this section the surface wetted radius and wetted depth are presented as a function of volume of applied water (L), respectively. Volume of applied water is a product of the application rate (L/h) and time (h). Figures show the relation between wetting radius (X) and wetted depth (Y) with volume of applied water for all real soil texture classes from SEISMIC database for 2 L/h discharge rate at 50 % depletion.

The influence of soil type on the wetting patterns is shown in Figures 4.8 and 4.9 which are a plot of the dimension of the wetted soil in the horizontal (X) and vertical (Y) directions as a function of volume of water applied, for all soil texture classes. As expected, the size of the wetting pattern in both directions increases with the volume of applied water. Wetted radius (X) at a given volume of applied water tends to be larger for fine-textured soils (silt loam, silty clay, clay loam, sandy silt loam and clay) and smaller for course-textured soils (sand, loamy sand, sandy clay loam and sandy loam). The wetted depth (Y) tends to be larger for coarse-textured soils, as sand, loamy sand and sandy clay. The smallest wetted depth occurred in fine-textured soils (silty clay loam, silty clay and silt loam).

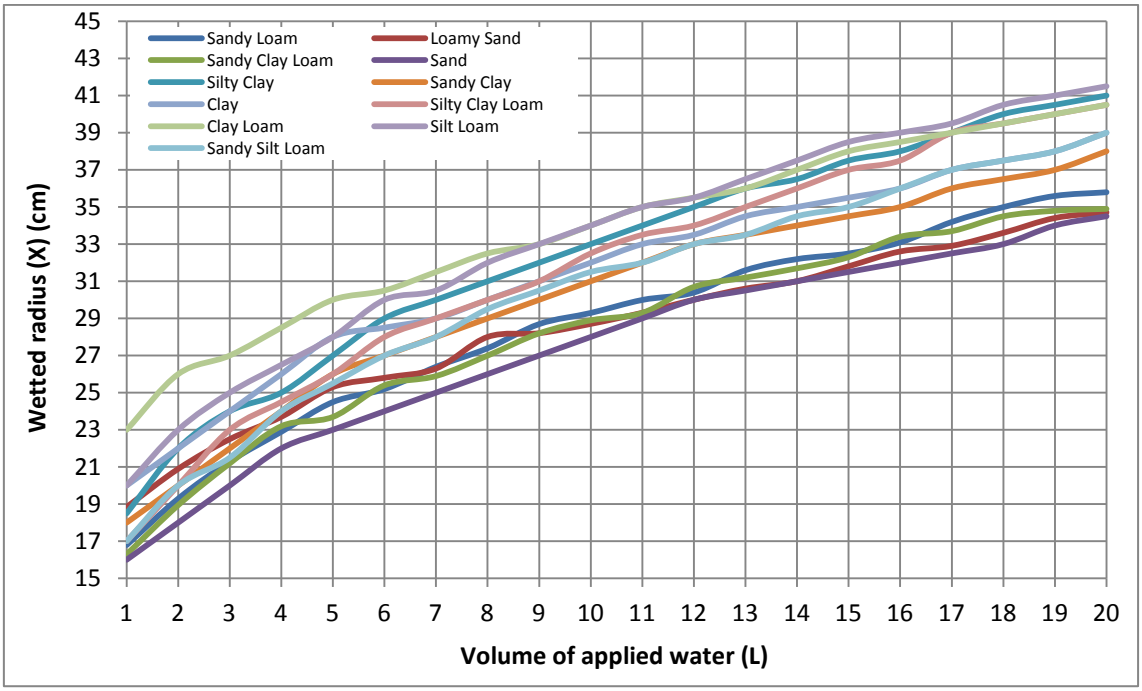

Figure 4.8: Dimensions of the wetted soil radius (X) as a function of volume of applied water for 11 soil texture classes, emitter discharge rate of 2L/h and at 50 % depletion.

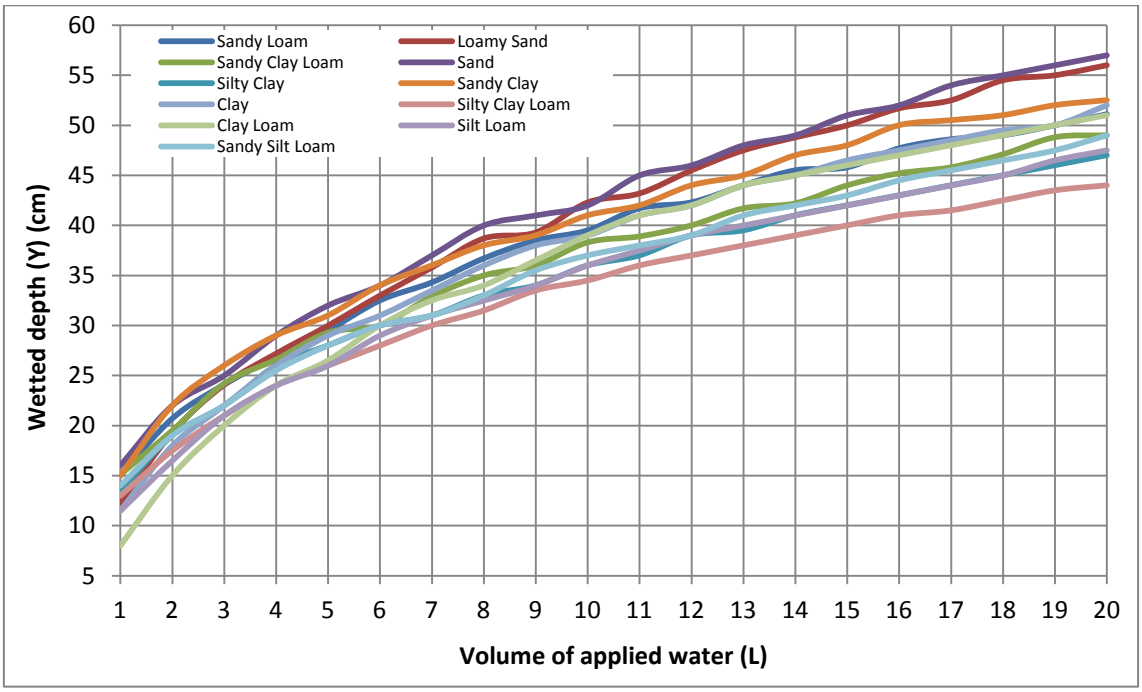

Figure 4.9: Dimensions of the wetted soil volume in vertical (Y) direction as a function of volume of applied water for 11 soil texture classes, emitter discharge rate of 2 L/h and at 50 % depletion.

Figures 4.8 and 4.9 also show that the wetting front in both directions (X and Y) moved faster at the beginning of the application, due to large capillarity pressure gradients (pressure difference per distance) between the water source and wetting front, and slowed down with increase in volume of applied water, as the wetting pattern moved away from the source. The increase was not linear. Later the pressure gradients get smaller and gravity starts to dominate. The figures also show that with the increase in volume of applied water, the wetted depth increased more than wetted radius, which is due to the gravity effect.

The wetted radius (X) and wetted depth (Y) for the two most contrasting soil textures, at the end of the application cycle, are compared in Figures 4.10 and 4.11. Horizontal and vertical water content profiles, at the soil surface and along the axis of symmetry, respectively, are plotted from the 2D moisture content distribution results obtained with the numerical simulations. The wetting front location can be defined as the location where the moisture content is greater than the initial moisture content (Bresler *et al.* 1971). The wetting front location in radial (X) direction is observed at 34.5 cm for sand and at 39 cm for clay. The wetting front location depth (Y) occurred at 57 cm for sand and at 52 cm for clay. Maximum water gradient in depth (Y) occurred at 57 cm for sand and at 52 cm for clay. The results show that the depth (Y) of the wetting pattern in the slowly permeable clay is smaller than in the highly permeable sand. On the other hand, the wetted radius of clay is bigger than that of the sand.

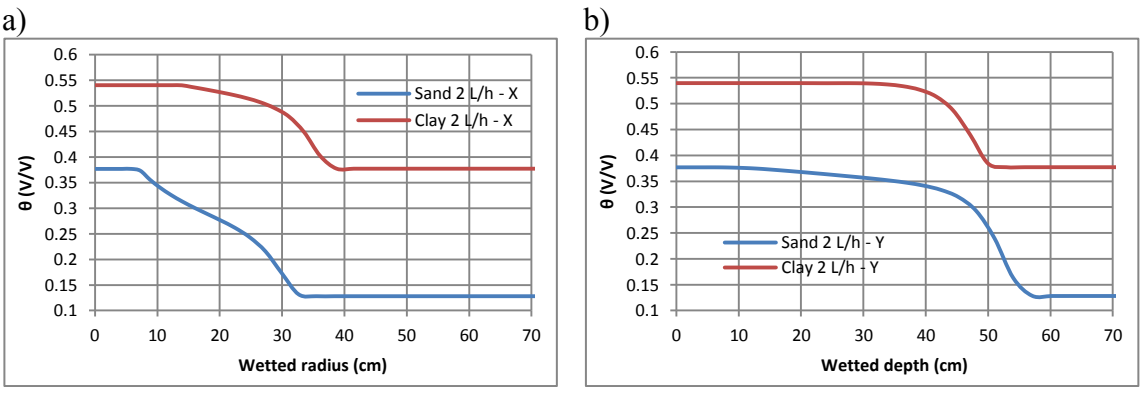

Figure 4.10: Wetted radius (a) and depth (b) for sand and clay soil at the end of the irrigation cycle (20 L of water applied).

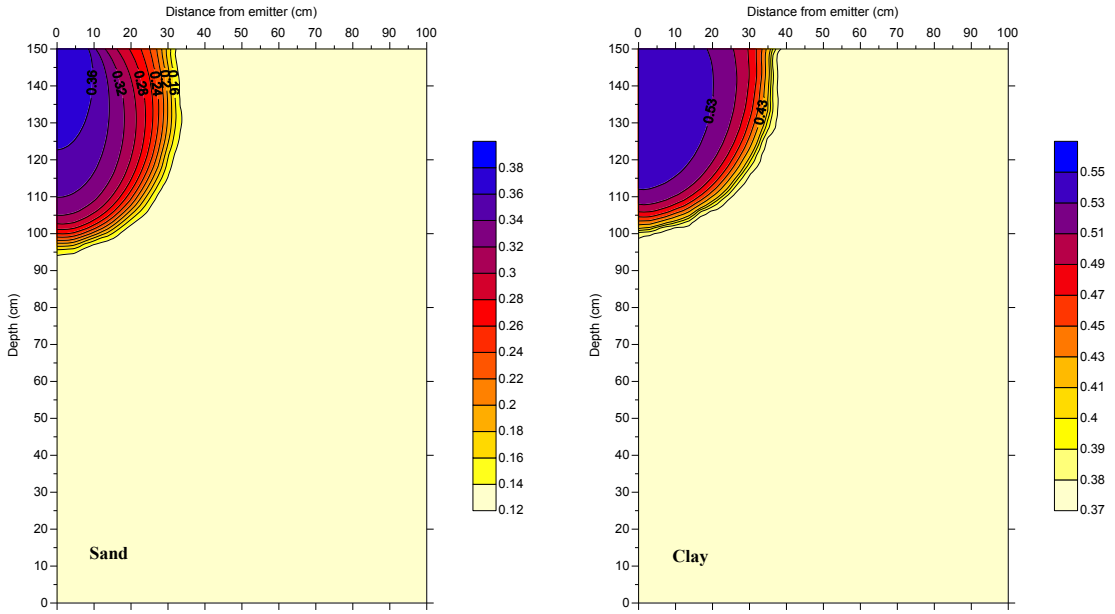

Figure 4.11: Water content distribution for sand and clay soil as simulated with Hydrus-2D/3D, at the end of irrigation cycle.

Comparisons of the maximum X and Y obtained for each soil at the end of last cycle of irrigation is shown in Figure 4.12.

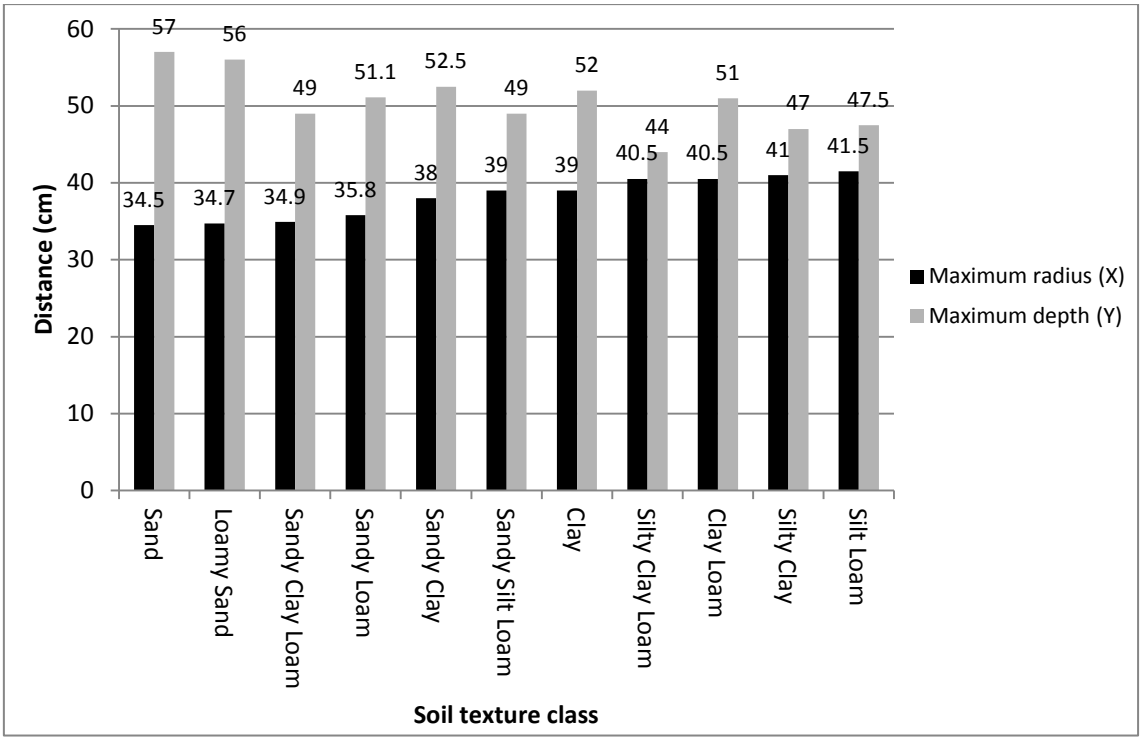

Figure 4.12: Maximum radius (X) and depth (Y) of wetting pattern at the end of irrigation cycle for all soil texture classes.

It can be seen that the maximum water spread in horizontal (X) direction occurred in silt loam soil (41.5 cm) and in horizontal (Y) direction for sandy clay (152 cm) soil. Minimum water spread in horizontal (X) direction can be observed for loamy sand (56 cm) soil and in vertical (Y) for sand soil (57 cm). The results show the same trend as that of the numerical soils as discussed in the previous section. The wetting patterns for coarse-textured soils tend to extend in vertical (Y) direction more than in horizontal (X) one. This is due to high infiltration capacity (or *Ks*) of coarse-textured soils, where water infiltrates easily through the soil profile and the domination of gravity forces. On the other hand, in fine-textured soils, where, the wetting patterns tends to move more in horizontal (X) than in vertical (Y) direction because of high capillarity forces, especially at the beginning of water application.

To illustrate how soil texture affects the geometry of wetting pattern, Figure 4.13 shows the ratio of wetted depth (Y) to wetted radius (X) at the end of irrigation cycle (20 L of water applied). The Y/X rate of 1 means that wetted depth (Y) and wetted radius (X) have about the same distance – the wetting pattern shape is round and capillarity forces are dominating. Ratio close to 2 shows that the wetted depth is larger than the wetted diameter and that the gravity forces dominate.

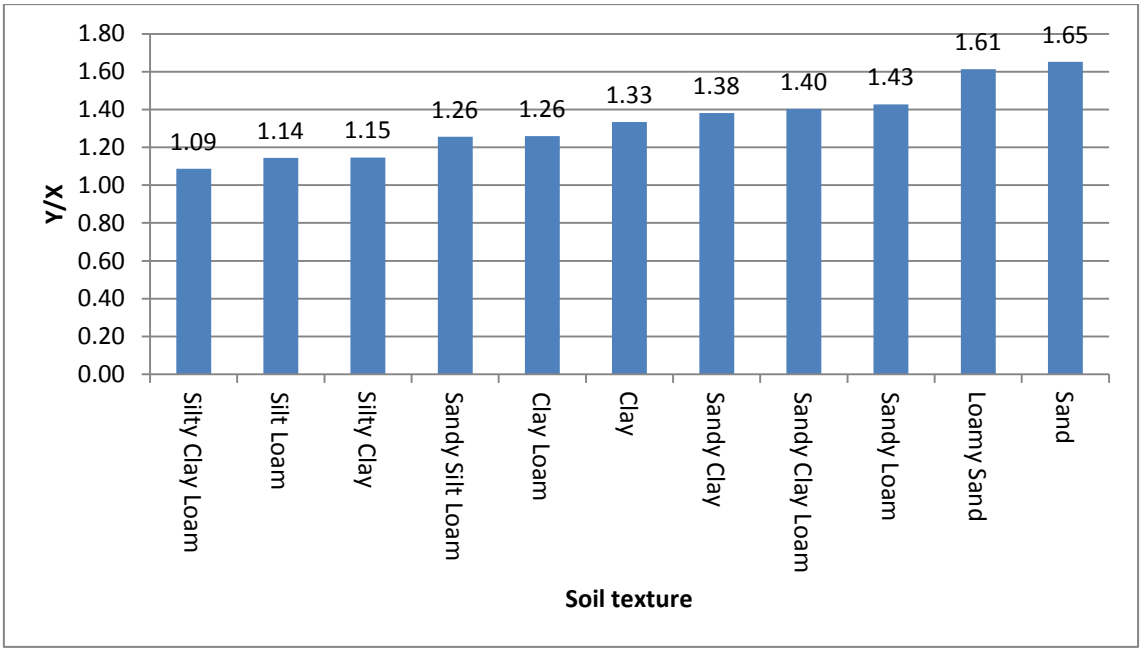

Figure 4.13: The ratio of wetted depth (Y) to wetted radius (X) at the end of the irrigation cycle (20 L of water applied).

In Figure 4.13 the coarse-textured soils (sand and loamy sand) have Y/X ratio above 1.6, showing that the wetting pattern depth is larger than the wetted diameter. Gravity has a profound effect in these soils. The ratio for fine-textured soils (silty clay loam, silty clay and silt loam), is 1.1, showing that the wetting pattern depth and diameter have about the same length and in that case the capillarity forces dominate.

4.1.2 Influence of discharge rates

Measurements of dimensions of wetting patterns for three contrasting soil texture classes, as a function of volume of applied water (irrigation duration) for the three different surface drip emitter discharge rates (Q), are given in Figure 4.14.

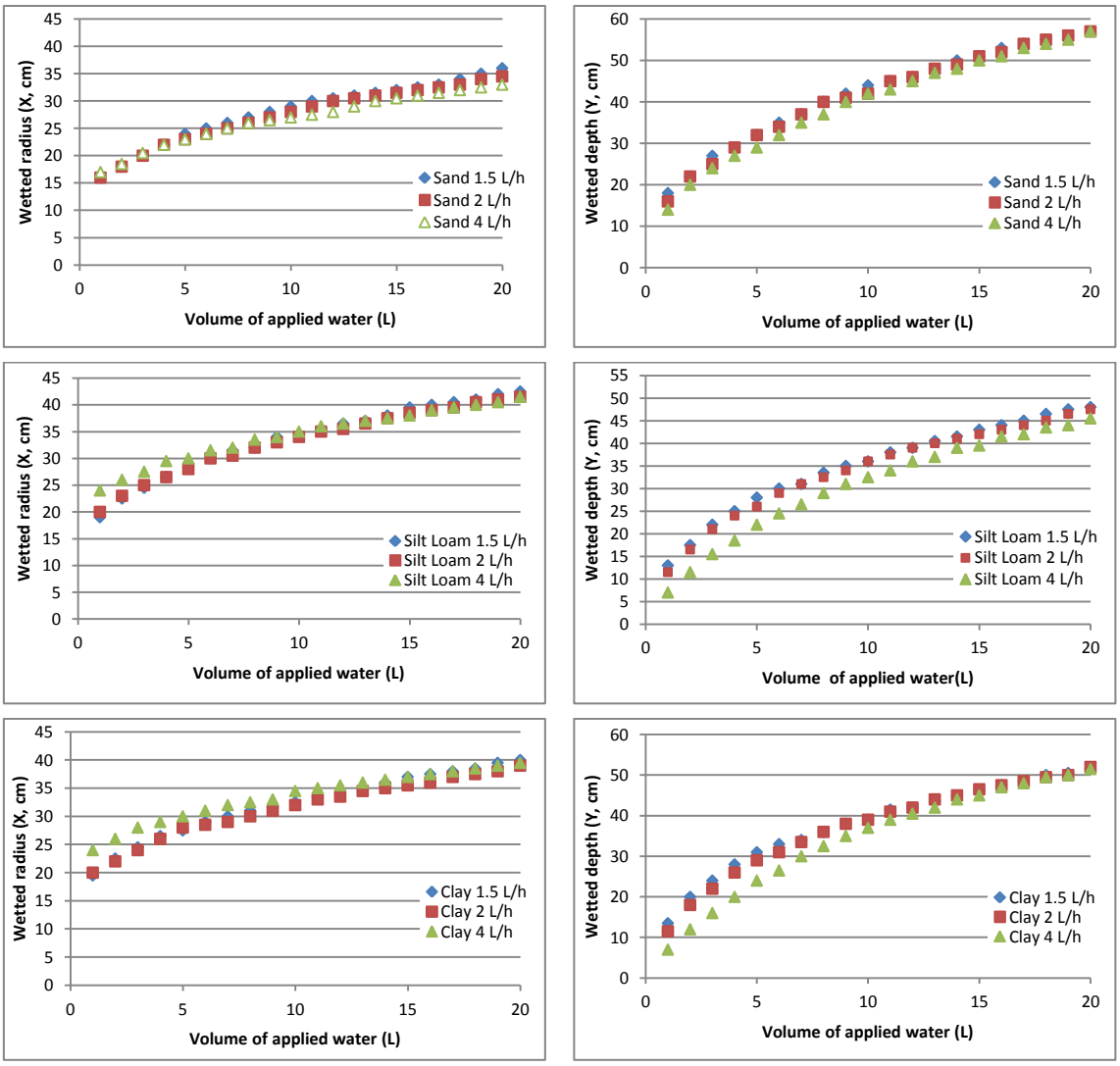

Figure 4.14: Measured simulated wetting pattern dimensions in three texture-contrasting soils as a function of volume of applied water for different water application rates.

In the silt loam and clay soils the higher emitter discharge rate (4 L/h) produced a bigger wetted radius at the beginning of irrigation. This was not true for the sand soil, where differences between different emitter discharge rates had minimal or almost no effect on the wetted radius at the beginning of irrigation, or up to 9 L of water applied. Therefore, in the sand soil, differences only occurred at the end of irrigation, where the lower flow rate resulted in a slightly larger wetted radius, as discussed earlier. Conversely, at the end of water application almost no differences in the size of the wetted radius occurred in silt loam and clay soil. The wetted depth increased with a decrease in emitter discharge rate in the silt loam and clay soils. However, this effect vanished after 15 L of applied water in the clay. In the sand soil emitter discharge rate had almost no effect on the wetted depth.

Because it is hard to see the differences in wetting pattern dimensions in Figure 4.14, the wetted radius (X) and wetted depth (Y) are at the end of water application for the three discharge rates and the three soils plotted in Figure 4.15.

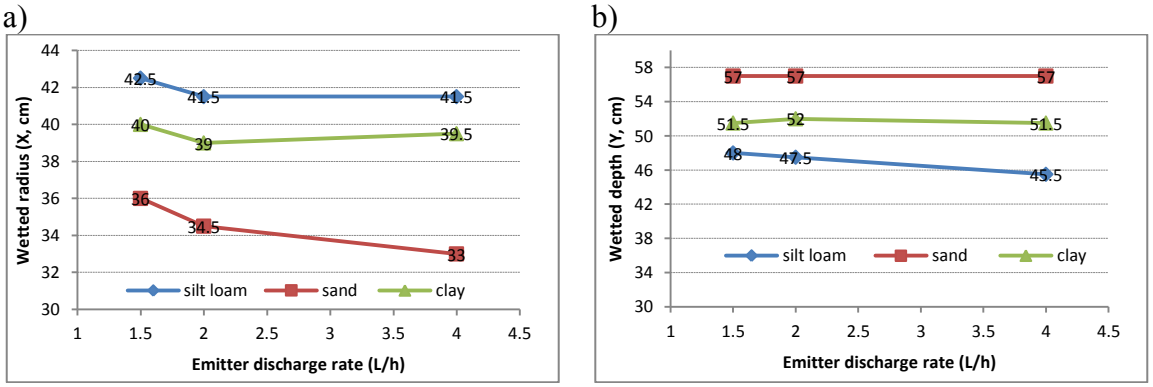

Figure 4.15: Wetted radius X (cm) (a) and wetted depth Y (cm) (b) at the end of water application (20 L of water applied) for three different emitter discharge rates and different soil textures.

At the end of water application (20 L) the emitter discharge rate slightly affected radial water movement in all cases. Decreased discharge rates resulted in a slight increase in the wetting pattern radius for all soils. In the silt loam soil the discharge rates of 2 L/h and 4 L/h produced the same wetted radius of 41.5 cm, whereas the discharge rate of 1.5 L/h produced a slightly larger radius (42.5 cm). Similarly, in the clay soil, 1.5 L/h resulted in a radius of 40 cm in comparison to radii of 39 and 39.5 cm for the 2 L/h and

4 L/h treatments, respectively. In the sand the difference was larger, with emitter discharge rates of 1.5, 2 and 4 L/h producing a wetted radius of 36, 34.5 and 33 cm, respectively. Conversely the discharge rate had no effect on the wetted depth in the sand and clay soils. The only effect of discharge rates was observed in the silt loam where 1.5, 2 and 4 L/h resulted in wetted depth of 48, 47.5 and 45.5 cm respectively. The findings of Cote *et al*. (2003) for subsurface drip irrigation suggested that, when the emitter discharge rate decreases, both the wetted radius and depth increase. This is contradictory to the findings of Skaggs *et al*. (2010) who concluded that, for subsurface drip irrigation investigated with numerical simulations and field experiments, emitter discharge rates had no significant effect. In our case, the discharge rates, under surface drip irrigation, only affected the wetted radius in the sand soil and the wetted depth in the silt loam.

The moisture content distribution obtained with the numerical simulations of water infiltration from surface emitters in the silt loam, sand and clay soils is shown in Figure 4.16. The wetting patterns for three contrasting soil types and the three emitter discharge rates are compared at the end of irrigation cycle (at 20 L of water applied). Note that the water content distribution is represented by colour scales which are different for each soil texture. The initial moisture content, corresponding to 50 % depletion, is represented by the red colour and varies between 0.128 and 0.377.

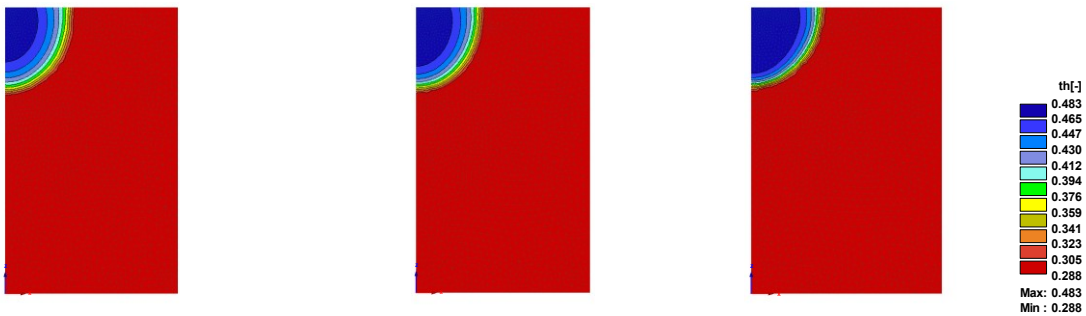

Silt loam, 1.5 L/h (at 13.33 h) Silt loam, 2 L/h (at 10 h) Silt loam, 4 L/h (at 5 h)

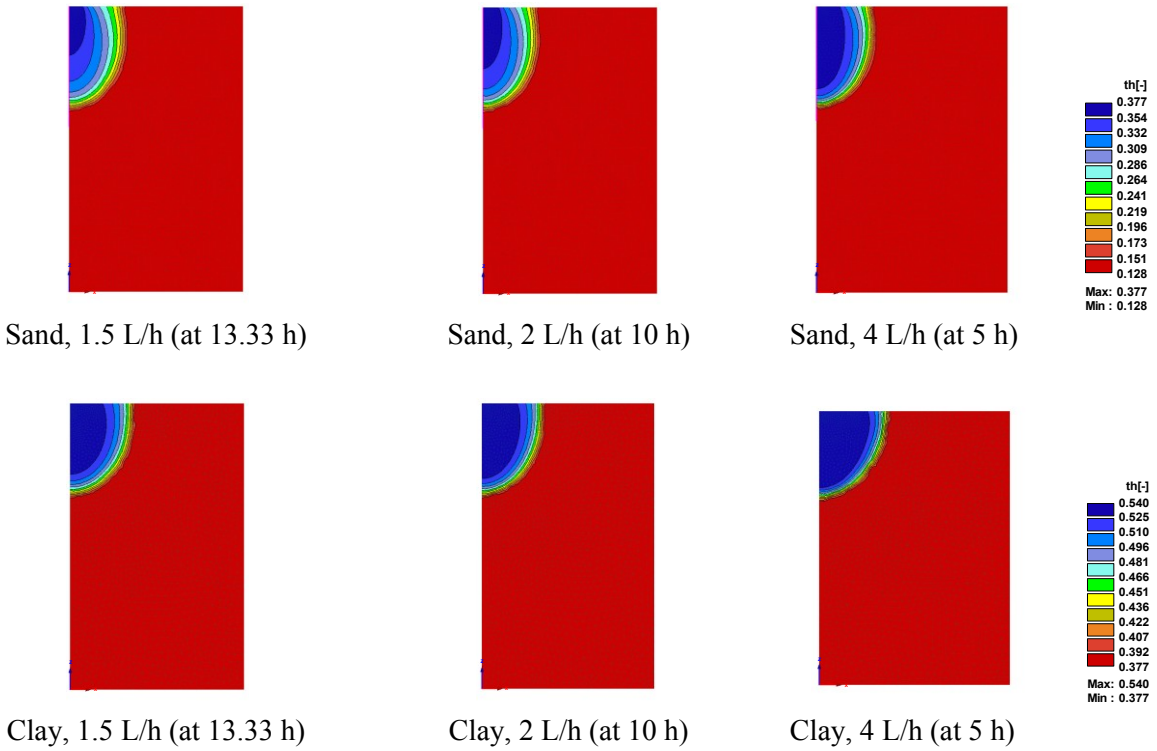

Figure 4.16: Simulated water distribution around the surface drip emitter for three emitter discharge rates of 1.5, 2 and 4 L/h and 20 L of water applied for three soil texture classes.

The different flow rates had a small effect on the final size of the wetting pattern as can be seen on Figure 4.15 and figure 4.16, but large differences in the position of the saturated (dark blue colour) wetted front were observed as shown in Figure 4.17

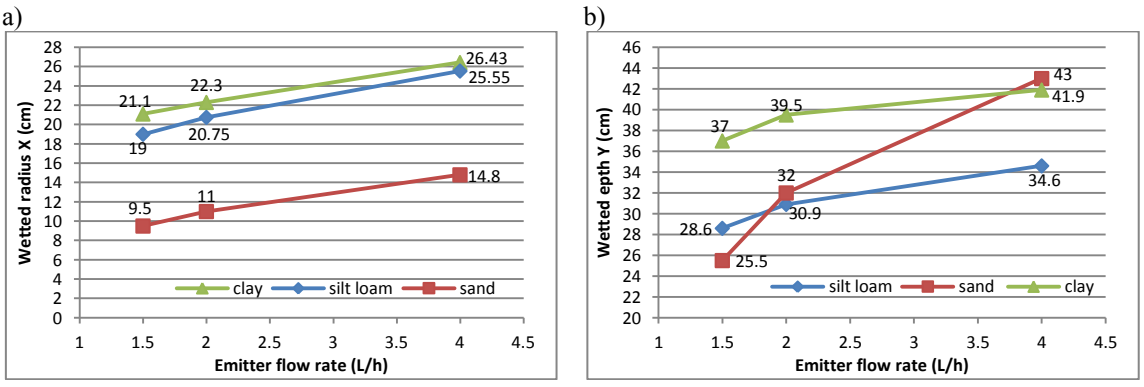

Figure 4.17: Wetting front close to saturation in X (cm) (a) and Y (cm) (b) direction at the end of water application (20 L of water applied) for three different emitter discharge rates and different soil textures.

The saturated moisture content θ_s in the sand is 0.377. The radius of the wetted front close to saturation (> 0.354) was 9.5, 11 and 14.8 cm for the 1.5, 2 and 4 L/h emitter discharge rates, respectively. The observed depths were 25.5, 32 and 43 cm for the three discharge rates, respectively. The saturated moisture content θ_s in the silt loam is 0.483. The radius of the wetter front close to saturation (>0.465) was 19, 20.75 and 25.55 cm for the 1.5, 2 and 4 L/h emitter discharge rates, respectively and observed depths were 28.6, 30.9 and 34.6 cm for the three discharge rates, respectively. For clay soil the saturated moisture content θ_s is 0.540. The radius of the wetted front close to saturation (> 0.525) was 21.1, 22.3 and 26.43 cm for the 1.5, 2 and 4 L/h emitter discharge rates, respectively. The observed depths were 37, 39.5 and 41.9 cm for the three discharge rates, respectively. It is therefore apparent that flow rate has a much larger effect on the position of the saturated front compared than on the position of the wetting front. When only the wetted front close to saturation is taken into account, higher Q (L/h) result in larger saturated radius and depth. This was more pronounced for wetted depth in the soils with coarser texture and can be clearly seen for sand soil (Figure 4.17).

Additional insight into any other possible effects of different discharge rates on soil water distribution can be gained by plotting wetted depth and wetted radius against water content (θ) (Figure 4.18).

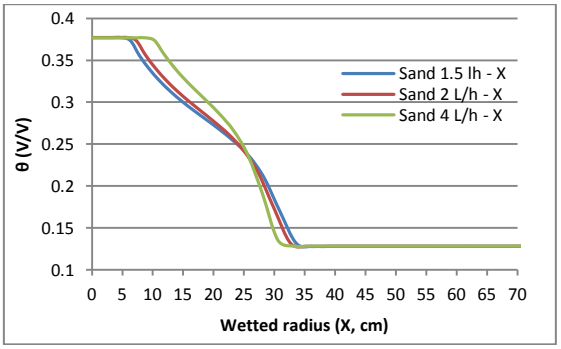

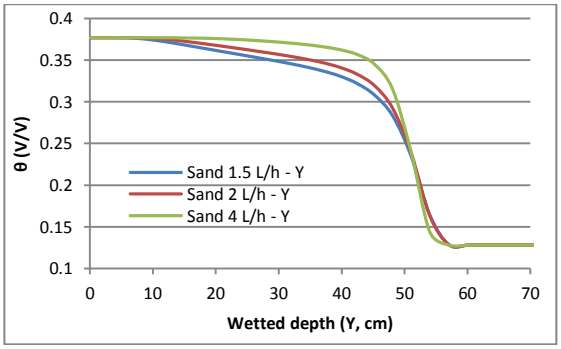

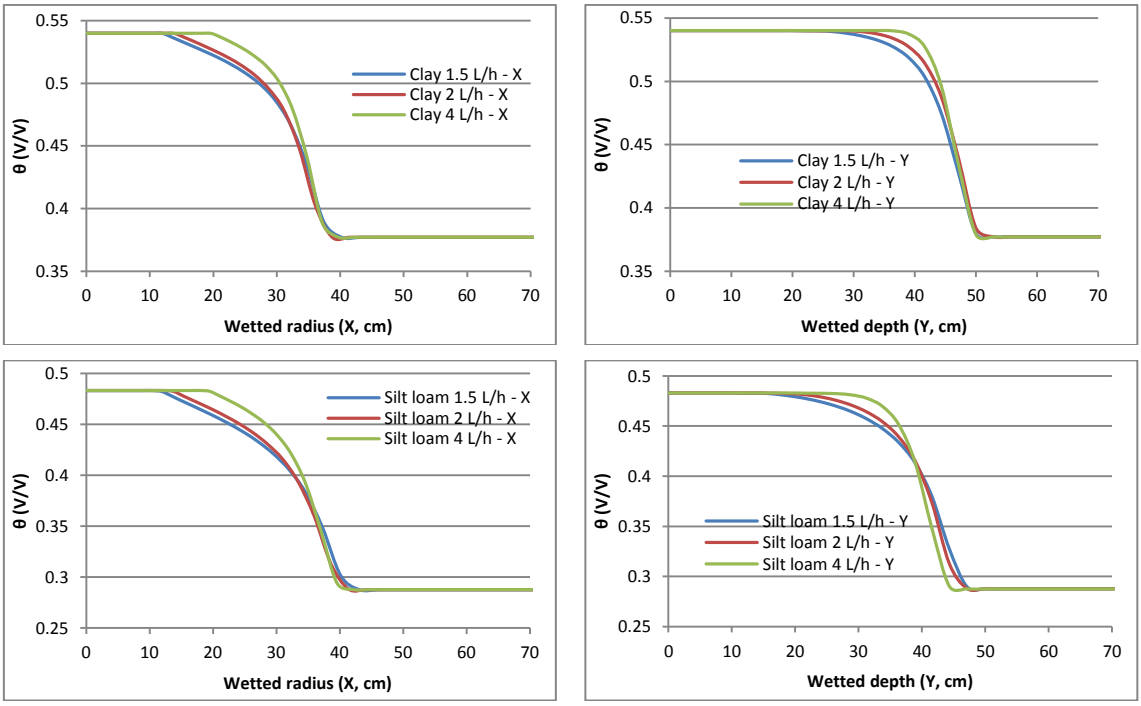

Figure 4.18: Wetted radius and wetted depth for three soils with different emitter discharge rates at the end of irrigation (20 L of water applied).

These water content profiles correspond to the end of water application (20 L of water applied). From Figure 4.18 it can be seen that, at the saturated front, larger water content gradients are produced with the higher emitter discharge rate. This results in a sharper front and larger changes in water content over smaller distances. This is true for all soil textures and in both directions. As mentioned earlier, the results also show that the radius and depth of the saturated zone increased with emitter discharge rate. These results are in agreement with Mostaghimi *et al*. (1982) and Bar-Yosef and Sheikholslami (1976) in horizontal (X) direction for a sand soil, where for a given volume of water applied, the higher emitter discharge rates produced slightly smaller wetted radius. For silt loam and clay soil, 2 and 4 L/h emitter discharge rates had no effect on wetted radius and a 1.5 L/h discharge rate produced a slightly larger wetted radius. This is probably due to the longer application time needed for the 1.5 L/h emitter to apply the same amount of water, therefore allowing more time for soil moisture to redistribute in a radial direction due to capillary forces. Higher emitter discharge rates caused faster horizontal (X) water spreading and shorter application time, allowing less time for water to redistribute, through capillarity. Emitter discharge rate had no effect on wetted depth (Y) of sand and clay, but small effect for silt loam, where a higher

emitter discharge rate resulted in smaller wetted depth, which is in agreement with Bresler *et al*. 1971, Li *et al*. (2003, 2004), Levin *et al*. (1979) and Khan *et al*. (1996), but in disagreement with studies of Mostaghimi et al., 1982 and Bar-Yosef and Sheikholslami, 1976, where increase in emitter discharge rate resulted in increased wetted depth.

When only the wetting pattern close to saturation is considered, the influence of emitter discharge rate had a bigger effect on radius and depth of wetting pattern in all soils. An increase in emitter discharge rate resulted in increase in depth (Y) and radius (X) of the saturated wetting pattern. This is similar to the results of Levin *et al*. (1971), where the highest emitter discharge rate resulted in the furthest wetting pattern advance in both directions for sand soil. However, the discharge rates they used were higher (8 L/h) and their initial water content of the soil was chosen close to field capacity. These results also agree with Bresler *et al*. (1971), Levin *et al.* (1979), Khan *et al*., (1996) and Li *et al*. (2003, 2004), but just for wetted radius (X). In their case the wetted depth decreased with increase of emitter discharge rate, which was not true in this study. The differences in saturated wetted radius occurred because of the nature of the surface boundary condition, which was calculated as presented with Equation 11. The radius of application was bigger for a bigger emitter discharge rate for a given soil. All the changes therefore occurred in the radius of application, which resulted in calculated length as presented in Table 4.1. In general, the radius of saturated wetting pattern depends on the *Ks* of the soil and discharge rate of the emitter.

Table 4.1: Radius (X) of application for different soils and emitter discharge rates (*Q*)

Q (L/h)	Radius (X) (cm)		
	Sand	**Silt loam**	**Clay**
1.5	6.28	11.91	12.05
2	7.26	13.75	13.92
4	10.27	19.45	19.68

The differences in the length of application radius for different emitter discharge rates are very similar to the measured changes in radius (X) of saturated wetting patterns achieved with different emitter discharge rates. A higher emitter discharge rate resulted

in increase in the soil wetted depth close to saturation. This is in agreement with Mostaghimi *et al*. (1982) and Bar-Yosef and Sheikholslami (1976).

It has to be noted, that wetting patterns were observed in both directions immediately after termination of irrigation, allowing no time for redistribution of soil moisture content. According to Levin *et al*. (1977), the advantage gained by using high emitter discharge rates to extend wetting pattern lateral movement in sand (Nahal Sinai soil and Gilat loam) is valid only for a short time during the first irrigation cycle and after 24 h of moisture redistribution this difference is reduced to negligible amount. Also, in the study of Skaggs *et al*. (2011) it was concluded that none of the studies for sandy loam, testing different emitter discharge rates and pulsed irrigation produced a wetting pattern that was different from any others.

In order, to establish the proper spacing between the emitters, to give complete lateral soil wetting, the shape of the wetting pattern has an important role. For example, in sand soil the emitter spacing for emitter flow rate of 4 L/h should be at least 60 cm (2X) (Figure 4.18). At that spacing, the soil in the middle, between 2 successive emitters will be too dry and plants will experience a certain degree of stress. Therefore it is important to know the desired soil moisture content (or % depletion) at which plants easily extract water from the soil. If the emitter spacing is too close, the neighbouring emitters overlap and the water content adds up and can, in this case, exceed the field capacity of the soil, resulting in drainage and therefore lost water.

4.1.3 Influence of initial conditions

Different initial soil moisture conditions are, in this study, presented as % of depletion of the available water (AW) which corresponds to the amount of water between field capacity (FC) and permanent wilting point (PWP). % depletion represents the % of AW that is no longer available. A field capacity corresponding to a moisture content at 10 kPa (-100 cm) matric potential was chosen for all three soils. The size of the wetting pattern in a horizontal (X) and vertical (Y) direction was measured for three soils (sand, silt loam and clay) and three different initial soil moisture conditions corresponding to depletions of 30 %, 50 % and 70%.

The dimensions of the wetting patterns for the three soils as a function of the volume of applied water (irrigation duration) and for the three soil moisture depletions are represented in figure 4.19.

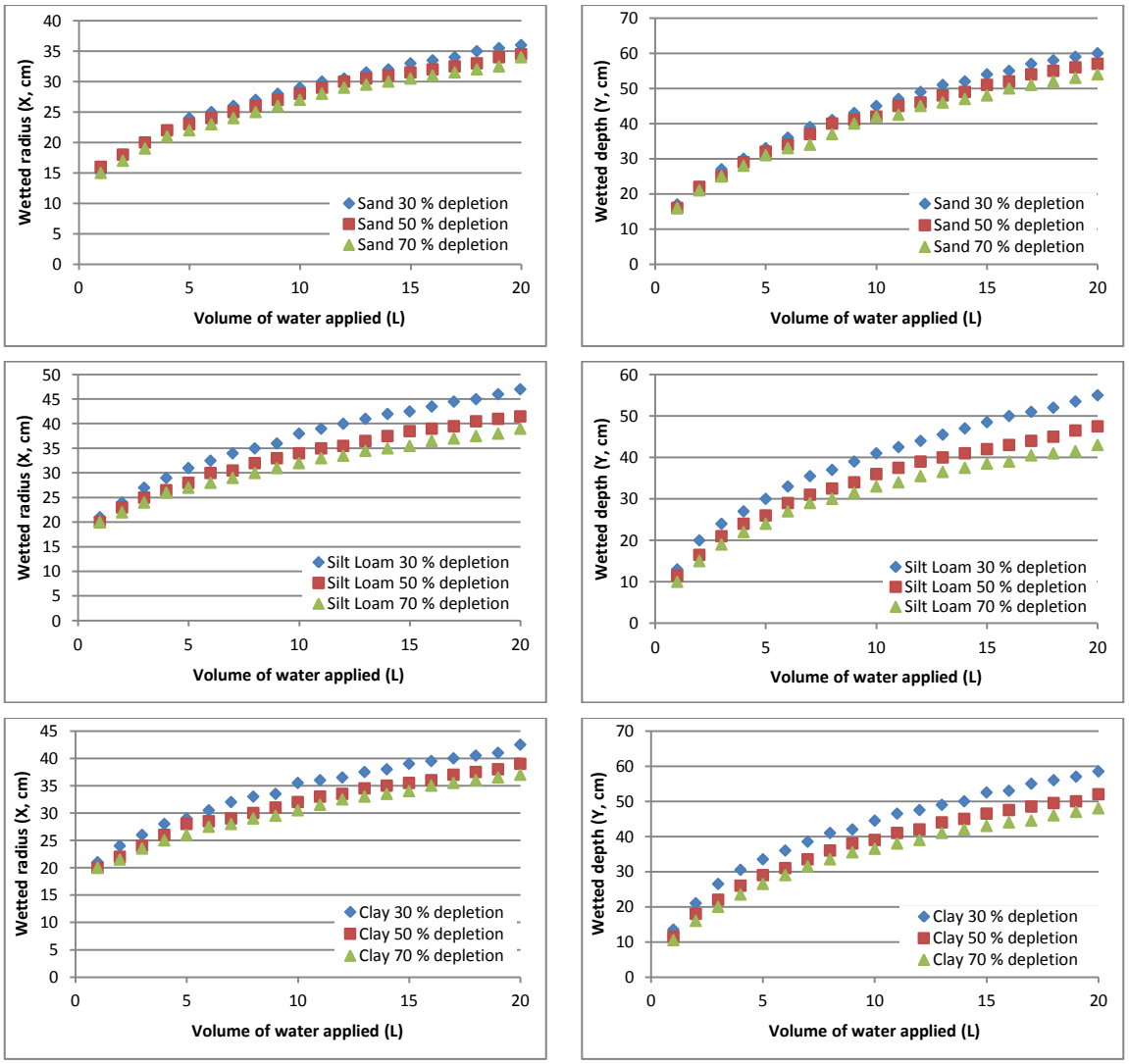

Figure 4.19: Measured simulated wetting pattern dimensions in three texture-contrasting soils as a function of volume of applied water for different soil water initial conditions (represented as depletion in % of selected FC).

Silt loam soil resulted in the biggest wetted radius for all depletions, followed by clay and sand soil. Just the opposite is true for wetted depth, where sand resulted in the biggest wetted depth for all depletions, following by clay and silt loam soil. Higher soil moisture initial conditions (lower depletions) caused an increase in spreading in a radial

direction and wetted depth for all soils. This data agree with results of previous studies of subsurface drip irrigation (e.g. Provenzano, 2007; Skaggs *et al*., 2010) and surface drip irrigation (e.g. Li *et al*., 2003, 2004).

Figure 4.20 shows the maximum wetted radius and wetted depth, reached at the end of water application for the three depletions and three different soils. 30, 50 and 70 % depletion produced a wetted radius of 47, 41.5 and 39 cm in silt loam soil, 42.5, 39 and 37 cm in clay soil and 36, 34.5 and 34 cm in sand soil, respectively. A wetted depth for 30, 50 and 70 % depletion was equal to 60, 57 and 54 cm for sand soil, 58.5, 52 and 48 cm for clay soil and 55, 47.5 and 43 cm for silt loam soil, respectively. Increase of the wetting pattern is larger in a vertical (Y) than in a horizontal (Y) direction.

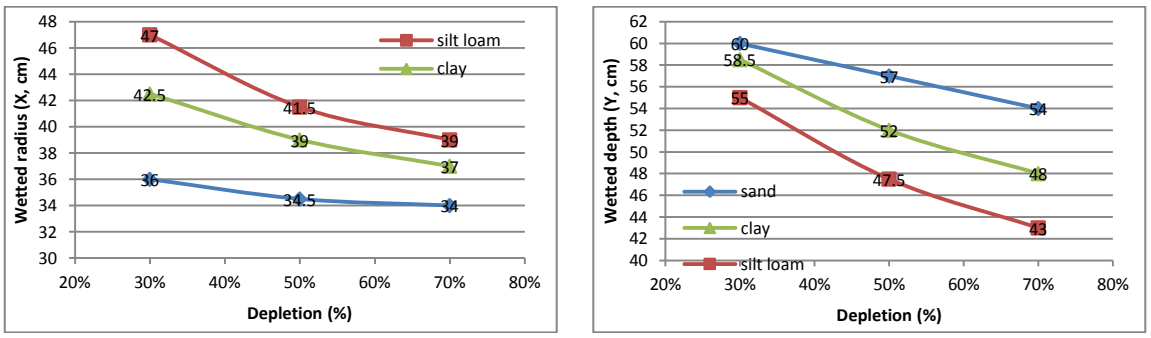

Figure 4.20: Wetted radius (X, cm) and wetted depth (Y, cm) in three soils for three initial soil moisture conditions (% depletions) at the end of water application (20 L of water applied).

Soil depletion had a larger effect on fine-textured soil (clay and silt loam) in both directions. The explanation for this effect can be found in soil's particle size, and consequently, air-filled pore spaces. Because depletion (%) was calculated, based on FC of each soil at -100 cm suction (matric potential), the sand soil had, at that suction, more air-filled pore space (or less available water) than other fine-textures soils. Therefore, applying different percentages of depletion to an already dry sand soil did not cause much difference in initial water content. Changes between 70 % depletion and 30 % depletion resulted in initial volumetric water content differences of 0.0085, 0.068 and 0.042 in the silt loam, clay and sand, respectively as presented in Figure 4.21. Therefore

the small variation in initial soil moisture content in the sand, explains the smaller effect on wetted dimensions in both directions.

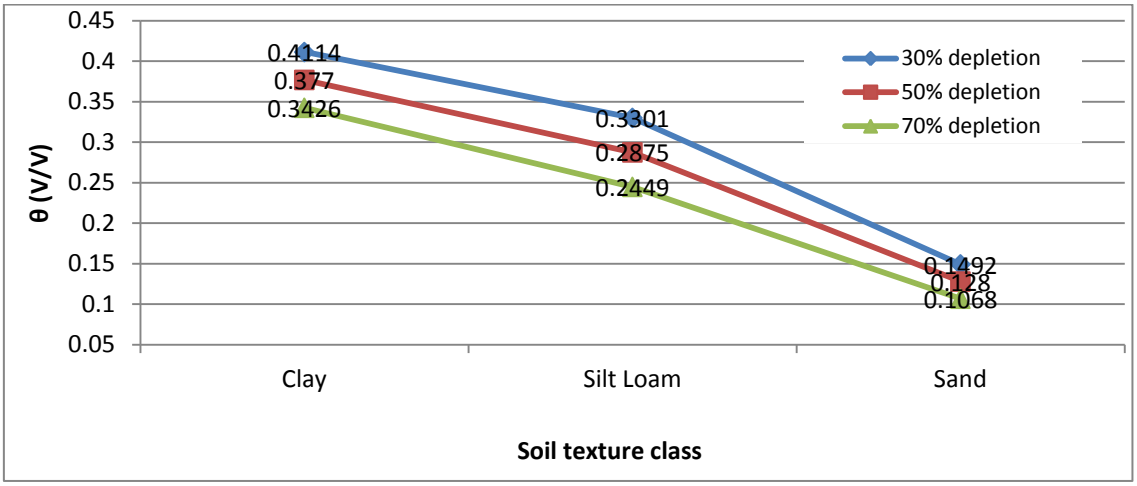

Figure 4.21: Values of water content corresponding to % depletion for three different soils.

Simulated water distribution in the sand, silt loam and clay soil, using 2 L/h emitter discharge and the three different initial moisture contents, are presented on Figure 4.22. It is obvious, that the wetting pattern increased with an increase in initial soil moisture content (or a decrease in % depletion).

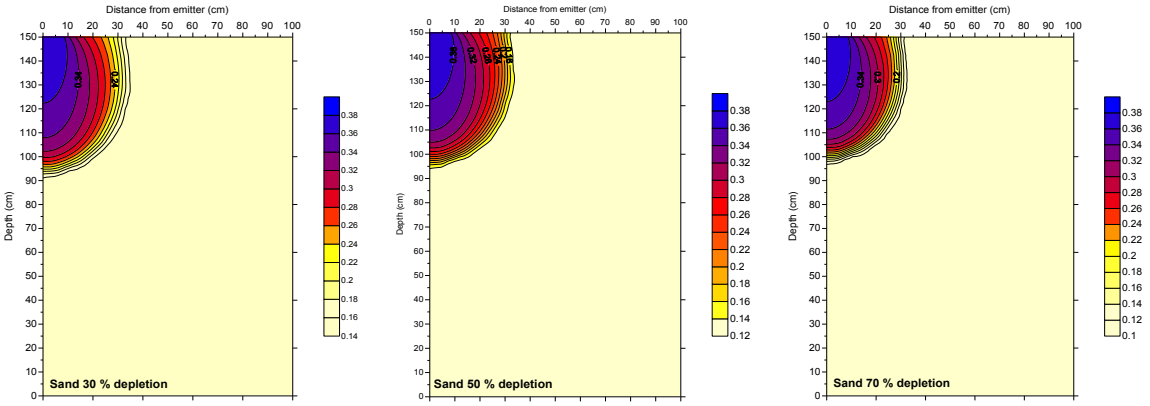

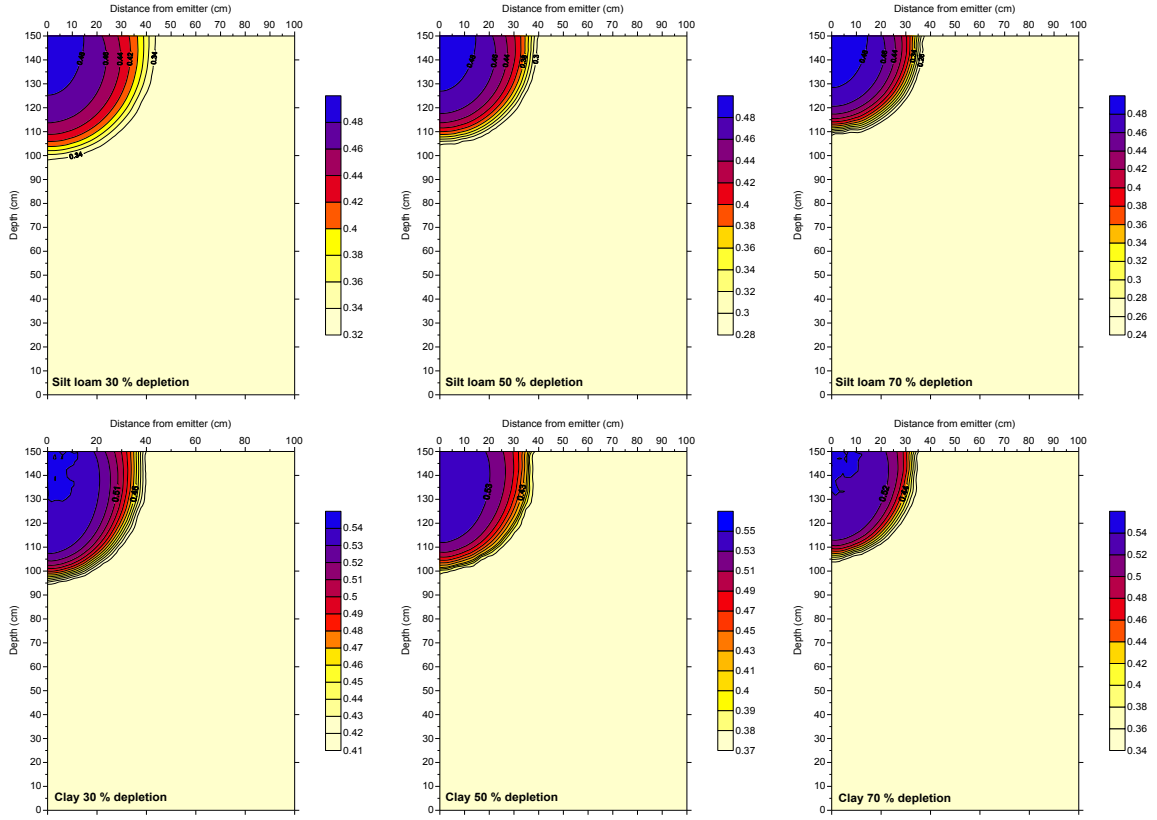

Figure 4.22: Simulation of water distribution in sand, silt loam and clay with 30 %, 50 % and 70 % depletion at the end of water application (20 L applied).

Additional insight into any other possible effects of different soil moisture initial conditions on soil water distribution can be gained by plotting wetted depth and wetted radius against θ (Figure 4.23). The figures show that the wetting pattern for all soils and in both directions increased with higher initial soil moisture (or lower depletion percentage). This was expected, because with higher soil moisture content less pore volume is available for water which has to infiltrate a larger soil volume. Water content gradients were in general sharper (steeper) in Y (depth) direction compared to X (radial) direction. In both directions water content gradients at the wetting front got sharper with decrease in initial soil moisture content.

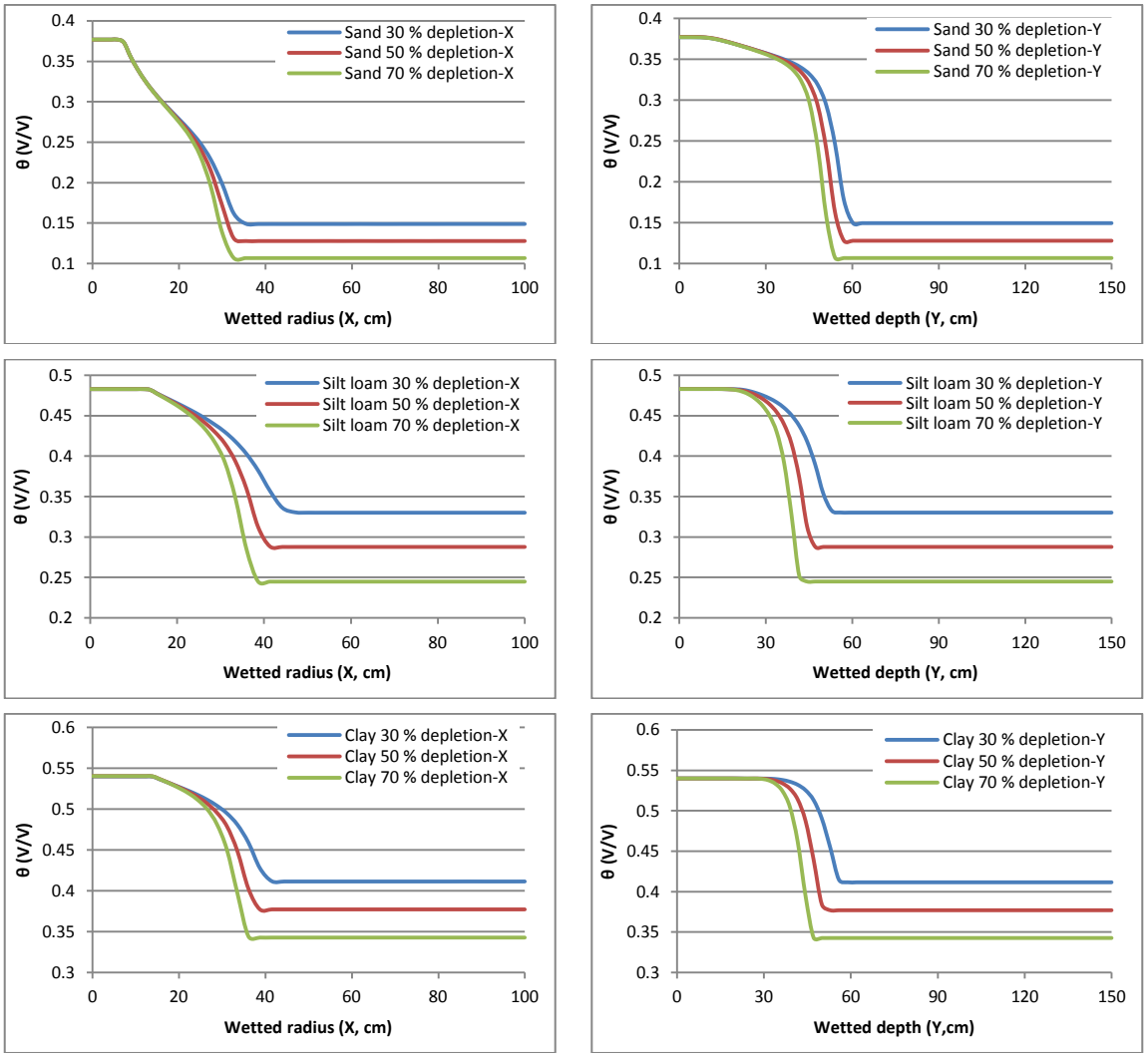

Figure 4.23: Simulated wetted radius and wetted depth for three soils with different initial soil moisture conditions (depletions) at the end of irrigation (20 L of water applied).

Overall, an increase in initial soil moisture content resulted in an increase in the size of the wetting pattern in both directions, and produced a less sharp water content gradient at the wetting front. Results confirm the conclusions of Skaggs *et al*. (2010), where higher initial soil water content increased water spreading from shallow subsurface and surface drip irrigation systems, with larger spreading in the vertical than in the horizontal direction. The larger overall spreading is due to a decrease in the available pore space at higher moisture content while the lower horizontal than vertical spreading can be explained by lower capillary forces at larger initial moisture content (smaller depletions).However, the rate of increase in the wetted depth and wetted radius on Figure 4.19 is not higher for dryer soils (70 % depletion) as it would be expected

because of higher capillary forces at the wetting front. This is because the rate of wetting pattern increase is governed by the infiltration rates at the soil surface, which is constant at 2 L/h in this case. Also, as can be seen in figure 4.23, less sharp water content gradients at the wetting front are produced in the soils with higher moisture content due to lower capillary pressure gradients.

4.1.4 Comparison with soil tank experiments

Figure 4.24 to 4.26 show the comparison between the experimental and simulated wetting patterns for the sand, the sandy loam and the silty clay loam for continuous applications with surface drip emitter discharge rates (Q) of 0.1, 0.5, 1, 1.5 and 2 L/h. Note that for the sandy loam and the silty clay loam Q higher than 0.1 or 0.5 L/h could not be used. This because these higher rates resulted in water spreading across the entire soil surface area of the tank before any meaningful measurements could be achieved.

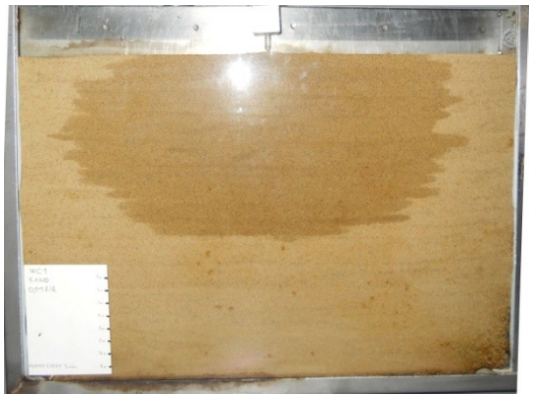

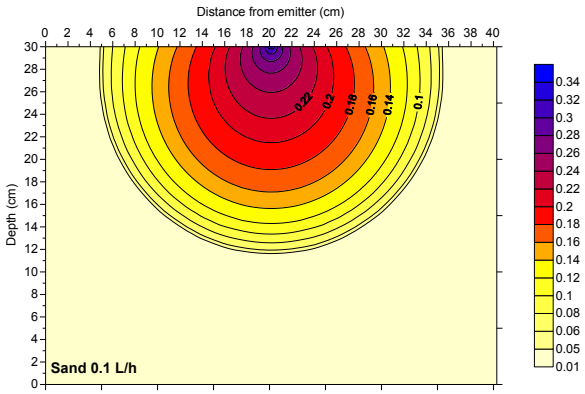

Sand 0.1 L/h at the end of irrigation cycle – 84 min (0,15 L of water applied)

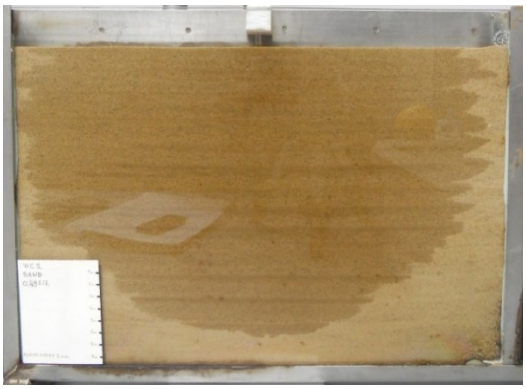

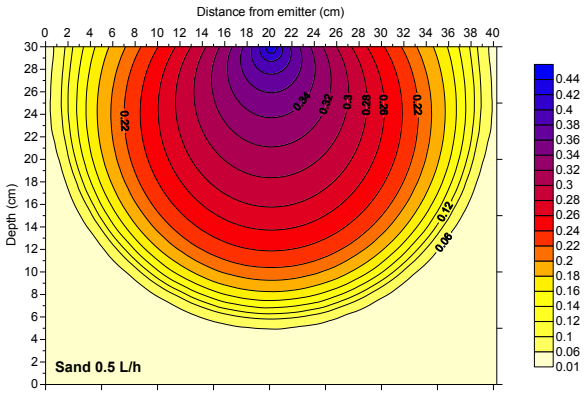

Sand 0.5 L/h at the end of irrigation cycle – 50 min (0,40 L of water applied)

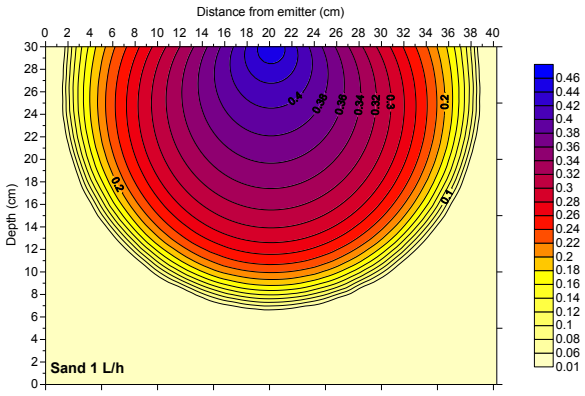

Sand 1 L/h at the end of irrigation cycle – 26 min (0,47 L of water applied)

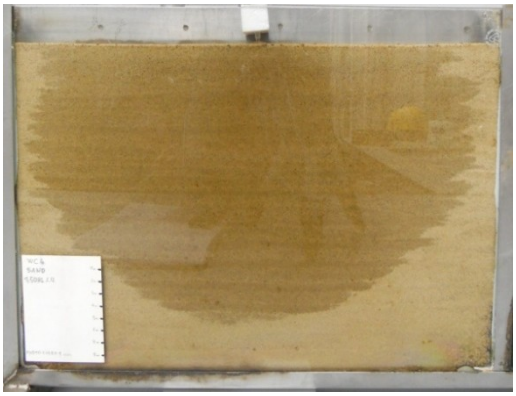

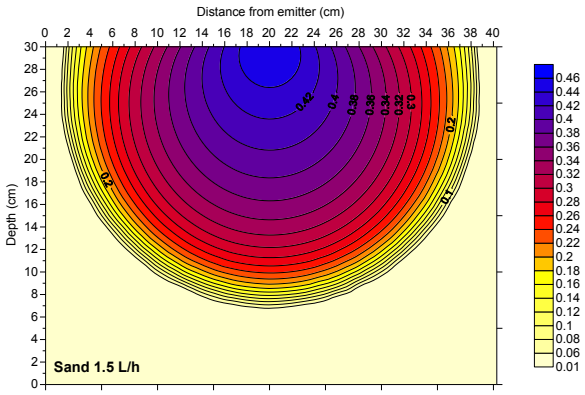

Sand 1.5 L/h at the end of irrigation cycle – 19 min (0,48 L of water applied)

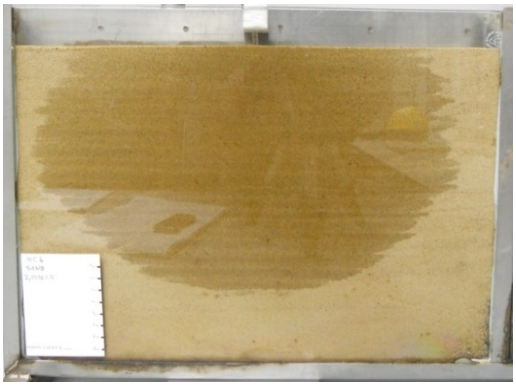

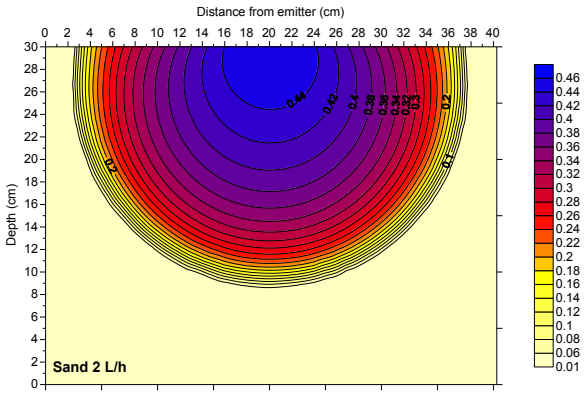

Sand 2 L/h at the end of irrigation cycle – 13 min (0,44 L of water applied)

Figure 4.24: Measured and simulated wetting patterns for sand at the end of the water application with *Q* variation from 0.1 to 2 L/h.

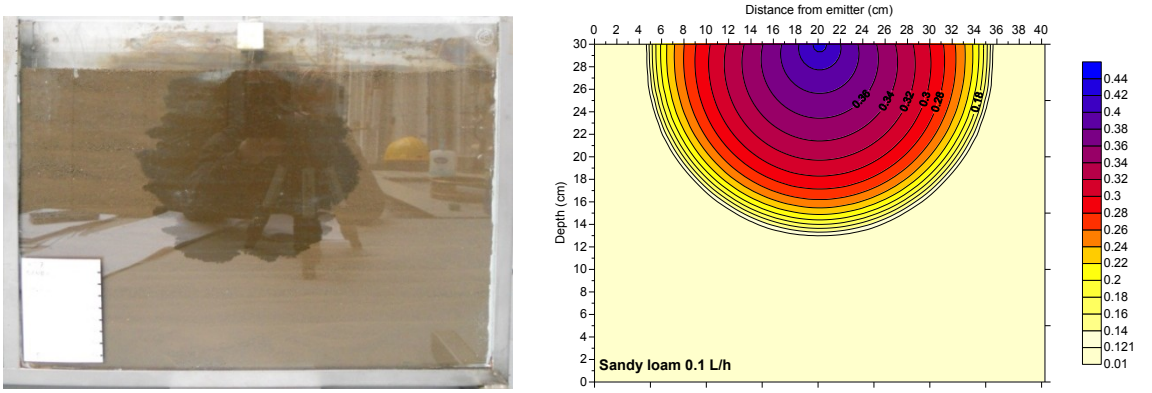

Sandy loam 0.1 L/h at the end of irrigation cycle – 130 min (0,2 L of water applied)

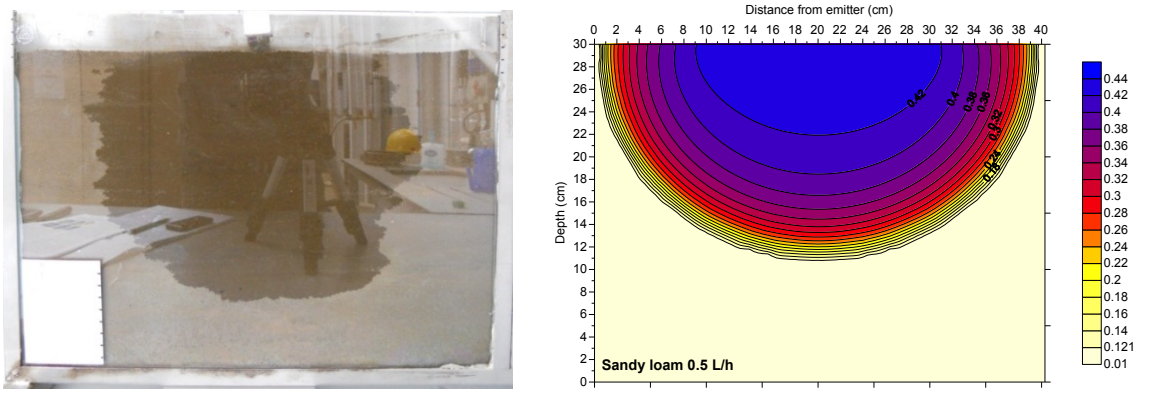

Sandy loam 0.5 L/h at the end of irrigation cycle – 49 min (0,40 L of water applied)

Figure 4.25: Measured and simulated wetting patterns for sandy soil at the end of water application with *Q* from 0.1 to 0.5 L/h.

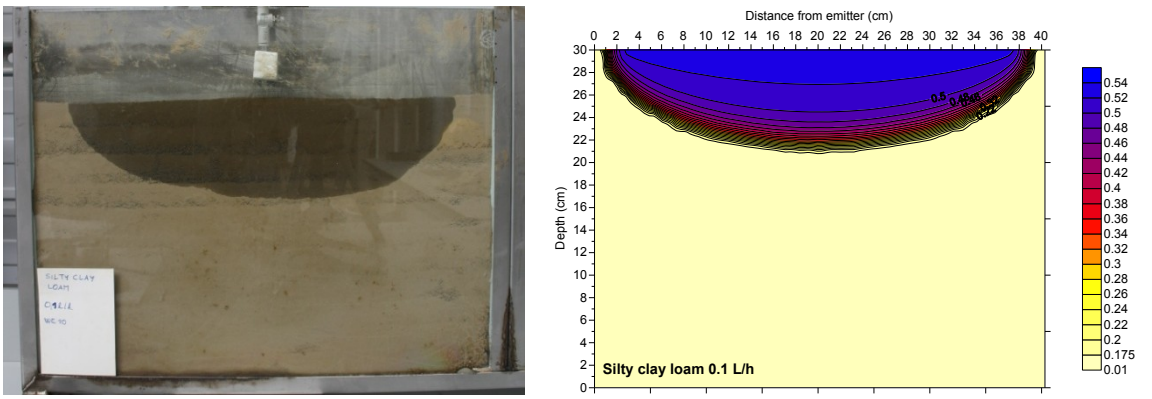

Silty clay loam 0.1 L/h at the end of irrigation cycle – 120 min (0,23 L of water applied

Figure 4.26: Measured and simulated wetting patterns for silty clay loam at the end of water application with *Q* of 0.1 L/h.

It is clear from the comparisons above that, in general, the depths and diameters of simulated and measured wetting patterns are in good agreement for the sand and silty clay loam soils. However, despite a relatively good agreement between measured and simulated wetted depth in the sandy loam soil, the discrepancy between measured and simulated diameters is larger.

Measured and simulated depth and diameter, as a function of time, for three different soil types and various emitter discharge rates, are shown in figures 4.27 to 4.29.

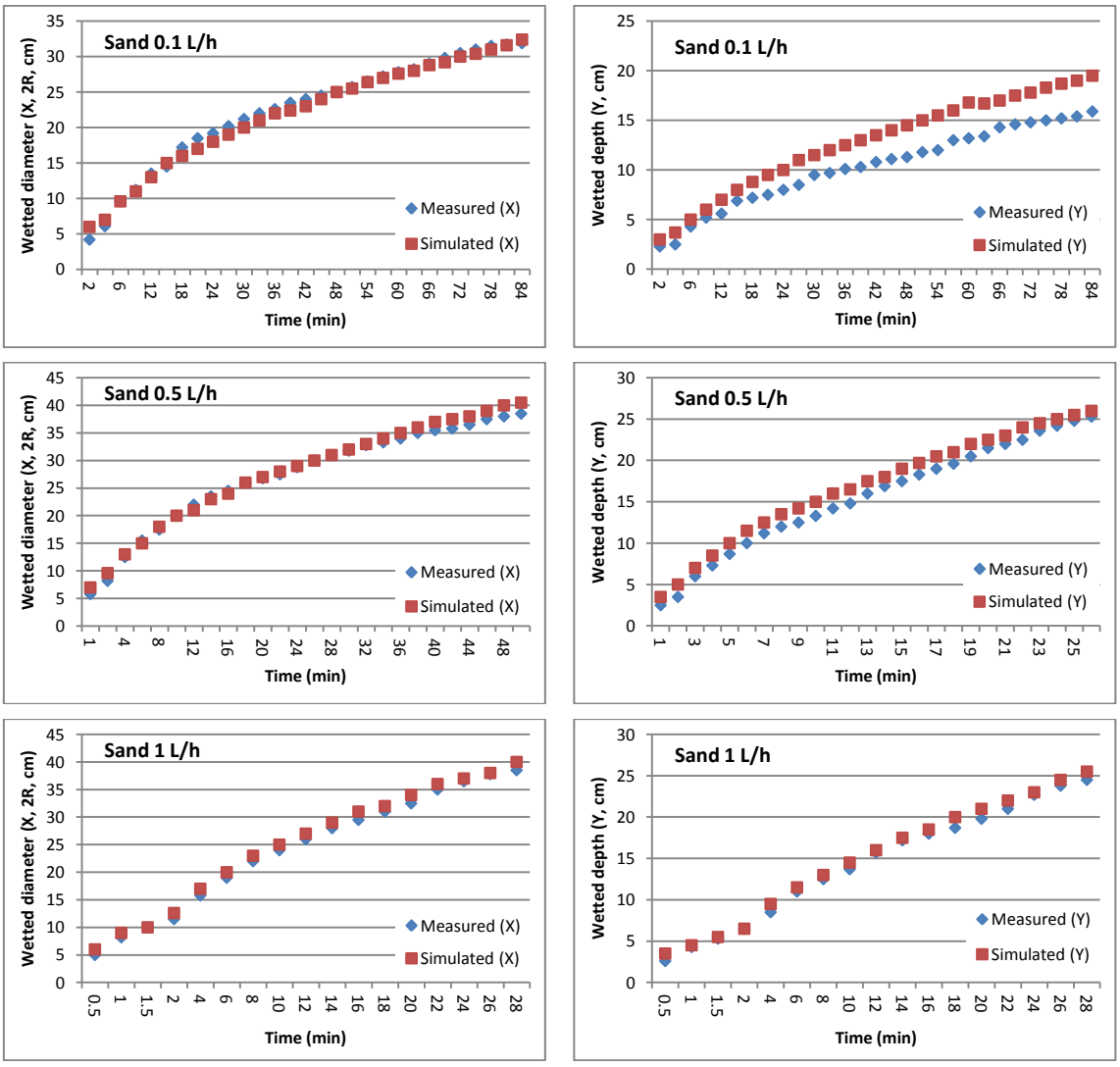

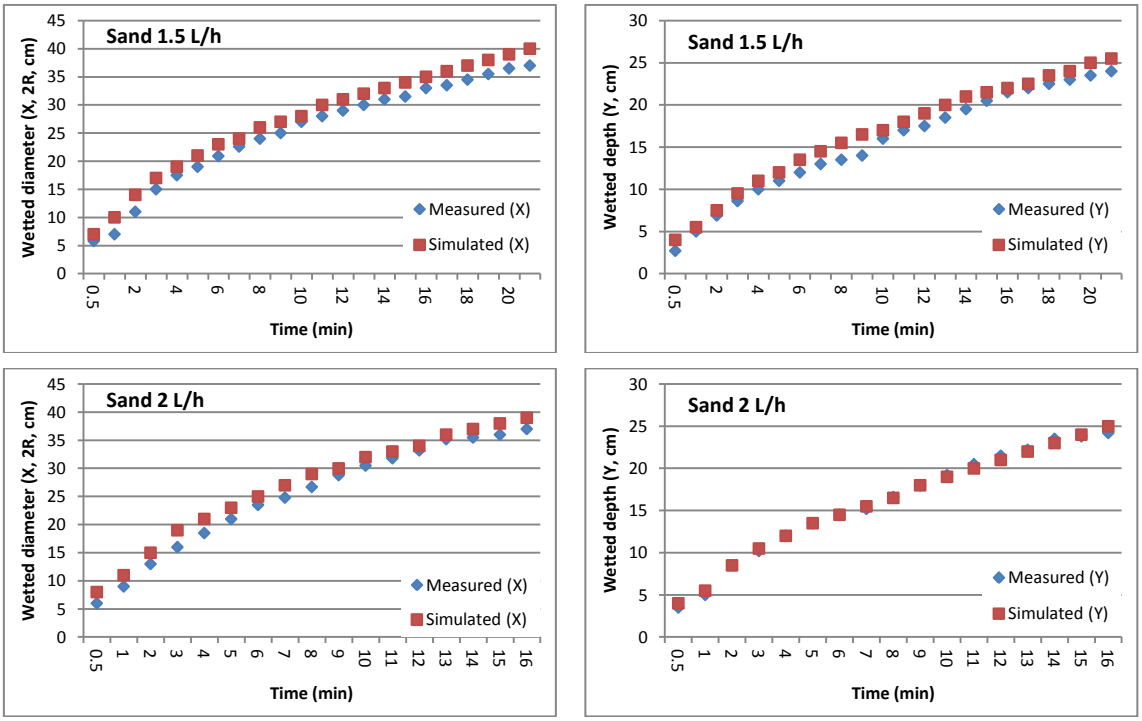

Figure 4.27: Measured and simulated wetted diameter (right side) and depth (left side) as a function of time for sand soil at different *Q*.

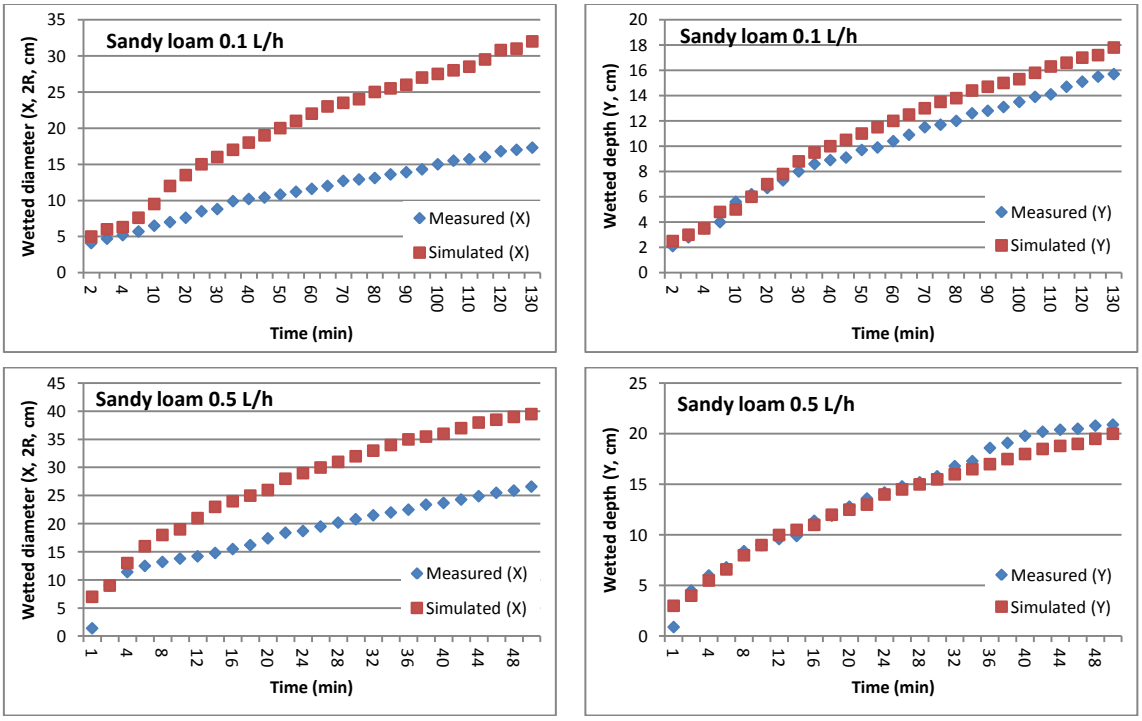

Figure 4.28: Measured and simulated wetted diameter (right side) and depth (left side) as a function of time for sandy loam soil at different *Q*.

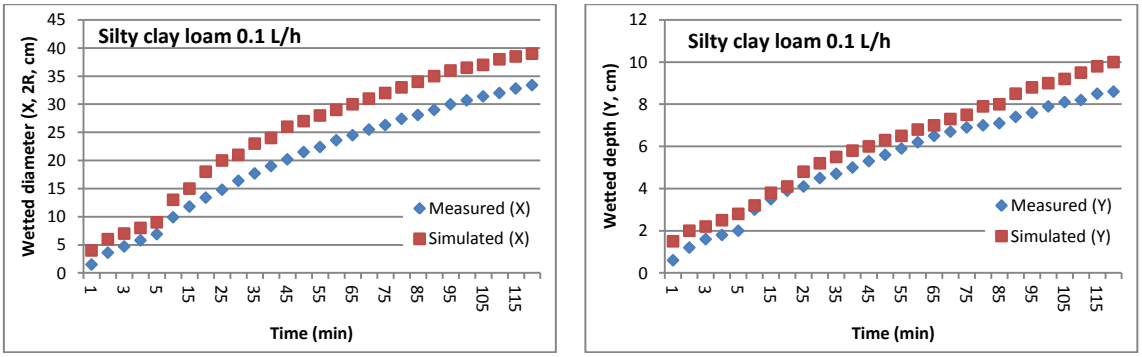

Figure 4.29: Measured and simulated wetted diameter (right side) and depth (left side) as a function of time for silty clay loam soil at different *Q*.

Measured and simulated wetting pattern dimensions for the sand and silt clay loam soils are in very good agreement, from the start to the end of water application. As mentioned above a large discrepancy occurs between the measured and simulated wetting pattern diameter for the sandy loam soil, where Hydrus-2D/3D overestimated the wetted distance. This discrepancy is unlikely to be due to errors in the characterisation of the hydraulic parameters of the soil, since these are comparable to those of other sandy loams found in both the Hydrus and SEISMIC databases. The lack of lateral spreading reflects low capillary pressures at the wetting front, and further numerical simulations (data not shown) show that large increases in the parameter α, to a value well above that of sands, are needed to match the wetted diameter observed experimentally. The photographs of the tank show, what appears to be, a layer of material made of coarser particles at the soil surface which may reduce the initial lateral spreading of water. Why such a segregation of particles has occurred during packing remains unclear.

Calculation of the root-mean-square-error (RMSE) for the measured and simulated wetting pattern dimensions represents the mean distance between measured and simulated depth and diameter of wetting pattern. The RMSE (Equation 13), as given by Kandelous *et al.* (2011) and Phogat *et al.* (2011), is given as:

$$RMSE = \sqrt{\frac{1}{n}\sum_{i=1}^{n}(Mi - Si)^2} \qquad 13$$

where *Mi* and *Si* are observed and simulated values and *n* is the number of observations. The RMSE values for each trial are given in table 4.2.

Table 4.2: Root mean square error (RMSE) between measured and simulated wetting pattern diameters (X) and depths (Y) for *Q* (L/h) ranged from 0.1 to 2 L/h.

Soil texture	RMSE (cm)									
	Q									
	0.1 L/h		0.5 L/h		1 L/h		1.5 L/h		2 L/h	
	X	Y	X	Y	X	Y	X	Y	X	Y
Sand	0.8	2.6	1.0	1.3	1.0	0.7	2.2	1.3	1.9	0.4
Sandy loam	9.9	1.4	9.9	1.0	-	-	-	-	-	-
Silty clay loam	5.0	0.8	-	-	-	-	-	-	-	-

The RMSE values ranged from 0.4 to 2.6 cm for the sand, from 1.0 to 9.9 cm for the sandy loam and from 0.8 to 5.0 for the silty clay loam soil. Overall the error was smaller for the wetted depth (Y) than the wetted diameter (X). The comparison in Table 4.2 shows that the model predicted correctly the vertical distribution of water (wetted depth) for all soils, with RMSE values < 2.6 cm. Good predictions of horizontal distribution were also obtained for the sand with RMSE values < 2.2 cm over the four flow rates. However, as noticed above the model simulations did not match the horizontal spreading in the sandy loam and resulted in RMSE values of 9.9 cm for both emitter discharge rates. The error was smaller in the silty clay loam with a RMSE of 5.0 cm.

Figures 4.30 and 4.31 show the wetted diameter and wetted depth as a function of volume of applied water for different emitter discharge rates as measured during the tank experiments.

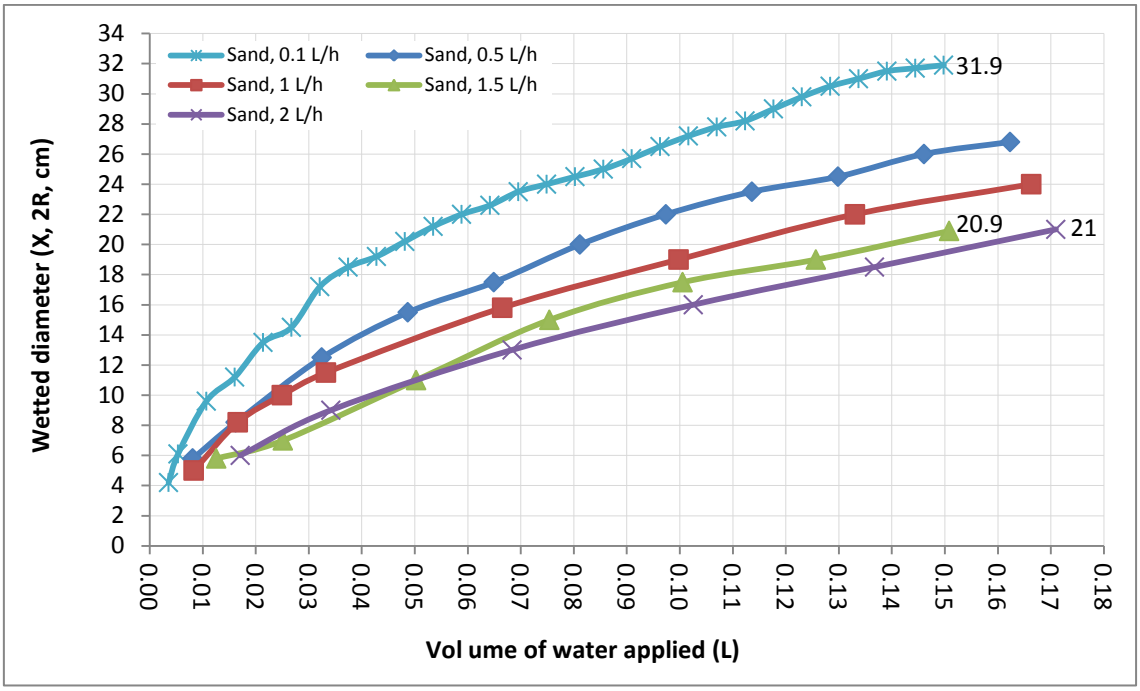

Figure 4.30: Measured wetted diameter in sand soil as a function of volume of applied water for different emitter application rates.

Figure 4.30 shows, that Q (L/h) had influence on soil wetted diameter. As Q (L/h) decreased, the wetted diameter increased. The wetted diameter at 0.15 L of water applied varied from 18.9 to 31.9 cm depending on the Q (L/h). These results are in agreement with the results observed for the sand soil from the SEISMIC database presented in section 4.1.2.

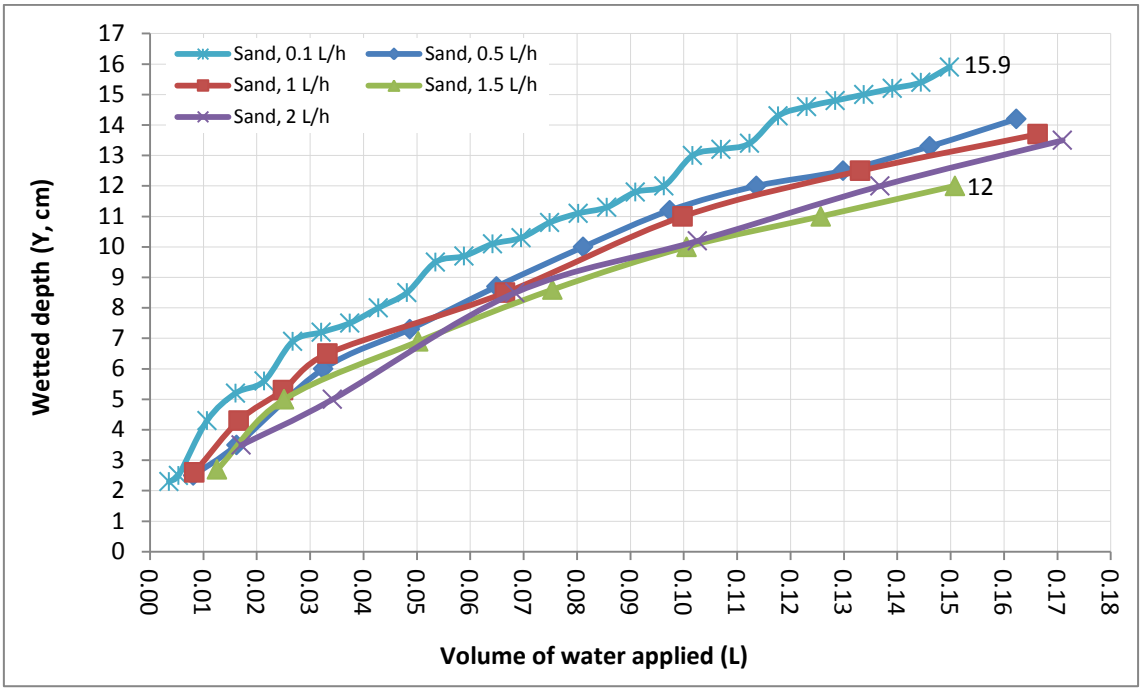

Figure 4.31: Measured wetted depth in sand soil as a function of volume of applied water for different emitter application rates.

Figure 4.31 shows that Q (L/h) in the sand influenced the wetted depth. In general, as the emitter discharge rate decreased the wetted depth increased but the influence was smaller than in the horizontal direction. At 0.15 L, the wetted depth for the Q of 0.1, 0.5, 1, 1.5 and 2 L/h was 15.9, 13.5, 13, 12.5 and 12 cm, respectively. These results are in contradiction with the results for sand soil from SEISMIC database, where Q (L/h) had no influence on the wetted depth in the sand soil. However, the emitter discharge rates used for SEISMIC soils were several orders of magnitude higher than those used in soil tank simulations but only varied by a factor of 2.7 (from 1.5 to 4 L/h) whereas for the soil tank simulations they varied by a factor of 20 (from 0.1 to 2 L/h). When the emitter discharge rates of the same magnitude (1.5 and 2 L/h) are used to compare both, SEISMIC and soil tank numerical simulations, the results show almost the same trend (Y for 1.5 and 2 L/h in SEISMIC soils is 57 cm for both cases and in soil tank simulations 1.5 L/h produces 12 cm and 2 L/h 12.5 cm deep wetting pattern).

4.1.5 Correlations between soil texture, hydraulic properties and horizontal and vertical wetting pattern dimensions

To analyse the effect of the soil texture, emitter discharge rates (Q), volume of applied water and soil hydraulic properties *(α, n, Ks* and free pore space, θ_f) on wetted radius and wetted depth, multiple linear regression analyses were carried out. θ_f was calculated subtracting initial soil moisture content from θ_s. The purpose of the analysis was to identify if any of the above parameters can explain the variation of soil wetting pattern radius and depth. Analysis was performed for the Hydrus-2D/3D simulations results for SEISMIC soils with all different emitter flow rates and initial soil moisture conditions (% depletion), presented in Tables 3.5, 3.6 and 3.7 in section 3.2.2.

All above soil parameters were used in multiple linear regression analysis and their effects on wetting pattern radius (X) and depth (Y) were examined. Pareto chart of effects was used to represent the effects of soil texture and hydraulic properties on X and Y (Figure 4.32 and 4.33). The Pareto chart's purpose is to highlight the most important parameters, among typically, a large set of parameters. The p value of 0.05 indicates which parameters are statistically significant. t-test checks the significance of individual regression coefficients.

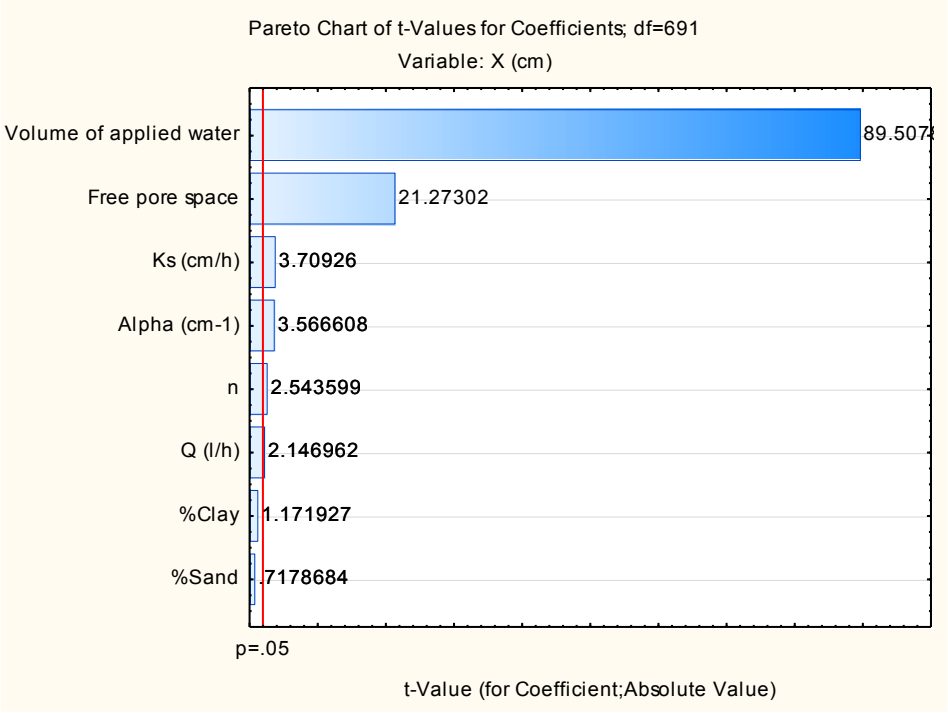

Figure 4.32: Pareto chart showing the relative frequency of soil parameters, affecting the radius (X) of wetting pattern.

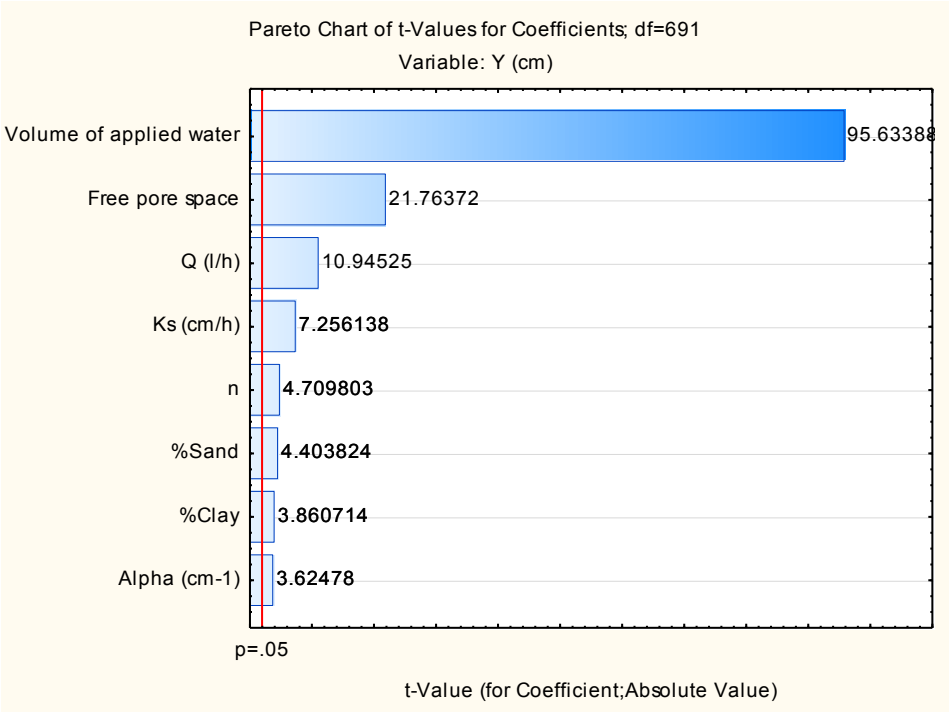

Figure 4.33: Pareto chart showing the relative frequency of soil parameters, affecting the depth (Y) of wetting pattern.

Figure 4.32 shows that volume of applied water (L), θ_f, *Ks* (cm/day) and α (cm^{-1}) have the highest significance in predicting the wetted radius (X) and are therefore used to build a model. All parameters, except % of clay and % of sand, are statistically significant. In figure 4.33 the volume of applied water, θ_f , *Q* (L/h) and *Ks* (cm/day) have the highest significance in predictions of wetted depth (Y) and, although all the other parameters are statistically significant, they add very little to wetted depth explanation. In both cases the parameters with lower or without statistical significance were removed from the model and new predictions, presented in Table 4.3, were made.

Table 4.3: Multiple regression equations describing the relationship between soil parameters and soil wetted radius (X) and depth (Y).

Dependent variable	Independent variable	Equation	Adj. R^2	p
X (cm)	Volume of water (V) (L), α (cm^{-1}), θ_f, *Ks* (cm/h)	$x = -57.9*\alpha - 34.14*\theta_f + 0.94*V + 0.09*Ks + 31.52$	0.92	$p < 0.001$
Y (cm)	Volume of applied water (V) (L), *Q* (L/h), θ_f, *Ks* (cm/h)	$y = 1.22*Ks - 1.27*Q - 90.8*\theta_f + 1.87*V + 31.8$	0.92	$p < 0.001$

The volume of applied water (L), θ_f, *Ks* (cm/day) and α (cm^{-1}) explained 92 % of variability of the wetted radius (X). Volume of applied water (L), θ_f, *Q* (L/h) and *Ks* (cm/h) explained 92 % of variability of wetted depth (Y). Analysis showed that independent variables, presented in Table 4.3, sufficiently explained the variability of X and Y. The full model, including all variables from Figures 4.32 and 4.33, explained 92 % of variability of X and 94 % of variability of Y.

Figure 4.34 shows observed vs. predicted values for relationship X and volume of applied water (L), θ_f, *Ks* (cm/h) and α (cm^{-1}). Predicted values cluster closely and homogeneously around the 1:1 line, indicating a good fit of the linear model. On that basis it can be concluded that the volume of applied water (L), θ_f, *Ks* (cm/h) and α (cm^{-1}) provides a good fit for the dependent variable of X (wetted radius). Figure 4.35 shows observed vs. predicted values for relationship Y and Volume of applied water θ_f, *Q* (L/h) and *Ks* (cm/h). Predicted values cluster quite closely and homogenously around

the 1:1 line. It can be concluded that volume of applied water, free pore space (θ_f), Q (L/h) and Ks (cm/h) provide a good fit for wetted depth (Y).

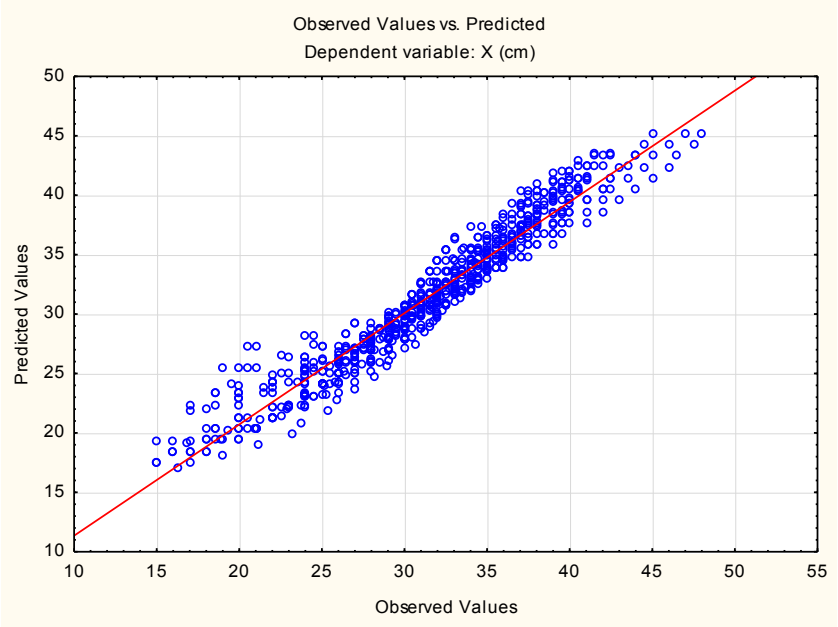

Figure 4.34: Observed values of X (cm) against those predicted from the relationship between X and volume of applied water (L), θ_f, Ks (cm/h) and α (cm^{-1}).

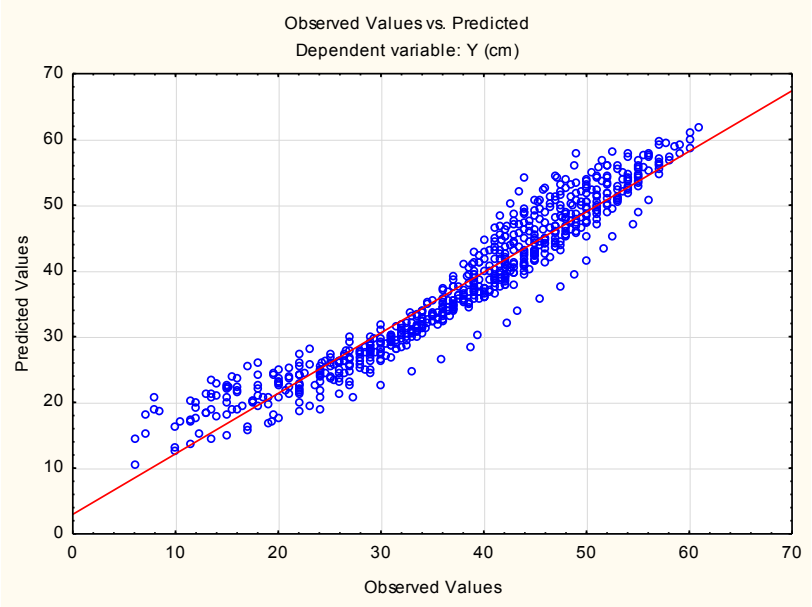

Figure 4.35: Observed values of Y (cm) against those predicted from the relationship between Y and volume of applied water, free pore space, Q (L/h) and Ks (cm/day).

Empirical models for predicting wetting patterns dimensions

Several models proposed that wetting pattern radius (X) and depth (Y) are mostly influenced by volume of applied water, as suggested by Li *et al*. (2003), emitter discharge rate (*Q*), saturated hydraulic conductivity (*Ks*) but also changes in volumetric water content ($\Delta\theta$) (Amin and Ekhmaj, 2006). In all these models, the radius (X) and depth (Y) of the wetting patterns are power functions of the above parameters rather than linear functions. In order to take this into account, the multiple regression analysis was run again, but now looking at log X and log Y against logarithm of volume of applied water (V), emitter discharge rate (*Q*), saturated hydraulic conductivity (*Ks*) as well as changes in water content ($\Delta\theta$). This allows assessing the predictive capabilities of these existing empirical models.

Li et al. (2003) model

Li *et al*. (2003) suggested that the surface wetted radius (X) and wetted depth(Y) are simply controlled by emitter discharge rate (*Q*) and time (t), which product is equal to the volume of water applied. On the basis of correlative analysis they suggested the following equations for the duration of irrigation necessary to achieve a desired radial and vertical wetting at a given emitter discharge rate:

$$x = 13.85(Q \times t)^{0.29} \quad 14$$

$$y = 8.69(Q \times t)^{0.53} \quad 15$$

These equations, however, were based on experimental results obtained for only one loam soil. Here, this simple model is tested against the data obtained with the Hydrus-2D/3D simulations. The relations obtained with the multiple regression analysis are presented in Table 4.4 and Figure 4.36.

Table 4.4: Multiple regression equations describing the relationship between log of volume of applied water (L) and log of soil wetted radius (X) and depth (Y).

Dependent variable	Independent variable	Equation	Adj. R^2	p
X (cm)	Volume of applied water (L)	$x = 18.2 \times V^{0.24}$	0.75	$p < 0.001$
Y (cm)	Volume of applied water (L)	$y = 12.9 \times V^{0.47}$	0.88	$p < 0.001$

The volume of applied water explained 75 % and 88 % of variability in wetted radius (X) and wetted depth (Y), respectively. Figure 4.36a and 4.36b show that observed vs. predicted values are quite scattered around the 1:1 line, indicating a poor fit of the simplified model proposed by Li *et al*. (2003).

a) b)

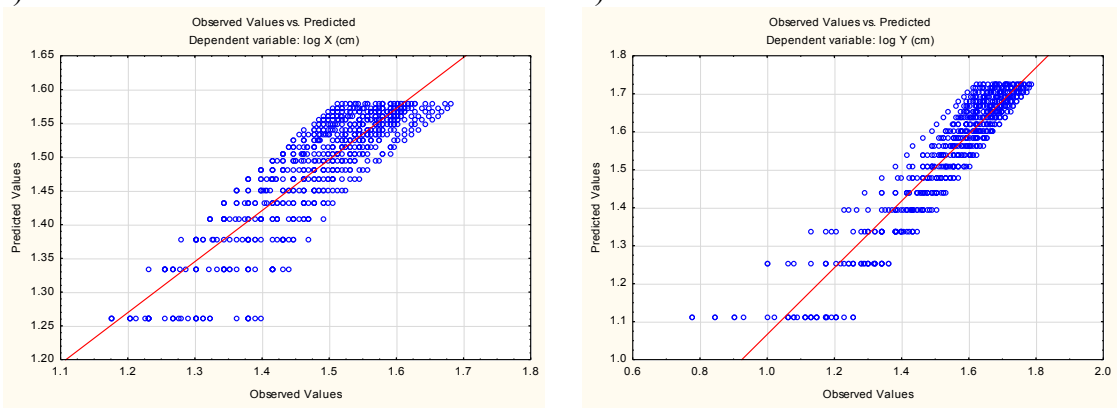

Figure 4.36: Observed values of log X (cm) (a) and log Y (cm) (b) against those predicted from the relationship between X and Y and log of volume of applied water.

Amin and Ekhmaj (2006) model

The model of Amin and Ekhmaj (2006) is presented is section 2.2.3. The results of the multiple regression analysis are presented in Table 4.5 and Figure 4.37. The change in volumetric water content ($\Delta\theta$) was calculated to be half of the θ_s as suggested by Kandelous and Šimunek (2010).

Table 4.5: Multiple regression equations describing the relationship between log of volume of applied water (L), *q* (L/h), *Ks* (cm/h), $\Delta\theta$ and log of soil wetted radius (X) and depth (Y).

Dependent variable	Independent variable	Equation	Adj. R^2	p
X (cm)	Volume of applied water (L), *Q* (L/h), *Ks* (cm/h), $\Delta\theta$	$x = 27.29 \times \Delta\theta^{0.146} \times Q^{0.018} \times Ks^{-0.122} \times V^{0.244}$	0.92	$p < 0.001$
Y (cm)	Volume of applied water (L), *Q* (L/h), *Ks* (cm/h), $\Delta\theta$	$y = 8.83 \times \Delta\theta^{-0.265} \times Q^{-0.131} \times Ks^{0.057} \times V^{0.473}$	0.92	$p < 0.001$

The of volume of applied water *V* (L), *Q* (L/h), *Ks* (cm/h) and $\Delta\theta$ explained 92 % of variability in both wetted radius (X) and wetted depth (Y).). Figure 4.37a and 4.37b show that observed vs. predicted values cluster quite closely to the 1:1 line, indicating a good fit of the model.

a) b)

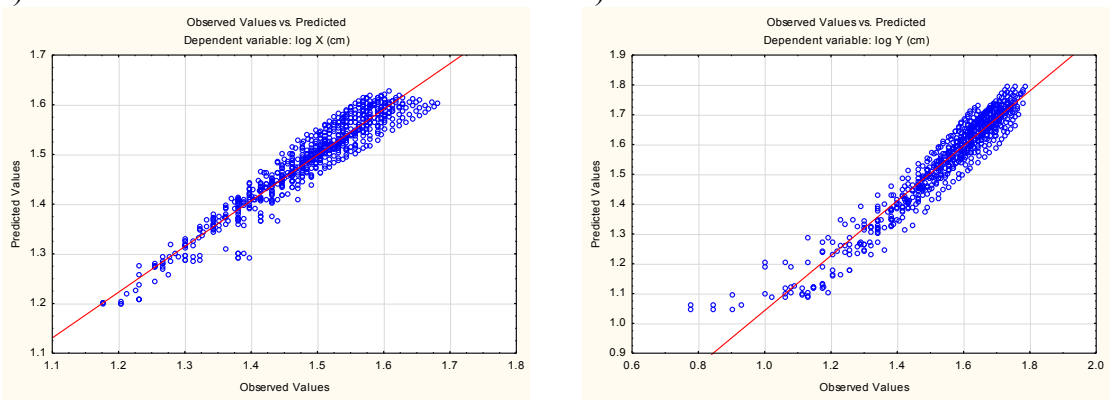

Figure 4.37: Observed values of log(X) (a) and log(Y) (b) against those predicted from the relationship between X and Y and log volume of applied water, log *Q*, log *Ks* and log $\Delta\theta$.

The size of the wetting pattern is a function of the available pore space into which water can infiltrate and therefore depends on both saturated water content, θ_s, (equivalent to total porosity), and initial moisture content θ_i. In the model of Amin and Ekhmaj (2006), this is not accurately represented by the parameter $\Delta\theta$ since the available or free pore space is $\theta_f = \theta_s - \theta_i$ and not $\theta_s/2$. Using θ_f *as* opposed to $\Delta\theta$ in the multiple regression leads to an improvement in the predictions where the model now explains 93 % of variability in wetted radius (X) and 95 % of variability in wetted depth (Y).

The linear multiple regression analysis presented above found that the combination of volume of applied water (L), free pore space θ_f, α (cm^{-1}) and *Ks* (cm/h) are the most important parameters, affecting wetting pattern movement in horizontal direction (radius – X). In vertical direction (depth – Y) the most important parameter are volume of applied water (L), free pore space (θ_f), *Ks* (cm/h) and *Q* (L/h). However, the analysis of log transformed values showed that prediction can be improved with less parameters (volume of water applied, *Q* and *Ks*) providing that indicators of available pore volume such as $\Delta\theta$ or θ_f are included. This is important, because as opposed to complex hydraulic parameters such as the van-Genuchten parameters, the parameters in these models are readily available or easy to measure. These findings corroborate the study of Kandelous and Šimůnek (2010), where the empirical model of Amin and Ekhmaj (2006) provided better results than the Schwartzman and Zur (1986) model, discussed in section 4.1.6. It can be therefore concluded that the influence of initial water content should be included in empirical models for estimating surface drip irrigation wetting patterns.

Comparison with exiting experimental data

The adopted models of Li *et al.* (2003) and Amin and Ekhmaj (2006) were compared to experimental results published by Li *et al*. (2003) (Figure 4.38). The positions of the wetted fronts are shown for different emitter discharge rates of 2.0, 5.0, and 7.8 L/h. The soil was a loam with 54 % sand, 34 % silt and 12 % clay and with *Ks* of 1.85 cm/h. Approximately 13.3 L of water was applied in all cases

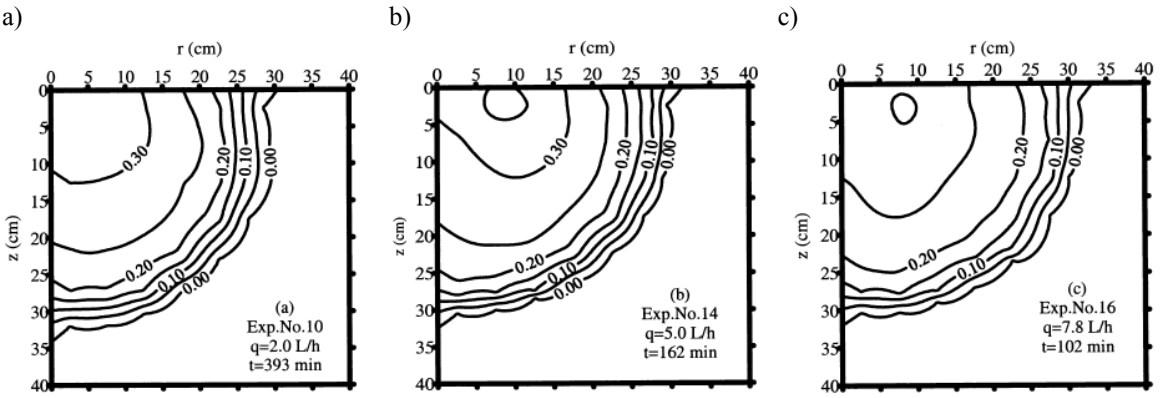

Figure 4.38: Change in volumetric water content distribution for 2.0 (a), 5.0 (b), and 7.8 (c) L/h emitter application rates after adding approximately 13.3 L of water. After Li *et al*. (2003)

These data are compared to predictions of modified Amin and Ekhmaj (AE) and Li *et al*. (2003) (L) model in Table 4.6.

Table 4.6: Observed wetting pattern geometry in Li *et al*. (2003) paper compared to predicted wetting pattern geometry of modified Amin and Ekhmaj (2006) (AE) and Li *et al*. (2003) (L) models.

	Wetted radius (X) (cm)					Wetted depth (Y) (cm)				
Q(L/h)	**Observed[1]**	**AEi[2]**	**AEe[3]**	**Li[4]**	**Le[5]**	**Observed**	**AEi**	**AEe**	**Li**	**Le**
2	30	39	27,7	33.9	29.3	34	41.7	29.2	43.5	34,2
5	32	39.7	27,7	33.9	29,3	32	37	26.6	43.5	34,2
7.8	34	40	27.6	33.9	29,3	32	35	25.4	43.5	34,2

[1] Observed geometry of wetting pattern in Li et al. (2003)
[2] Improved Amin and Ehhmaj (2006) model using θ_f
[3] Existing Amin and Ekhmaj model
[3] Improved Li et al. (2003) model fitted to the data from this study
[4] Existing Li *et al*. model

Table 4.6 shows that the wetted radius and wetted depth predicted from the models with coefficients obtained by fitting them data from this study were not in good agreement with Li *et al*. (2003) results from laboratory experiments. Note that Li *et al*. (2003) model provides more accurate predictions simply because the coefficient of the model were obtained for a single soil using the data presented in Figure 4.38. It is likely that the Amin and Ekhmaj (2006) model can predict wetting pattern geometries for a wider range of soils and emitter discharge rates under surface point source emitter.

4.1.6 Comparison with existing simple analytical model

According to Schwartzman and Zur (1986), the wetted soil volume under a point source is mainly dependent on the hydraulic conductivity of the soil (*Ks*), the emitter discharge rate (*Q*) and the total volume of applied water (V). They used dimensional analysis to develop an analytical model to predict horizontal and vertical wetting pattern positions under surface drip irrigation. The following functions were considered for wetted soil dimensions under point source:

$$x = f_1(V, Q, Ks) \quad 16$$

$$y = f_2(V, Q, Ks) \quad 17$$

where y (cm) is depth of the wetting and x (cm) is diameter of the wetted soil volume at its widest point.

In order to reduce the number of variables, the dimensionless forms of the above parameters were presented as below.

$$V^* = V\left(\frac{Ks}{Q}\right)^{\frac{3}{2}} \quad 18$$

$$y^* = y\left(\frac{Ks}{Q}\right)^{\frac{1}{2}} \quad 19$$

$$x^* = x\left(\frac{Ks}{Q}\right)^{\frac{1}{2}} \quad 20$$

Then the dimensionless parameters, as V^*, x^* and y^* were extracted from experimental or simulated results. It was assumed, that the relationship between the dimensionless parameters was:

$$x^* = A_1 V^{*n_1} \quad 21$$

$$y^* = A_2 V^{*n_2} \quad 22$$

where, A_1, A_2 n_1 and n_2 are constants for the cylindrical flow model.

Then, to convert dimensionless equations to dimensional ones, the relationship in equations 18, 19 and 20 are used, which results in following equations.

$$x = A_1 V^{n_1} \left(\frac{Ks}{Q}\right)^{\frac{3n_1}{2} - 1/2} \quad 23$$

$$y = A_2 V^{n_2} \left(\frac{Ks}{Q}\right)^{\frac{3n_2}{2} - 1/2} \quad 24$$

Based on results, presented by Bresler (1978) for a point source surface dripper they estimated the model's constants through regression analysis to obtain the equations 25 and 26. The soils used in Bresler (1971) were Gilat loam (48 % sand and 20 % clay), which is a clay loam according to UK textural triangle, and Sinai sand (97 % sand and 1 % clay). Both soils come from Israel. The *Ks* was 2.4×10^{-6} m/s for Gilt loam and 7.6×10^{-6} m/s for Sinai sand soil. Two emitter discharge rates used were 1.1×10^{-6} m^3/s (4 L/h) and 5.6×10^{-6} m^3/s (20 L/h). Therefore, the combined effect of emitter discharge rates, soil hydraulic properties and water application times on wetting pattern geometry, used to develop this model, are based on Bresler's (1978) results and are presented on Figure 4.39. The figure shows computed contours which represent the position of the wetting front for various times for above mentioned soils and emitter discharge rates.

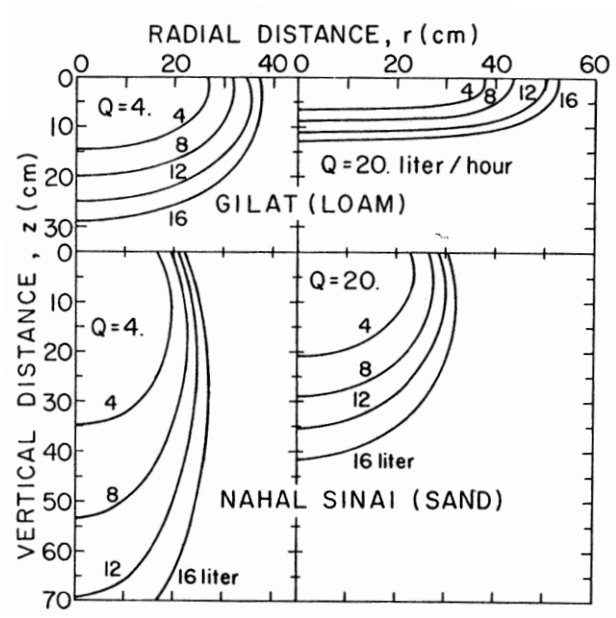

Figure 4.39: Wetting front position as a function of emitter discharge rate (*Q*) and cumulative infiltration (L) for two soils. After Bresler (1978)

With converting dimensionless equations using equations 23 and 24 to dimensional ones, the result was as follows.

$$x=1.82\ V^{0.22}\left(\frac{Ks}{Q}\right)^{-0.17} \qquad 25$$

$$y=2.54\ V^{0.63}\left(\frac{Ks}{Q}\right)^{0.45} \qquad 26$$

It is worth noting, that the predicted values using this model were not compared to those obtained with laboratory or field experiments.

In this section the Schwartzman and Zur (1986) analytical model is tested against the data obtained with the Hydrus-2D/3D simulations presented in section 4.1.2.

The dimensionless wetted radius (x^*), wetted depth (y^*) and amount of water applied (V^*) were calculated from the X and Y data obtained with the numerical simulations for

each volume of applied water V, using the appropriate values of *Ks* for each soil texture and the known emitter discharge rate.

Figure 4.40 and 4.41 show the relationship between *V**, *x** and *y** for the results obtained with the 11 soil textures, the three flow rates and the three different initial moisture contents.

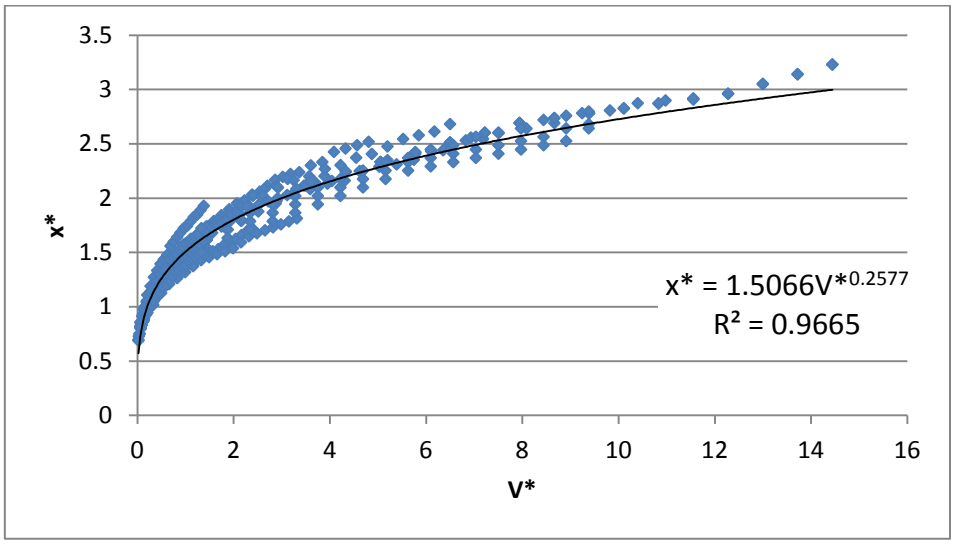

Figure 4.40: Relationship between *V and *x** obtained from simulated results for at treatments.**

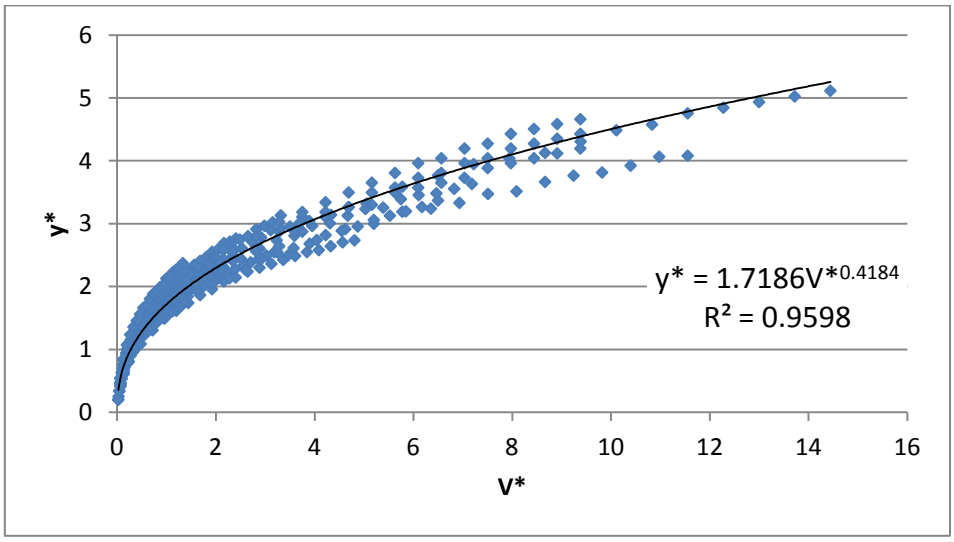

Figure 4.41: Relationship between *V and *x** obtained from simulated results for all treatments.**

The relationship between dimensionless V^* and x^* from Figure 4.40 resulted in following power equation with value R^2 of 0.97.

$$x^* = 1.51V^{*0.26} \quad (27)$$

Similarly, the relationship between dimensionless V^* and y^* from Figure 4.41 resulted in following power equation with value R^2 of 0.96.

$$y^* = 1.72V^{*0.42} \quad (28)$$

Values of constants A_1, A_2 n_1 and n_2, regarding to equations 21 and 22 from the model, were 1.51, 1.72, 0.26 and 0.42, respectively. With converting dimensionless equations 27 and 28 to dimensional ones, using equations 23 and 24, resulted in the following relation (equations 29 and 30).

$$x=1.51\ V^{0.26}\left(\frac{Ks}{Q}\right)^{-0.113} \quad (29)$$

$$y=1.72\ V^{0.42}\left(\frac{Ks}{Q}\right)^{0.128} \quad (30)$$

The performance of improved Schwartzam and Zur model is illustrated on Figures 4.42 and 4.43. Observed and predicted values for wetted radius and depth were transformed, using logarithmic transformation. Linear regression analysis of the results was done and correlation coefficient (R^2) of 0.95 for wetted radius and of 0.89 for wetted depth, were observed.

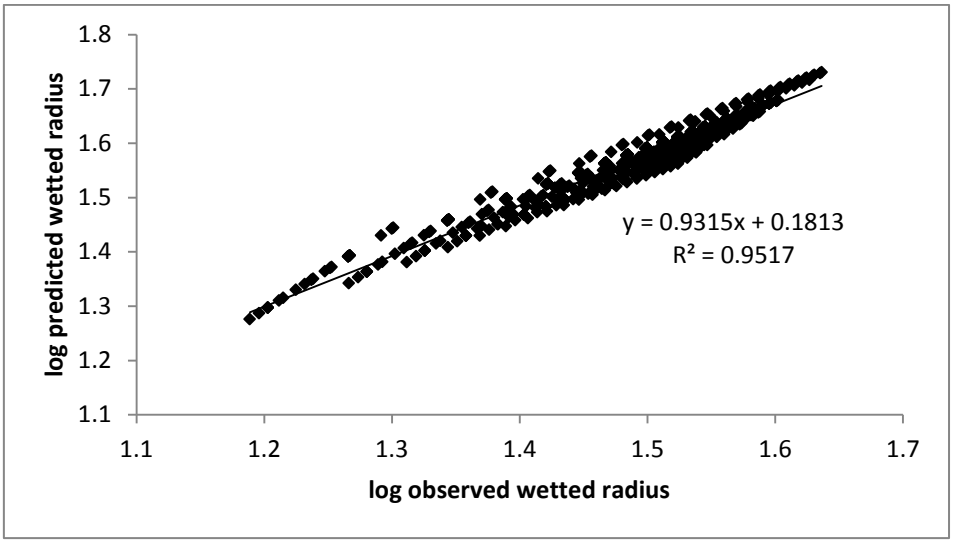

Figure 4.42: Logarithmic observed and simulated wetted radius (X) under surface drip emitter using improved Schwartzman and Zur model.

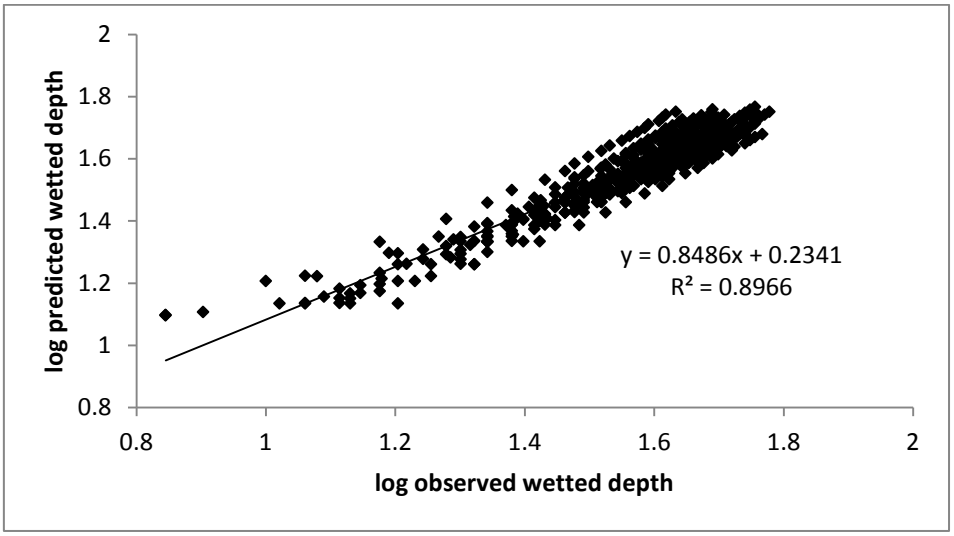

Figure 4.43: Logarithmic observed and simulated wetted depth (Y) under surface drip emitter using improved Schwartzman and Zur model.

Predicted radius and depth of the wetted soil around a point source surface emitter, based on improved Schwartzman and Zur model were in good agreement with observed (measured) data. For further analysis, the RMSE (Equation 13, section 4.1.4) and EF (Modelling efficiency) (Equation 31) statistical parameters were used to test the performance of the improved model against observed values and the existing model. EF, as given by Smith *et al.* (1996) *"provides a standard method for assessing the accuracy of simulations by comparing the variance of predicted from observed values*

to the variance of observed values from the mean of the observations." In other words, this is a comparison of the efficiency of the selected model (improved Schwartzman and Zur) to the efficiency of a very simple predictive model - the mean value of the observations.

The EF is given as:

$$EF = \frac{(\sum_{i=1}^{n}(Mi - \bar{M})^2 - \sum_{i=1}^{n}(Si - Mi)^2)}{\sum_{i=1}^{n}(Mi - \bar{M})^2} \quad 31$$

where, *Mi* and *Si* are measured and observed values, $\bar{M}$ is the mean of the observed (measured) data and *n* is the number of observations.

EF value has the maximum at 1, in which case the predicted values perfectly match with the observed ones. When EF value is less than 0, the simulated values are worse than simply using the observed mean. In that case model is not performing well.

RMSE and EF values were compared separately for the improved and existing Schwartzman and Zur (1986) model and for each of the simulated combinations, as given in Table 4.7. The RMSE values between measured and predicted wetted radius ranged from 0.41 cm to 4.71 cm for the improved model and from 2.63 to 11.69 for the existing model. Values between measured and predicted depth ranged from 0.74 to 9.95 for improved model and from 1.76 cm to 63.29 cm for existing model. EF values between measured and predicted wetted radius varied from 0.99 to 0.32 for the improved model and from 0.82 to -6.18 for model. EF for wetted depth varied from 0.99 to -0.19 for the improved model and from 0.98 to -43.97 for the existing model.

Table 4.7: Statistical analysis of improved model performance in comparison to existing model.

			Wetted radius (X, cm)				Wetted depth (Y, cm)			
	Q[1]	IC[2]	RMSE[3]		EF[4]		RMSE		EF	
Soil	(L/h)	(%)	I[5]	E[6]	I	E	I	E	I	E
Sandy Loam	2	50	0.41	4.44	0.99	0.32	2.32	47.29	0.95	-20.37
Loamy Sand	2	50	2.97	9.07	0.55	-3.19	4.40	20.44	0.87	-1.75
Sandy Clay Loam	2	50	0.77	3.08	0.98	0.67	5.69	62.26	0.65	-41.49
Sand	2	50	0.83	4.72	0.98	0.21	0.74	50.73	0.99	-17.73
Silty Clay	2	50	2.20	3.86	0.88	0.63	2.93	32.15	0.90	-11.17
Sandy Clay	2	50	0.50	5.20	0.99	0.17	1.74	31.48	0.97	-8.04
Clay	2	50	1.31	8.58	0.94	-1.59	3.22	13.59	0.92	-0.47
Silty Clay Loam	2	50	2.53	3.20	0.86	0.77	6.04	42.73	0.53	-22.62
Clay Loam	2	50	1.62	9.99	0.89	-3.10	4.96	4.35	0.83	0.87
Silt Loam	2	50	1.03	6.52	0.97	-0.12	0.78	17.35	0.99	-2.00
Sandy Silt Loam	2	50	1.92	3.07	0.90	0.75	4.42	47.26	0.80	-22.42
Silt loam	1.5	50	2.59	4.19	0.85	0.60	1.07	23.84	0.99	-4.83
Sand	1.5	50	1.12	2.63	0.96	0.78	0.83	63.29	0.99	-29.66
Clay	1.5	50	0.81	5.95	0.98	-0.09	2.23	20.48	0.95	-2.87
Silt loam	4	50	1.71	10.61	0.88	-3.62	2.44	35.58	0.95	-9.23
Sand	4	50	3.79	9.41	0.32	-3.19	3.15	26.83	0.93	-3.85
Clay	4	50	2.62	11.69	0.64	-6.18	5.22	1.76	0.84	0.98
Silt loam	2	30	4.71	3.16	0.59	0.82	4.95	12.32	0.82	-0.13
Sand	2	30	0.83	3.90	0.98	0.56	2.96	48.41	0.94	-13.97
Clay	2	30	1.67	5.86	0.92	0.03	8.31	9.15	0.54	0.44
Silt loam	2	70	1.24	8.46	0.95	-1.45	9.95	61.09	-0.19	-43.97
Sand	2	70	1.77	5.72	0.89	-0.16	5.21	11.90	0.77	-0.18
Clay	2	70	2.54	9.84	0.74	-2.92	1.12	16.24	0.99	-1.37

[1] Emitter discharge
[2] Soil moisture initial conditions (% depletion from FC)
[3] Root mean square error
[4] Modelling efficiency
[5] Improved Schwartzman and Zur model
[6] Existing Schwartzman and Zur model

Total performance of the improved model was good, with average EF of 0.85 for wetted radius and 0.82 for wetted depth. Average EF of existing (unimproved) model was -0.84 and -11.12 for wetted radius and depth, respectively. The RMSE values indicated the

same differences between each model's performances. The improved model resulted in average RMSE values of 1.80 cm for wetted radius and 3.68 cm for wetted depth. Average RMSE values for the existing model were 6.22 cm for wetted radius and 30.46 cm for wetted depth. Overall, both improved and existing models predicted soil wetted radius better than wetted depth. Statistical analysis of the improved model showed some discrepancies between simulated and observed wetting pattern predictions in sand, silt loam and clay soils with higher emitter discharge rates and lower soil moisture initial conditions. The reason for this can be found in the higher number of soils with the same emitter discharge rate and initial soil moisture conditions used in the model modification procedure. The model can be used for wide range of soil types, initial soil moisture conditions and emitter discharge rates (from 1.5 to 4 L/h) and up to maximum 20 L of water applied.

The values of the constants A_1, A_2 n_1 and n_2 of the Schwartzaman and Zur (1986) model when fitted to the data of this study were 1.51, 1.72, 0.26 and 0.42, respectively. In comparison, the same parameters, of A_1, A_2 n_1 and n_2 of existing Schwartzaman and Zur (1986) model, were 1.82, 2.54, 0.22 and 0.63, respectively. Existing model of Schwartzman and Zur is based on two soils and two different emitter discharge rates of Bresler (1978) research and is as such unlikely to represent the best fit for all soils from textural triangle. The new model constants result from the best fit for many more soil textural classes, three different emitter discharge rates and different initial soil moisture conditions. The Schwartzaman and Zur (1986) model results, using both our new and the old model constants, were compared to experimental results published by Li *et al*. (2003) (Figure 4.44) as described below (Table 4.8).

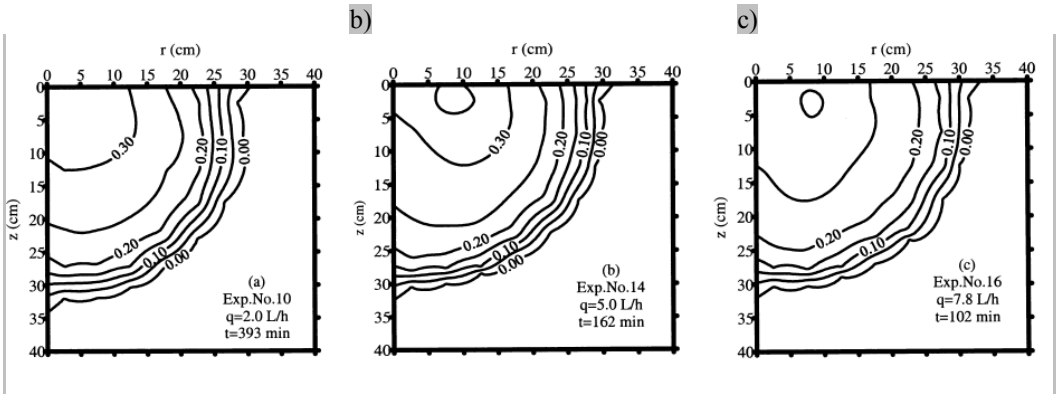

Figure 4.44: Change in volumetric water content distribution for 2.0 (a), 5.0 (b), and 7.8 (c) L/h emitter application rates after adding approximately 13.3 L of water. After *Li et al.* (2003)

The predicted and observed wetted depth and radius are compared in Table 4.8.

Table 4.8: Observed wetting pattern geometry in Li *et al.* (2003) paper compared to predicted wetting pattern geometry of improved Schvartzman and Zur model (M) and existing Schwartzman and Zur model (E).

	Wetted radius (X)			Wetted depth (Y)		
Q **(L/h)**	**Observed[1]**	**M[2]**	**E[3]**	**Observed**	**M**	**E**
2	30	38	48	34	37	45
5	32	42	56	32	33	30
7.8	34	44	61	32	31	24

[1] Observed geometry of wetting pattern in Li et al. Paper
[2] Schwartzman and Zur model with new constants
[3] Schwartzman and Zur model with old constants

The results show that the wetted radius and wetted depth predicted with Schwartzman and Zur model were in better agreement with Li *et al.* (2003) results when using the new model constants.

To get an equation for the radius of the wetted soil volume, the equations 29 and 30 can be combined as follows:

$$x = 1.08\, y^{0.62} \left(\frac{Ks}{Q}\right)^{0.25} \qquad 32$$

Above equation 32 can be used to get the relationship between soil wetted radius (X) and depth (Y) and Q for given soil type (Ks). Wetted radius (Y) represents half of the emitter spacing and has to be multiplied by 2, to get emitter spacing for continuous non-overlapping geometry (wetted strip of soil). Wetted depth (Y) in this equation is not an independent parameter, but represents the rooting depth of the specified crop.

5 Conclusions and recommendations

5.1 Conclusions

The influence of the soil texture, soil hydraulic properties and irrigation system design parameters on the size of the wetted area under point source surface irrigation was studied numerically with the model Hydrus-2D/3D, and experimentally with simple two-dimensional soil tanks experiments.

The influence of soil type (texture) and volume of applied water on soil wetting pattern dimensions, for all soil texture classes from SEISMIC database, was investigated. As expected, the size of the wetting pattern in both directions increased with the volume of applied water. The increase was not linear and the wetting front in both directions moved faster at the beginning of the water application, and slowed down with increase in volume of water applied, as the wetting pattern moved away from the source. The wetted radius for a given volume of applied water tended to be larger for fine-textured soils (silt loam, silty clay, clay loam, sandy silt loam and clay) and smaller for coarse-textured soils (sand, loamy sand, sandy clay loam and sandy loam). The wetted depth tended to be larger for coarse-textured soils such as sand, loamy sand and sandy clay. The smallest wetted depth occurred in fine-textured soils such as silty clay loam, silty clay and silt loam. As the volume of applied water increased, the rate of increase in wetted depth was larger than that in wetted radius, which was due to the gravity effects. In the coarse-textured soils (sand and loamy sand), where gravitational flow tends to dominate, the wetting pattern depth was larger than the wetting pattern diameter. In fine-textured soils (silty clay loam, silty clay and silt loam), the wetting pattern depth and diameter had about the same length.

The study of influence of different emitter discharge rates was conducted to investigate the influence on dimensions of wetting patterns for three contrasting soil texture classes. At the end of water application, the emitter discharge rates slightly affected radial water movement in all cases. Decreased discharge rates resulted in a slight increase in the wetting pattern radius for all soils. Conversely emitter discharge rate had no effect on the wetted depth in the sand and clay soils. The only effect of discharge rates was

observed in the silt loam. The different flow rates had a small effect on the final size of the wetting pattern in all experiments conducted, but large differences in the position of the wetted front close to saturation were observed. Higher emitter discharge rates resulted in larger saturated wetting pattern radius and depth in all experiments. The effect was even more pronounced for wetted depth in the soils with coarser textures (sand soil). At the saturated front, larger water content gradients were observed with the higher emitter discharge rates treatments. This was true for all soil textures and in both directions. However, those results are based on numerical simulations and for only three emitter discharge rates. In addition, the results of discharge rates influence on the wetting pattern dimensions were analysed at the end of the irrigation cycle and may have been different at the early stages of irrigation (i.e. different volume of water applied). In the soil tank experiments with the sand soil, a decrease in emitter discharge rate resulted in an increase in wetted diameter and wetted depth. These results were in agreement with the simulated wetted diameter of the SEISMIC database sand, but not with the simulated wetted depth. However, the emitter discharge rates used in the numerical simulations were much larger than those used in the soil tank experiments.

The study of the influence of different initial soil moisture conditions on the size of the wetting pattern in horizontal and vertical directions were studied for three contrasting soil textures. Higher initial soil moisture conditions caused larger wetting pattern sizes in both horizontal and vertical directions for all soils. Different initial soil moisture conditions had larger effect on the fine-textured clay and silt loam soils in both directions. Also, an increase in initial soil moisture content resulted in less sharp water content gradient at the wetting front for all soils.

The performance of the Hydrus-2D/3D model was tested by comparing it to simple two-dimensional soil tank experiments. In general, the depths and diameters of simulated and measured wetting patterns were in very good agreement for the sand and silty clay loam soils. However, despite a relatively good agreement between measured and simulated wetted depth in the sandy loam soil, Hydrus-2D/3D overestimated the wetted diameter and the discrepancy was large. The RMSE values ranged from 0.4 to 2.6 cm for the sand, from 1.0 to 9.9 cm for the sandy loam and from 0.8 to 5.0 for the silty clay

loam soil. Overall the error was smaller for the wetted depth than the wetted diameter. Why a large discrepancy occurred between the measured and simulated wetting pattern diameter for the sandy loam soil was unclear, but is unlikely to be due to errors in the characterisation of the hydraulic parameters of the soil. They may be due to a thin layer of material made of coarser particles at the soil surface which may reduce the initial lateral spreading of water.

The linear multiple regression analysis found that the combination of volume of applied water, free pore space (θ_f), α and *Ks* are the most important parameters, affecting wetting pattern movement in horizontal direction. They explained 92 % of variability of the wetted radius. In vertical direction the most important parameters are volume of applied water, free pore space (θ_f), *Ks* and *Q*, they explained 92 % of variability of the wetted depth. The analysis of log transformed values showed that prediction can be improved with less parameters (volume of water applied, *Q* and *Ks*) providing that indicators of available pore volume such as $\Delta\theta$ or θ_f are included. The multiple regression showed that the of volume of applied water, *Q*, *Ks* and $\Delta\theta$ explained 92 % of variability of wetted radius and 92 % of the variability of wetted depth. Using θ_f *as* opposed to $\Delta\theta$ in the multiple regression leads to an improvement in the predictions where the model now explains 93 % of variability in wetted radius and 95 % of variability in wetted depth. It can be therefore concluded that the influence of initial water content should be included in empirical models for estimating surface drip irrigation wetting patterns.

The simple analytical model of Schwartzman and Zur (1986) was tested against the data obtained with the Hydrus-2D/3D simulations. The values of the model constants A_1, A_2 n_1 and n_2 of the Schwartzaman and Zur (1986) model when fitted to the data of this study were 1.51, 1.72, 0.26 and 0.42, respectively. In comparison, the same parameters, of A_1, A_2 n_1 and n_2 of existing Schwartzaman and Zur (1986) model, were 1.82, 2.54, 0.22 and 0.63, respectively. The existing model of Schwartzman and Zur is based on two soils and two different emitter discharge rates and is as such unlikely to represent the best fit for soils from all textural classes. The new model constants result from the

best fit for many more soil textural classes, three different emitter discharge rates and different initial soil moisture conditions.

5.2 Recommendations

Further improvements of this work can be done in the means of practical integration into field work and additional modelling and irrigation scenario analysis. Below the areas, that need particular attention, are listed:

- Further study and simulations are needed to include the missing interactions between surface drip irrigation and specific plant root water uptake and transpiration.
- Analysis of Hydrus-2D/3D simulations using the new surface drip boundary condition which allows dynamic evaluation of the wetted area.
- Analysis of wider simulated range of emitter discharge rates (e.g. 0.1 to 12 L/h) and initial soil moisture conditions (depletions), would contribute to amelioration of current analytical models and therefore better predictions of emitter spacing under different irrigation systems operating conditions.
- Analysis of wetting pattern sizes after allowing water to redistribute after irrigation cut off (e.g. for period of 24 h).
- Comparisons with field experiments (effect of soil layers, soil structure and soil management such as tillage).
- Soil tank experiments with more soil types are necessary to test further the predictive capability of Hydrus-2D/3D.
- Analysis of the effect of irrigation scheduling (time of day (night, day), pulsed irrigation) on the geometry of the wetting pattern.
- Numerical studies of subsurface drip irrigation using Hydrus-2D/3D new subsurface drip boundary condition.

References

Ah Koon, P.D., Gregory, P.J., Bell, J.P. (1990) Influence of drip irrigation emission rate on distribution and drainage of water beneath a sugarcane and a fallow plot. Agricultural Water Management, 17, 267-282

Amin, M.S.M., Ekhmaj, A.I.M. (2006) DIPAC-drip irrigation water distribution pattern calculator. In: 7th International micro irrigation congress, 10–16 Sept, PWTC, Kuala Lumpur, Malaysia

Angelakis, A.N., Rolston, D.E., Kadir, T.N., Scott, V.N. (1993) Soil-water distribution under trickle source. J. Irrig. Drain. Eng., 119, 484–500

ASAE standard ASAE S526.3 September (2007) Soil and water terminology. American Society of Agricultural and Biological Engineers (ASABE), St. Joseph, Michigan, 22 p.

Assouline, S. (2002) The effects of microdrip and conventional drip irrigation on water distribution and uptake, Soil Sci. Soc. Am. J., 66, 1630-1636

Bar-Yosef, B; Sheikholslami, M.R. (1976) Distribution of water and ions in soils irrigated and fertilized from a trickle source. Soil Science Society of America Journal, 40, 575-582

Bates, B.C., Kundzewicz, Z.W., Wu, S., Palutikof, J. P. (2008) Climate Change and Water. Technical Paper of the Intergovernmental Panel on Climate Change, IPCC Secretariat, Geneva, 210 p.

Ben-Gal, A., Lazarovitch, N., Shani, U. (2004) Subsurface drip irrigation in gravel-filled cavities. Vadose Zone J., 3, 1407–1413

Brandt, A., Bresler, E., Diner, N., Ben-Asher, I. K., Heller, J., Goldberg, D. (1971) Infiltration from a trickle source: I. Mathematical models. Soil Science Society of America, 35, 683-689

Bresler, E., Heller, J., Diner, N., Ben-Asher, J., Brandt, A., and Goldberg, D. (1971) Infiltration from a trickle source. II: Experimental data and theoretical predictions. Soil Sci. Soc. Am. Proc., 35, 683–689

Bresler, E. (1975) Two-dimensional transport of solutes during non-steady infiltration from a trickle source. Soil Science Society of America Proceedings, 39, 604-613

Bresler, E. (1978) Analysis of trickle-irrigation with application to design problems. Irrigation Science, 1, 3-17

Bruinsma, J. (2003) World Agriculture: Towards 2015/2030. An FAO Perspective. Earthscan, London, 444 p.

Bufon, V.B., Lascano, R.J., Bednarz, C., Booker, J.D., Gitz, D.C. (2011) Soil water content on drip irrigated cotton: comparison of measured and simulated values obtained with the Hydrus 2-D model, Irrigation Science, DOI: 10.1007/s00271-011-0279-z

Camp, C.R. (1998) Subsurface drip irrigation: a review. Trans ASAE 41, 1353–1367

Cook, F.J., Thorburn, P.J., Fitch, P., Bristow, K.L. (2003) Wet up: A Software Tool to Display Approximate Wetting Patterns from Drippers. Irrig. Sci., 22, 129-134

Cote, C.M., Bristow, K.L., Charlesworth, P.B., Cook, F.J., Thorburn, P.J. (2003) Analysis of soil wetting and solute transport in subsurface trickle irrigation, Irrig. Sci., 22, 143–156

Dahiya, R., Jhorar, J.B.S., Malik, R.S., Ingwersen, J., Streck, T. (2007) Simulation of water and heat transport in drip-irrigated sandy soil under mulched conditions, J. Indian Soc. Soil Sci., 55 (3), 233-240

Dasberg, S. and Or, D. (1999) Drip irrigation. Springer Verlag, Berlin, 162 p.

Dorenbos, J. and Pruitt, W.O. (1984) Crop Water Requirements - Guidelines for Predicting Crop Water Requirements. FAO Irrigation and Drainage Paper 24, FAO, Rome

Elmaloglou, S. and. Diamantopoulos, E. (2009) Simulation of soil water dynamics under subsurface drip irrigation from line sources, Agricultural Water Management, 96, 1587–1595

Evans, R.G., Wu, I.P., Smystrala, A.G. (2007) Design of Microirrigation Systems. Chapter 17, in: Glenn J. Hoffman, Robert G. Evans, Marvin E. Jensen, Derrel L. Martin, Ronald L. Elliott, Design and Operation of Farm Irrigation Systems. 2nd edition. ASABE Special Monograph, 633-683 p.

FAO (2002a). Irrigation manual. Planning, development monitoring and evaluation of irrigated agriculture with farmer participation, Module 9: Localized irrigation systems planning, design, operation and maintenance (English) Savva, A.P., FAO, Harare (Zimbabwe). Subregional Office for Southern and East Africa, 2002, 82 p.

FAO (2002b). Irrigation manual. Planning, development monitoring and evaluation of irrigated agriculture with farmer participation, Module 4: Crop Water Requirements and Irrigation Scheduling (English), Savva, A.P., Frenken, K., FAO, Harare (Zimbabwe). Subregional Office for Southern and East Africa , 2002, 138 p.

Fernandez-Galvez J., Simmonds, L.P. (2006) Monitoring and modelling the three-dimensional flow of water under drip irrigation, Agricultural Water Management, 83 (3), 197-208

Fischer, G., F.N. Tubiello, H. van Velthuizen and D. Wiberg (2007): Climate change impacts on irrigation water requirements: Effects of mitigation, 1990–2080. Tech. Forecasting Soc. Ch., 74 1083–1107

Gardenas, A, Hopmans, J.W., Hanson, B.R., Šimůnek, J. (2005) Two dimensional modeling of nitrate leaching for various fertigation scenarios under micro-irrigation. Agric Water Manag 74,219– 242

Hammami, M., Daghari, H., Balti, J., Maalej, M.. (2002) Approach for predicting the wetting front depth beneath a surface point source: Theory and numerical aspect. Irrig. Drain., 51 (4), 347–360

Kandelous, M.M., Liaghat, A., Abbasi, F. (2008) Estimation of soil moisture pattern in subsurface drip irrigation using dimensional analysis method. J Agri Sci 39 (2), 371–378 (in Persian), cited in Kandelous, M.M., and Šimůnek, J. (2010 b). Numerical simulations of water movement in a subsurface drip irrigation system under field and laboratory conditions using HYDRUS-2D, Agricultural Water Management, 97, 1070-1076

Kandelous, M.M. and Šimůnek, J. (2010a) Comparison of numerical, analytical and empirical models to estimate wetting pattern for surface and subsurface drip irrigation, Irrigation Sci. 28,435-444.

Kandelous, M.M., and Šimůnek, J. (2010 b) Numerical simulations of water movement in a subsurface drip irrigation system under field and laboratory conditions using HYDRUS-2D, Agricultural Water Management, 97, 1070-1076.

Kandelous, M.M., Šimůnek, J., van Genuchten, M.Th., Malek, K. (2011) Soil water content distributions between two emitters of a subsurface drip irrigation system, Soil Science Society of America Journal, 75 (2), 488-497

Keller, J. and Karmeli, D. (1974) Trickle irrigation design parameters. Transaction of the ASAE, **7**, 678-684

Keller, J. and Bliesner, R. (1990) Sprinkle and trickle irrigation. Chapman and Hall, New York. 739 p.

Khan, A.A., Yitayew, M., Warrick, A.W. (1996) Field evaluation of water and solute distribution from a point source. J. Irrig. Drain. Eng., ASCE, 22(4),221–227

Lafolie, F., Guennelon, R., Van Genuchten, M. (1989) Analysis of water flow under trickle-irrigation, I: theory and numerical solution. Soil Science Society of America Journal, 53, 1310-1318

Lamm, F.R., Ayars, J.E., Nakayama, F.S. (2007) Microirrigation for Crop Production - Design, Operation and Management. Elsevier Publications. 608 p.

Lazarovitch, N., Šimůnek, J., Shani, U. (2005) System dependent boundary condition for water flow from subsurface source. Soil Sci Soc Am J 69 (1), 46-50

Lazarovitch, N, Warrick, A.W., Furman, A., Šimůnek, J. (2007) Subsurface water distribution from drip irrigation described by moment analyses. Vadose Zone J 6, 116–123

Levin, I., Van Rooyen, P.C., Van Rooyen, F.C. (1979) The effect of discharge rate and intermittent water application by point source irrigation on soil moisture distribution pattern. Soil Science Society of America Journal, 43 (1), 8-16

Li, J., Zhang, J., Ren, L. (2003) Water and nitrogen distribution as affected by fertigation of ammonium nitrate from a point source. Irrig. Sci 22 (1), 12-30

Li, J., Zhang, J., Rao, M. (2004). Wetting patterns and nitrogen distributions as affected by fertigation strategies from a surface point source. Agricult. Water Manag., 67, 89–104

Lubana, P.P.S. and Narda, N.K. (2001) Modelling soil water dynamics under trickle emitters - a review. J. Agric. Eng. Res., 78 (3), 217–232

Mmolawa, K., and Or, D. (2000) Water and Solute Dynamics under a Drip-Irrigated Crop: Experiments and Analytical Model. Trans. ASAE 43, 1597-1608

Mostaghimi, S., Mitchel, J.K., Lembke, W.D. (1981) Effect of discharge rate on distribution of moisture in heavy soils irrigated from a trickle source. American Society of Agricultural Engineers, 81, 975-980

Mualem, Y. (1976) A new model for predicting the hydraulic conductivity of unsaturated porous media. Water Resour. Res., 12, 513–522

Patel, N. and Rajput, T.B.S. (2008) Dynamics and modeling of soil water under subsurface drip irrigated onion, Agricultural Water Management, 95 (12), 1335-1349

Peters, A. and Durner, W. (2008) Simplified Evaporation Method for Determining Soil Hydraulic Properties, Journal of Hydrology, 356, 147– 162

Philip, J.R. (1968) Steady Infiltration from Buried Point Sources and Spherical Cavities. Water Resour. Res. 4, 1039-1047

Philip, J.R. (1984) Travel-Times from Buried and Surface Infiltration Point Sources. Water Resour. Res 20, 990-994

Phogat, V., M. Mahadevan, and M. Skewes, and J. W. Cox, (2011). Modelling soil water and salt dynamics under pulsed and continuous surface drip irrigation of almond and implications of system design, Irrigation Science, 1-19 p. doi:10.1007/s00271-011-0284-2

Provenzano, G. (2007) Using HYDRUS-2D Simulation Model to Evaluate Wetted Soil Volume in Subsurface Drip Irrigation Systems, Journal of Irrigation and Drainage Engineering, 133 (4), 342–349

Radcliffe, D.E., Šimůnek, J. (2010) Soil physics with HYDRUS modeling and applications. CRC Press, Taylor & Francis Group, Boca Raton, 373 p.

Reinders F.B. (2007) Micro-irrigation: world overview on technology and utilization. 7th International Micro-Irrigation Congress in Kuala Lumpur, Malaysia. Available at: http://www.icid.org/nletter/micro_nl2006_4.pdf

Richards, L.A. (1931) Capillary conduction of liquids in porous mediums. Physics 1, 318–333

Rodríguez-Sinobas, L., Gil-Rodríguez, M., Sánchez, R., Losada, A., Castañón, G., Juana, L., Laguna, F.V., Benítez, J. (2010) Simulation of Soil Wetting Patterns in Drip and Subsurface Irrigation. Effects in Design and Irrigation Management Variables, Geophysical Research Abstracts, Vol.. 12, EGU 2010-15064

Schaap, M.G., Leij, F.J., van Genuchten, M.Th. (2001) ROSETTA: a computer program for estimating soil hydraulic properties with hierarchical pedotransfer functions. J. Hydrol., 251, 163–176

Schindler, U., (1980) Ein Schnellverfahren zur Messung der Wasserleitfa ¨higkeit im teilgesa¨ttigten Boden an Stechzylinderproben. Arch. Acker-u. Pflanzenbau u. Bodenkd. Berlin 24, 1–7. Cited in: Peters, A. and Durner, W. (2008) Simplified Evaporation Method for Determining Soil Hydraulic Properties, Journal of Hydrology, 356, 147– 162

Schmitz, G.H., Schutze, N., Petersohn, U. (2002) New strategy for optimizing water application under trickle irrigation. J. Irrig. Drain. Eng. ASCE 128 (5), 287–297

Schwartzman, M. and Zur, B. (1986) Emitter spacing and geometry of wetted soil volume. J. Irrigat. Drain. Eng., 112, 242-253

Skaggs, T.H., Trout, T.J., Rothfuss, Y. (2010) Drip Irrigation Water Distribution Patterns: Effects of Emitter Rate, Pulsing, and Antecedent Water. Soil Sci. Soc. Am. J. 74,1886–1896

Skaggs, T.H., Trout, T.J., Šimůnek, J., Shouse, P. J. (2004) Comparison of Hydrus-2D simulations of drip irrigation with experimental observations, J. of Irrigation and Drainage Engineering, 130 (4), 304-310

Smith, J.U., Smith, P. Addiscott, T.M. (1996) Quantitative methods to evaluate and cpompare soil organice matter (SOM) models. in DS Powlson, P Smith & JU Smith (eds), Evaluation of Soil Organic Matter Models Using Existing Long-Term Datasets. NATO Advanced Research Workshop : Papers., NATO ASI Series 1 edn, vol. 38, NATO ASI series I global environmental change, vol. 38, Springer-Verlag, Heidelberg, 181-200

Šejna, M., Šimůnek, J., van Genuchten, M.Th. (2011). The HYDRUS Software Package for Simulating Two- and Three-Dimensional Movement of Water, Heat, and

Multiple Solutes in Variably- Saturated Media, User Manual, Version 2.0, PC Progress, Prague, Czech Republic, 284 p.

Šimůnek, J., Huang, K., van Genuchten, M. Th. (1995) The SWMS_3D Code for Simulating Water Flow and Solute Transport in Three-Dimensional Variably-Saturated Media, Version 1 .O. Research Report No, 139, U.S. Salinity Laboratory, USDA, ARS, Riverside, California.

Šimůnek, J., Šejna, M., van Genuchten M.Th. (1996) Th e HYDRUS-2D software package for simulating water flow and solute transport in two dimensional variably saturated media. Version 1.0. IGWMC-TPS-53. Int. Ground Water Modeling Ctr., Colorado School of Mines, Golden.

Šimůnek, J., Šejna, M., van Genuchten, M.Th. (1999) The HYDRUS-2D software package for simulating two-dimensional movement of water, heat, and multiple solutes in variably saturated media. Version 2.0. IGWMC-TPS-53. Int. Ground Water Modeling Ctr., Colorado School of Mines, Golden.

Šimůnek, J., van Genuchten, M.Th, Šejna, M. (2006) The HYDRUS software package for simulating two- and three-dimensional movement of water, heat, and multiple solutes in variably-saturated media: Technical manual. Version 1.0. PC-Progress, Prague, Czech Republic

Šimůnek, J., van Genuchten, M.Th., Šejna, M. (2011) The HYDRUS software package for simulating two- and three-dimensional movement of water, heat, and multiple solutes in variably-saturated media: Technical manual. Version 2.0. PC-Progress, Prague, Czech Republic, 258 p.

Taghavi, S.A., Miguel, M.A., Rolston, D.E. (1984) Infiltration from trickle-irrigation source. Journal of Irrigation and Drainage Engineering. American Society of Civil Engineering, 10, 331-341

van Genuchten, M.T. (1980) A closed-form equation for predicting hydraulic conductivity of unsaturated soils. Soil Sci Soc Am J 44, 892–898

van Genuchten, M. Th., Leij, F. J., Yates, S. R. (1991) The RETC code for quantifying the hydraulic functions of unsaturated soils. Report No. EPA/600/2-91/065. R. S. Kerr Environmental Research Laboratory, U. S. Environmental Protection Agency, Ada, OK. 85 p.

Vermeiren, L., Jobling, G.A. (1984) Localized irrigation. FAO Irrigation and Drainage Paper 36, FAO-UN, Rome, Italy, 203 p.

Wang, F., Kang, Y., Liu, S. (2006) Effects of drip irrigation frequency on soil wetting pattern and potato growth in North China Plain. Agric. Water Manag. 79 (3), 248-264

Warrick, A.W. (1974) Time-dependent linearized infi ltration: I. Point sources. Soil Sci. Soc. Am. J. 38,383–386

Wind, G.P. (1968) Capillary conductivity data estimated by a simple method. In: Rijtema, P.E., Wassink, H. (Eds.), Water in the Unsaturated Zone, vol. 1. Proceedings of the Wageningen Symposium, 19–23 June 1966. Int. Assoc. Sci. Hydrol. Publ. (IASH), Gentbrugge, The Netherlands and UNESCO, Paris. Cited in: Peters, A. and Durner, W. (2008) Simplified Evaporation Method for Determining Soil Hydraulic Properties, Journal of Hydrology, 356, 147– 162

Wooding, R.A. (1968) Steady Infiltration from a Shallow Circular Pond. Water Resou. Res. 4, 1259-1273